ASSESSMENT OF ROLL-FORMED PRODUCTS INCLUDING THE COLD FORMING EFFECTS

A THESIS SUBMITTED TO
THE GRADUATE SCHOOL OF NATURAL AND APPLIED SCIENCES
OF
MIDDLE EAST TECHNICAL UNIVERSITY

BY

ALPER GÜNER

IN PARTIAL FULFILLMENT OF THE REQUIREMENTS
FOR
THE DEGREE OF MASTER OF SCIENCE
IN
MECHANICAL ENGINEERING

MAY 2007

Approval of the Graduate School of Natural and Applied Sciences

Prof. Dr. Canan ÖZGEN
Director

I certify that this thesis satisfies all the requirements as a thesis for the degree of Master of Science.

Prof. Dr. S. Kemal İDER
Head of Department

This is to certify that we have read this thesis and that in our opinion it is fully adequate, in scope and quality, as a thesis for the degree of Master of Science.

Prof. Dr. A. Erman Tekkaya	Prof. Dr. S. Engin Kılıç
Co-Supervisor	Supervisor

Examining Committee Members

Prof. Dr. Suat Kadıoğlu	(METU, ME)	
Prof. Dr. S. Engin Kılıç	(METU, ME)	
Prof. Dr. A. Erman Tekkaya	(Atılım Uni., MFGE)	
Assoc. Prof. Dr. Uğur Polat	(METU, CE)	
Asst. Prof. Dr. Serkan Dağ	(METU, ME)	

I hereby declare that all information in this document has been obtained and presented in accordance with academic rules and ethical conduct. I also declare that, as required by these rules and conduct, I have fully cited and referenced all material and results that are not original to this work.

Alper GÜNER

ABSTRACT

ASSESSMENT OF ROLL-FORMED PRODUCTS INCLUDING THE COLD FORMING EFFECTS

Güner, Alper
M.S., Department of Mechanical Engineering
Supervisor: Prof. Dr. S. Engin Kılıç
Co-Supervisor: Prof. Dr. A. Erman Tekkaya

May 2007, 149 pages

Roll-forming is an efficient sheet forming process that is used in manufacturing long parts with constant cross-section. The theoretical, experimental and numerical analyses of the process are limited since the sheet takes a complex 3D shape during the process.

In this study proper finite element method models to simulate the roll-forming process are examined both numerically and experimentally. In addition, the applicability of 2D plane strain models to the simulation of the process is investigated. To reveal the deformation of the sheet, important geometrical parameters of the sheet and the rollers are introduced. The effect of these parameters on the strain hardening and deformation of the sheet is analyzed at distinct parts of the sheet that undergoes different types of deformations. Having revealed the deformation mechanisms, the assumptions behind the theoretical knowledge is criticized.

The mentioned studies are verified with a case study in which a roll-formed product is analyzed under service loads. The manufacturing of the product and service load application are simulated and the results are compared with the experiments. In addition, effects of cold forming on the behaviour of the product under service loads are examined.

It is concluded that under some conditions, 2D plane strain simulations can be used to predict the strain hardening in the material that occurs during roll-forming and this hardening has a considerable effect on the response of the material under loading.

Keywords: Roll-Forming, Finite Element Method, Plane Strain, Strain Hardening.

ÖZ

HADDELİ ŞEKİLLENDİRİLMİŞ ÜRÜNLERİN SOĞUK ŞEKİLLENDİRME ETKİLERİNİ İÇEREREK DEĞERLENDİRİLMESİ

Güner, Alper
Yüksek Lisans, Makina Mühendisliği Bölümü
Tez Yöneticisi: Prof. Dr. S. Engin Kılıç
Ortak Tez Yöneticisi: Prof. Dr. A. Erman Tekkaya

Mayıs 2007, 149 sayfa

Haddeli şekillendirme sabit kesite sahip uzun parçaların üretimi için kullanılan verimli bir sac şekillendirme yöntemidir. Yöntemin kuramsal, deneysel ve sayısal incelemeleri sacın işlem sırasında aldığı karmaşık üç boyutlu şekil yüzünden sınırlıdır.

Bu çalışmada haddeli şekillendirme işleminin simülasyonunda kullanılabilecek sonlu eleman yöntemi modelleri sayısal ve deneysel olarak incelenmiştir. Ayrıca iki boyutlu düzlemsel genleme modellerinin işlemin simülasyonuna uygulanabilirliği araştırılmıştır. Sacın şekillenmesini incelemek için sacın ve tamburların önemli geometrik parametreleri ortaya çıkarılmıştır. Bu parametrelerin sacın farklı biçimde şekillenen kısımlarındaki deformasyona ve pekleşmeye olan etkileri incelenmiştir. Deformasyon mekanizmaları ortaya çıkarıldıktan sonra kuramsal bilgilerin arkasındaki kabuller eleştirilmiştir.

Bahsedilen çalışmalar, haddeli şekillendirilmiş bir ürünün servis yükleri altında incelendiği uygulamalı bir örnek ile doğrulanmıştır. Ürünün üretimi ve servis yüklerinin uygulanması simüle edilmiş ve sonuçlar deneylerle karşılaştırılmıştır. Ayrıca soğuk şekillendirmenin servis yükleri altındaki ürünün davranışına olan etkileri incelenmiştir.

Sonuç olarak, iki boyutlu düzlemsel genleme simülasyonlarının bazı koşullar altında malzemede haddeli şekillendirme esnasında oluşan pekleşmeyi tahmin etmek için kullanılabileceği ve bu pekleşmenin yükleme altındaki malzemenin tepkisini önemli ölçüde etkilediği anlaşılmıştır.

Anahtar Kelimeler: Haddeli Şekillendirme, Sonlu Eleman Yöntemi, Düzlemsel Genleme, Pekleşme.

To My Family

ACKNOWLEDGEMENTS

I would like to express my appreciation and thankfulness to Prof. Dr.-Ing. A . Erman Tekkaya for his encouragement and support that created this study.

I would like to thank Prof. Dr. S. Engin Kılıç for his kind help and support. I also wish to thank Prof. Dr. Suat Kadıoğlu, Asst. Prof. Dr. Serkan Dağ, and Assoc. Prof. Dr. Uğur Polat for their suggestions and comments.

I would like to thank Koray Demir, for his invaluable collaboration and friendship.

I would like to thank my colleagues Günter Domani and Martin Matheis. The support provided by HILTI A.G. is greatly acknowledged.

I send my best wishes to Asst. Prof. Serhat Erpolat and Celal Soyarslan who have supported my study with their kind help.

My best wishes to all former FEMLAB members, Oya Okman, Erkan Önder, Erge Koray, Nagihan Topçu, Canderim Önder, Muin Öztop, Mert Aygen, and Hasan Ali Hatipoğlu. The support provided by my colleagues Emrah Demirci, Tahsin Öpöz and Aylin Konez Eroğlu are greatly acknowledged. Thanks extend to Dilek Özgör and Gözde Eminoğlu for their support and friendship.

I would like to express my happiness to have such close friends like Ateş, Hoca, Murat, Engin, Hüsam, Tuçe, Birgül and Berat.

And to have Emine Kılıç, who has witnessed and shaped my undergraduate and graduate life and enriched this study with her contribution full of patience.

Güner Family members, Zuhal Güner, M. Nail Güner and Ögeday Güner, who have supported me through my life, deserve the largest credit. Every single page of this study is their work essentially and therefore dedicated to them.

TABLE OF CONTENTS

LIST OF TABLES

LIST OF FIGURES

CHAPTER 1

INTRODUCTION

1.1 An Overview of Metal Forming Processes

Manufacturing processes are defined broadly as the production of solid bodies with the required geometry and properties. The classification of manufacturing processes according to DIN 8530 can be seen in Table 1.1 [1].

Table 1.1 Classification of manufacturing processes [1]

<table>
<tr><td>Creation of Cohesion</td><td>Maintenance of Cohesion</td><td>Destruction of Cohesion</td><td colspan="2">Increase of Cohesion</td></tr>
<tr><td rowspan="4">1. Primary Forming
(Form generation)</td><td colspan="3">Shape (Form) Modification</td><td rowspan="4">5. Coating</td></tr>
<tr><td>2. Deforming</td><td>3. Separating</td><td>4. Joining</td></tr>
<tr><td colspan="3">6. Changing Material Properties</td></tr>
<tr><td>Rearrangement of particles</td><td>Removal of particles</td><td>Addition of Particles</td></tr>
</table>

Metal forming, which is classified under “Deforming” processes in Table 1.1, is one of the main production processes. It is defined by DIN 8580 as “manufacturing of a shape while retaining its mass and material cohesion”.

Metal forming processes provide numerous advantages to the manufacturer. Because of efficient utilization of material, these processes have superior characteristics over metal cutting operations. They provide high productivity in short production times. The dimensional accuracy of the final product is high within certain tolerances. The mechanical properties of the product are good, especially under dynamic loading conditions [1]. Because of the advantages mentioned above, this manufacturing technique is commonly utilized in industry.

Another classification of metal forming operations can be made according to the temperature of the workpiece at the beginning of the process. According to this criterion, the three main groups of processes are cold forming, warm forming and hot forming (Figure 1.1).

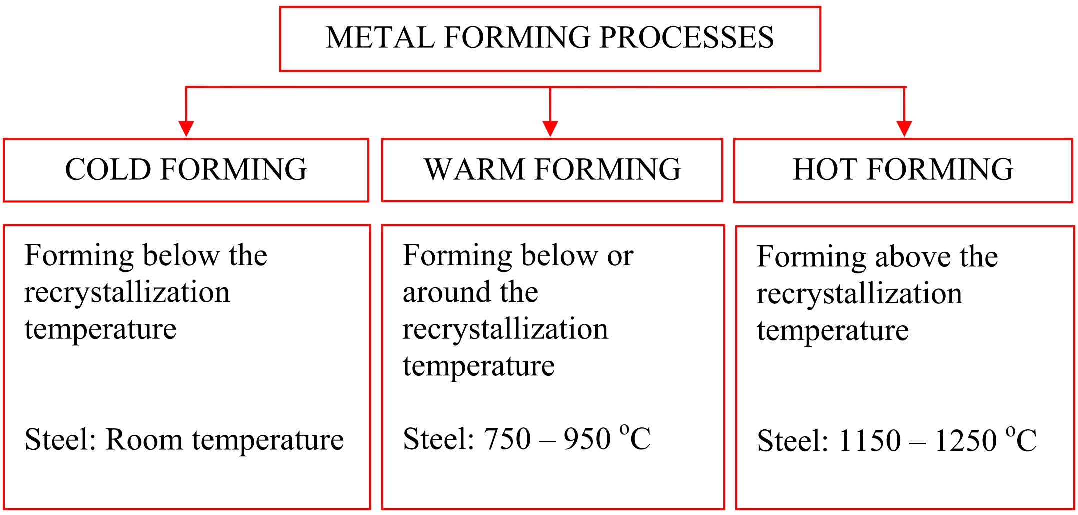

Figure 1.1 Classification of metal forming processes [1].

Hot forming is the forming of metal workpieces above their recrystallization temperature. Above their recrystallization temperatures, metals become more ductile providing easy manufacturing of large and complex shaped workpieces. However, hot forming processes have critical disadvantages. The dimensional tolerances are hard to control due to cooling stage of the workpiece, therefore surface quality of the final product can not be achieved as good as in cold forming.

Cold forming is performed below recrystallization temperature of the workpiece. The main advantages of the process are high strength of the products, better dimensional precision and surface finish and less waste of material. Near-net shape and net-shape products can be manufactured by this method. The main disadvantages are, necassity of high forming loads and limited formability and ductility of materials at low temperatures.

Warm forming is defined as forming around the recrystallization temperature of the workpiece. Warm forming aims to collect the advantages of both cold and hot forming in terms of required forces, formability and final product properties such as surface finish and dimensional tolerances.

Metal forming processes can also be classified according to the workpiece geometry and stress state during the process as bulk forming operations and sheet forming operation. In bulk forming operations, spatial workpieces are formed. Generally large changes in cross-section and thickness are observed. Material flows in all directions and multi-axial compressive stress states occur in bulk forming. In sheet forming, planar wokpieces such as sheets and plates are formed. Generally two-axial stress states are observed in sheet forming and wall thickness of the workpiece remains almost the same [1]. In sheet forming, relatively small forces are needed in comparison with bulk forming operations.

Forming processes are either steady state or non-steady-state according to the relation of the deformation patterns with process duration. In steady-state processes such as extrusion and rolling, the deformation patterns are independent of time. However in non-steady-state- processes like forging or upsetting, deformation patterns depend on the process time [1].

A final classification of metal forming processes can be seen in Figure 1.2 which is according to the primary stress in the deformation zone. As can be seen, metal forming operations can be classified according to various parameters and in all of these classifications increasing number of operation types can be identified. In this section only the main classes of operations are introduced.

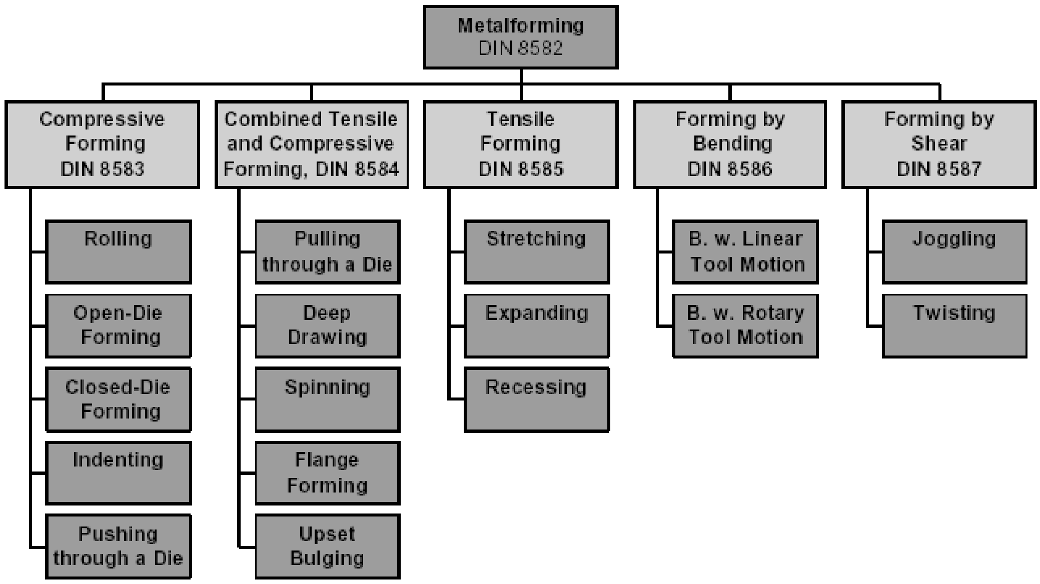

Figure 1.2 Classification of metal forming according to the primary stress in the deformation zone [1]

1.2 Fundamental Features of the Roll-Forming Process

There are numerous definitions in the literature for roll-forming. However, some of them limited themselves by using specific expressions which are not in general applicable or lost their validity through the time. The most comprehensive definition can be found in Reference [2], which is proposed by Kiuchi et al. According to this definition: “In a roll-forming process, pairs of profile rolls arranged in tandem transversally bend a moving metal sheet and make it into a product which has a designated cross-sectional profile" (Figure 1.3).

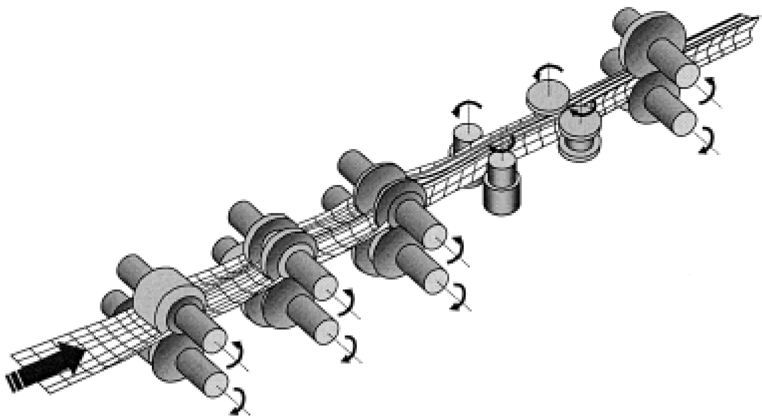

Figure 1.3 Schematic representation of roll-forming [3]

All materials that can be bent can also be roll-formed. Therefore, cold and hot finished carbon steel, stainless steel, aluminum and copper can be used in roll-forming [4]. It does not matter if the material is pre-painted or pre-coated. The thickness of the material being roll-formed may range from 0.1 mm up to 19 mm. The thickness of the material is usually limited by the size of available machinery. In length of the product there is no actual limit. The facilities that will handle the product limit the length of the production.

Since roll-forming is a continuous process high production speeds can be attained. 25-30 m/min is the most widely used speed range in roll-forming. 0.5 and 240 m/min are the unusual extremes of the process [4].

Roll-formed products are used widely in all areas of daily life. Some of the application areas are; roof panels, window and door frames, construction of cable carriage ways on the ceilings, construction of shelves, etc. Sample characteristic products can be seen in Figure 1.4.

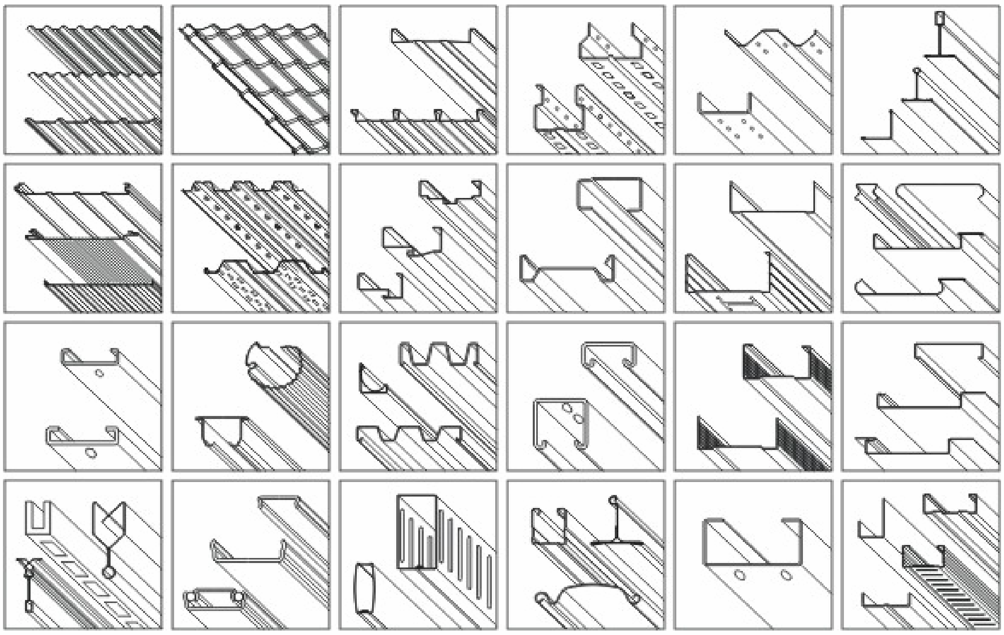

Figure 1.4 Range of roll-formed products [5]

The advantages of roll-forming can be listed as;

- High production capability: 1500-1800 m per working hour is a usual rate in roll-forming [4].
- Roll-formed sections have a higher strength to weight ratio than those which are hot rolled or extruded [6].
- Roll-forming does not injure fine surface finish of the raw material. Painted and electroplated material can be formed without damage to the coating [7].
- Roll-forming operation can be combined with other auxiliary operations such as piercing, notching, welding and perforation. These operations increase the production time by delaying the continuous feed of the sheet, but also add value to the product [4].

According to the classifications of metal forming presented in Section 1.1, roll-forming is a steady-state, sheet forming process. Since no occurrence of warm or hot roll-forming is encountered in the literature, the process is treated as cold forming. Therefore the name “roll-forming” actually stands for “cold roll-forming” in this study. According to the Figure 1.2 roll-forming is a process dominated by bending which is governed by rotary tool motion.

To understand the roll-forming process deeply, some definitions should be clarified since these are used extensively in the literature. Some widely used definitions are;

Web: The base of a cross-section which does not undergo any rotation (Figure 1.5).
Flange: The part of the cross-section which rotates about an axis around the web (Figure 1.5).
Roller: The rotary dies which bend the sheet (Figure 1.6).
Roll-set: A pair of rollers designed to give a specific shape to the sheet passing through (Figure 1.6).
Roll-stand: The roll-set is attached to the roll-stand with all its gears and shaft. In other words roll-stand carries the roll-set. Roll-stand can also be referred as “stand or “station” (Figure 1.6).

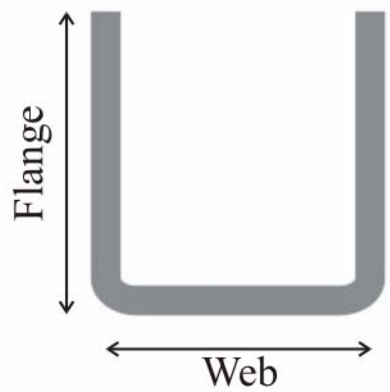

Figure 1.5 Flange and web of a section

The roll-forming machines used in the industry are quite similar. Basically they consist of a wide base which supports a bed on which a series of roll stands are mounted. Each roll-stand consists of one pair of rollers. Roll-forming machines with overhung spindles are suitable for light gage products since the rollers are supported only from one side (Figure 1.6). However, outboard support type machines can handle all types of sections. Hence, today outboard support type machines are preferred in the industry (Figure 1.7).

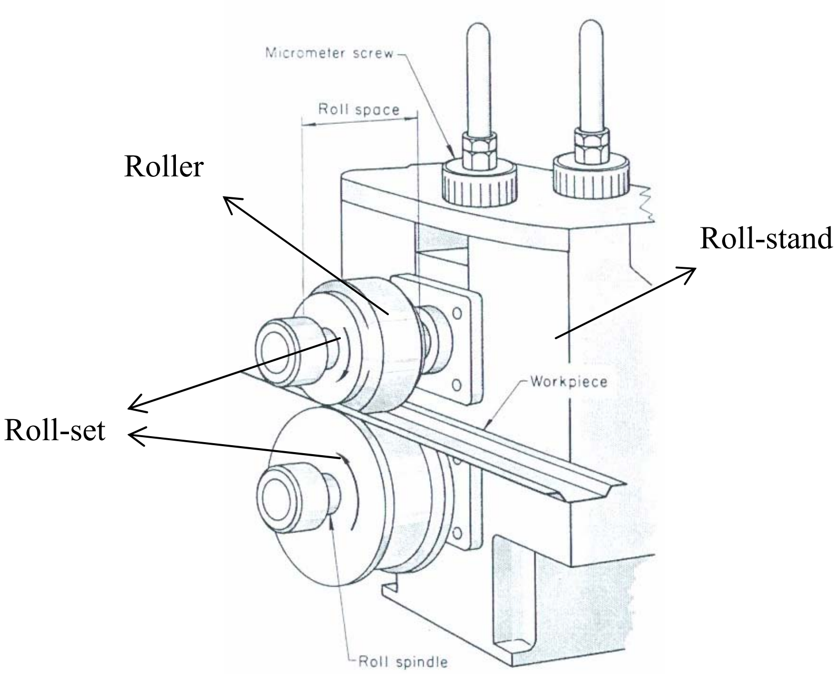

Figure 1.6 Roll-forming machine with overhung spindle [4]

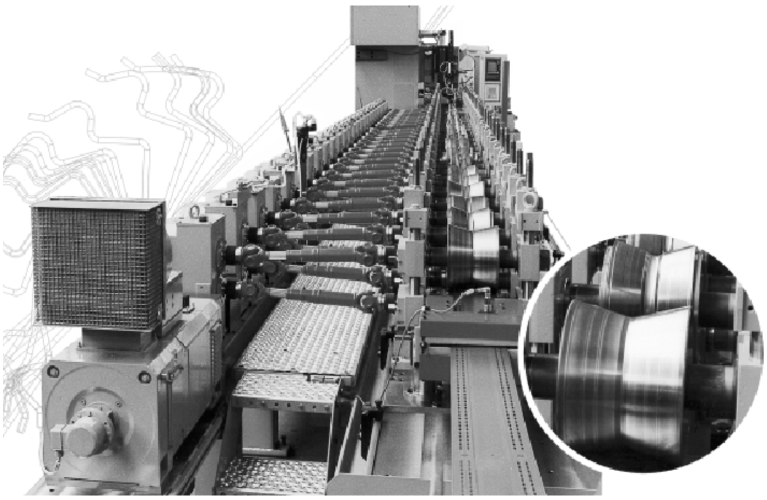

Figure 1.7 Roll-forming machine with outboard support [8]

1.3 Motivation of the Study

In the literature a number of papers admits that roll-forming is more an art than a science nowadays since the process is not revealed with all respects. Because of the complex deformation patterns in roll-forming, most of the works are limited to simple geometries such as U and V channels. In addition, numerical simulation of the process is a cumbersome work in terms of model preparation and computation duration. Hence, simplifications are needed to simulate roll-forming.

Moreover, analysis of the effects of cold forming on the final product is another critical issue. The design of products is generally performed disregarding the cold forming effects. However, it is known that residual stresses and plastic strains will occur in the material after cold forming operations. Therefore, these effects should be included in the design of the roll-formed sections. However, in the literature only a few studies are related to that topic.

Therefore, roll-forming is a relatively new process which has to be studied further with all its parameters. Furthermore, analysis of cold forming effects necessitates a deep knowledge of the process being investigated. Lack of studies on these subjects is the main motivation of the thesis work.

1.4 Aim and Scope of the Study

This thesis study will investigate how the roll-forming process affects the final product in terms of strain hardening and residual stresses. This is achieved in two major steps.

The first step is the research for an efficient numerical simulation method for the roll-forming process. Therefore different assumptions and simulation parameters are tried and compared to end up with an efficient method to simulate roll-forming.

In other words, the trade off between the accuracy of the results and the computation and model preparation time will be presented.

The next step is to study the deformation features of the roll-forming process. The strain hardening in different parts of the sheet will be revealed as a function of geometry of the sheet and the roll-sets.

In the final step, a case study is performed. A roll-formed product is tested under service loads both numerically and experimentally and the results are compared. The case study aims to clarify two major points;

- The simulation method presented in step one will be compared with the experimental results. Hence, the convenience of the method for this process will be discussed.
- The effects of strain hardening in roll-forming will be revealed by the performed experiments and numerical simulations.

The thesis work will be presented in six chapters. The upcoming chapter presents the literature that is made use of throughout the study. Chapter 3 discusses the simulation methods of the roll-forming process and Chapter 4 examines the deformation occuring in roll-forming including the effects of geometrical parameters. In Chapter 5, a case study is performed in which a roll-formed product is investigated both numerically and experimentally. The last chapter discusses the results and concludes the thesis work in addition with the further recommendations.

CHAPTER 2

LITERATURE SURVEY

2.1 Introduction

Because of the complexity of the roll-forming process, studies started with empirical observations. With the known experimental results, guidelines for the design of the roll sets for a defectless product have been proposed. These early studies are followed by theoretical works in which deformations occurring during roll-forming are identified and formulated. With the utilization of numerical methods and energy methods, detailed simulations of the process have been performed and deformation features of roll-formed products have been revealed for both simple and complex geometries. In this chapter empirical, analytical and numerical studies on investigation of the roll-forming process are presented. This is followed by a study on the effects of roll-forming process on the behaviour of a structural member under loads. As the last section, studies on the relation between Vickers Hardness Number and the yield stress will be presented since this knowledge will be used in validation of the numerical simulations throughout the thesis work.

2.2 Early Empirical Studies on Roll-Forming

Angel [9] proposed “Forming Angle Method” in order to achieve roll-forming without any defects in the final product. In this study it is assumed that a point at the edge of the section profile follows a straight line from the first roll-set to the last (Figure 2.1).

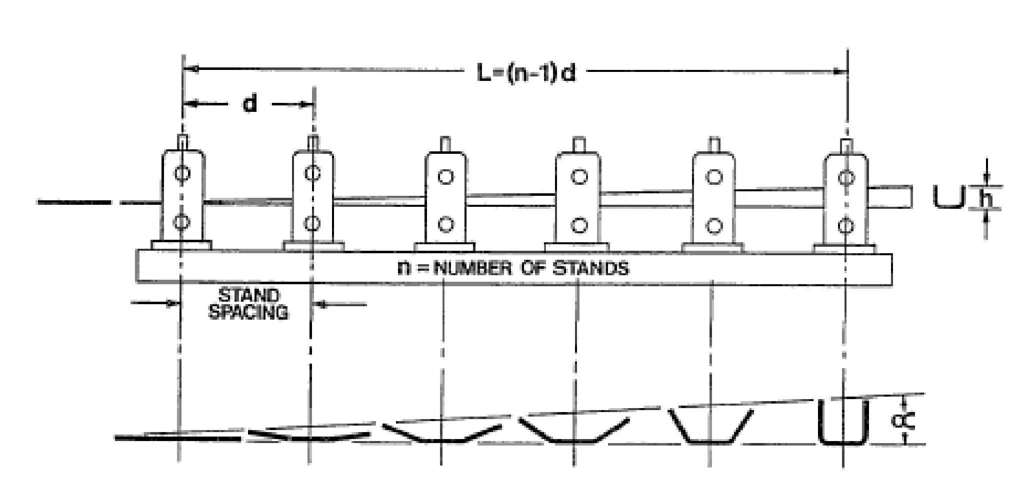

Figure 2.1 Forming Angle Method [9]

The forming angle α is given by

$$\cot(\alpha) = \frac{L}{h} = (n-1) \times \frac{d}{h} \tag{2.1}$$

where,

d= Interstand distance
h= Section height
α= Forming angle
L= Forming length
n= Number of stages required

The value of the forming angle is dependent on the ductility of the material being roll-formed. An average value of 1.4° is recommended for low carbon mild steels as a result of experiments performed.

Therefore;

$$\cot(\alpha) = \cot(1.5°) = 40.5 \tag{2.2}$$

and

$$n = 40.5 \times \frac{h}{d} + 1 \tag{2.3}$$

By the help of that study the number of stages for a specific geometry can be found roughly. However, it is clear that this method oversimplifies the roll-forming process.

To find the necessary number of stages, another method has been developed by Ona and Jimma [10]. A new parameter called shape factor is proposed. It is defined as;

$$\phi = F \cdot n \cdot t \tag{2.4}$$

where

F= Total length of all elements in the section in
n= Total number of bends
t= Thickness of the section

An element of a section is defined as a straight edge of a cross-section without any bends. In calculating the length *F*, only the elements which undergo deformation are considered. Therefore, the bottom web of a channel section is not considered in the calculation. Having found the shape factor, the value is input to a graph having the experimental results of successful roll-forming operations and the required number of stages *N* is found (Figure 2.2).

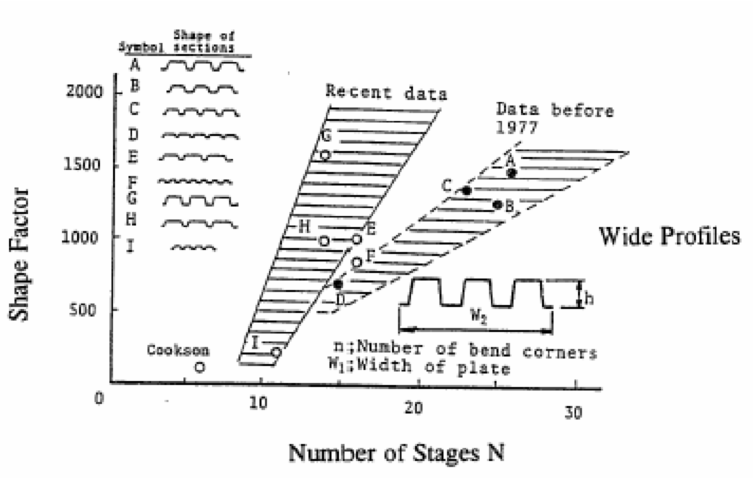

Figure 2.2 Shape Factor Method [10]

2.3 Theoretical Studies on Roll-Forming

Bhattacharyya et al. formulized the total work done to bend a metal sheet by roll-forming [11]. The deformation length of the sheet is also investigated. In this study, the total work is divided into two as bending work and stretching work. If the metal sheet is bent through an angle θ, the plastic bending work done per unit length is given as

$$W_b = \frac{1}{4} Y t^2 \theta \tag{2.5}$$

where, Y is the yield stress, θ is the bend angle and t is the sheet thickness.

Bhattacharyya et al. derived the expressions for stretching work by considering an infinitesimal element at the flange. Longitudinal engineering strain is found by considering two points on this element and calculating the displacement of these points and is given as

$$e = \frac{1}{2} x^2 \left(\frac{d\theta}{dz} \right)^2 \tag{2.6}$$

where x is the distance to the fold line and z-direction is the longitudinal direction.

Therefore, the plastic stretching work per unit volume is found as

$$W_s^{unit\ volume} = \frac{1}{2} Y x^2 \left(\frac{d\theta}{dz} \right) \tag{2.7}$$

Plastic work done by stretching per unit length of the sheet is found by integrating above expression along the flange. Therefore

$$W_s^{unit\ length} = \int_0^a \frac{1}{2} Y x^2 \left(\frac{d\theta}{dz} \right)^2 (t dx) = \frac{1}{6} Y a^3 t \left(\frac{d\theta}{dz} \right)^2 \tag{2.8}$$

where a is the flange length and t is the thickness of the sheet.

Hence the plastic stretching work for one bend is found as

$$W_s = \int_0^L \frac{Y a^3 t}{6} \left(\frac{d\theta}{dz} \right)^2 dz \tag{2.9}$$

The total plastic work per unit length is found by summing the work expressions for bending and stretching which is given as;

$$W_t = W_b + W_s = \frac{1}{4} Y t^2 \theta + \frac{1}{6} Y a^3 t \left(\frac{d\theta}{dz} \right)^2 \tag{2.10}$$

Then the general solution of $\theta(z)$ function which minimizes the total work is found as;

$$\theta(z) = \frac{3}{8} \frac{t}{a^3} z^2 + Az + B \tag{2.11}$$

Two constants A and B are found by applying the boundary conditions for θ. By equating $\theta'(0)$ to zero, the deformation length is found as;

$$L = \sqrt{\frac{8a\theta}{3t}} \tag{2.12}$$

Deformation length is defined as the length along which the bend angle of the sheet changes (Figure 2.3).

Substituting the θ function and the deformation length expressions in the total work equation yields the total work:

$$W_t = \frac{1}{6} Y t^2 L \theta \tag{2.13}$$

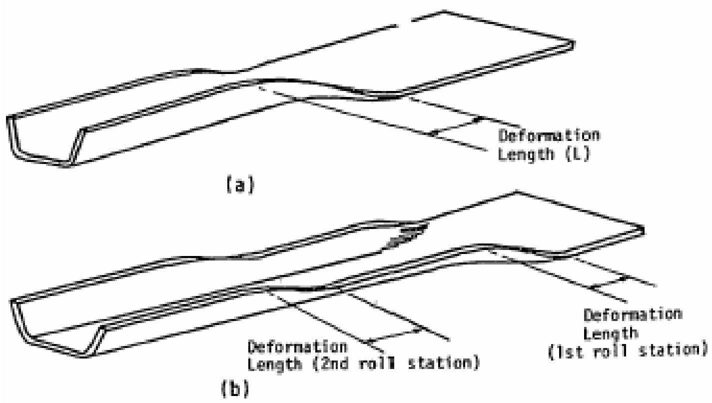

Figure 2.3 Deformation length in roll-forming [11]

Panton et al. [12] proposed the concept of geometric constraints in roll-forming. In this study, the sheet being roll-formed is investigated in 3 regions (Figure 2.4). In the first region the sheet does not undergo any deformation. In region 2, the sheet is deforming but it does not contact the rollers. In the last region the sheet is both deforming and in touch with the rollers. Therefore the sheet is not deforming through all the way. With this knowledge, the change of the bend angle of the sheet can be plotted with respect to the longitudinal traveled distance. This plot is named as “bend angle diagram” by the authors.

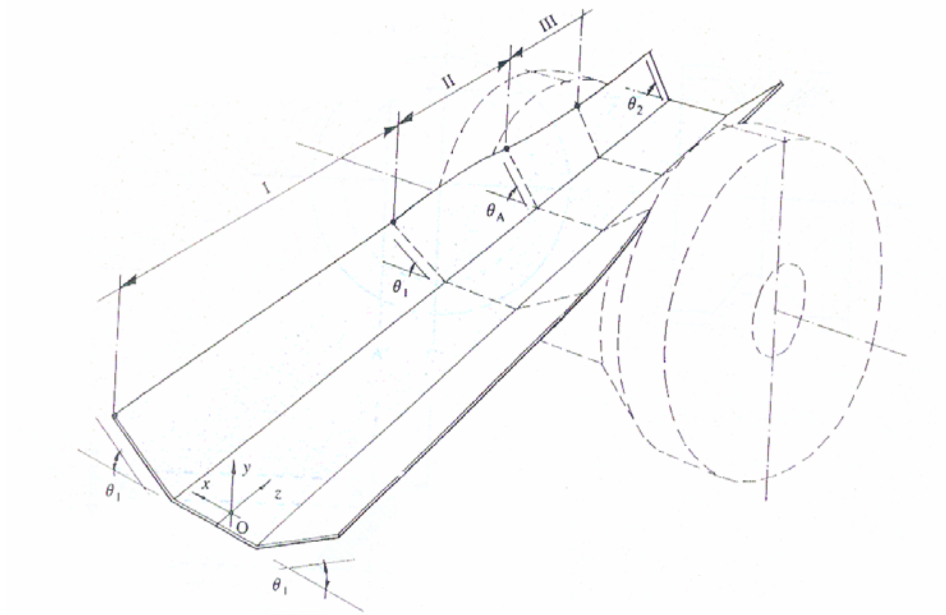

Figure 2.4 Three regions of deforming sheet [12]

In Figure 2.5, a bend angle diagram of a process which increases the bend angle from θ_1 to θ_2 is shown. In Region I, the bend angle is constant and equal to θ_1. In region II, the bend angle gradually increases until the sheet contacts the roller. The slope in Region III is accomplished by the rollers since the sheet is in contact with the roller. Therefore, if the roller profile is known, the part of the plot in Region III can be computed. To find the bend angle curve in region II the studies of Bhattacharyya et al. are benefited from [11]. In this study, the angle distribution along the longitudinal direction has been found for the deforming region. Panton et al. fitted that θ function between the first and the last regions.

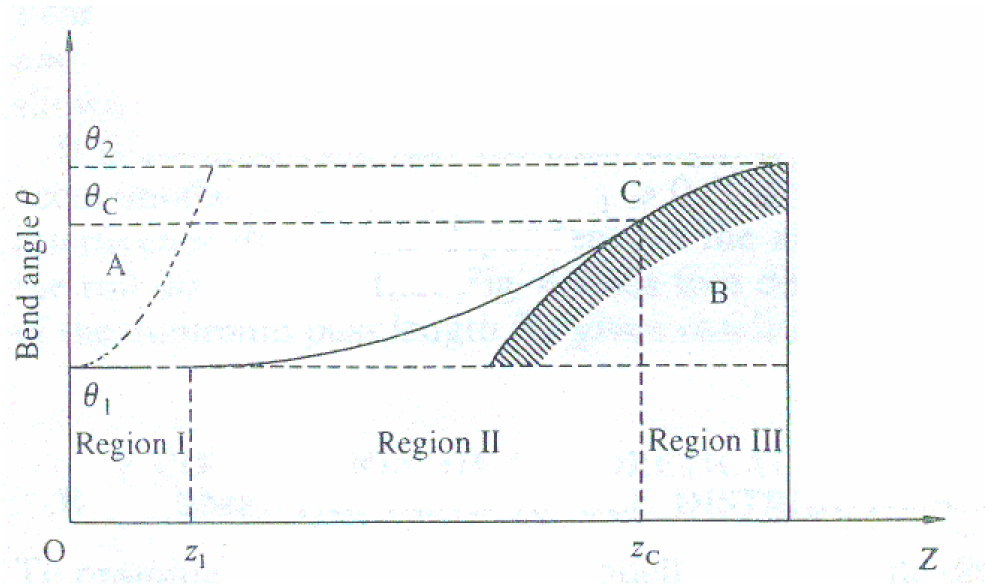

Figure 2.5 Bend angle diagram [12]

It was found previously that longitudinal engineering strain developing in roll-forming is a function of $\left({d\theta}/{dz}\right)^2$, [11]. Therefore, by the help of the Bend Angle Diagram the development of the engineering strain in roll-forming can be visualized and calculated. In Region I, the slope is zero. So there is no strain in region I. In region II the slope is gradually increasing and reaches its maximum at the end of region II. Therefore, engineering strain increases and reaches its maximum value when the sheet first contacts the roller. In region III, the slope decreases and drops to zero. Engineering strain also follows the same pattern. This engineering strain distribution along the sheet is verified with the experimental data obtained by locating strain gauges to the flange of a sheet specimen.

The formulations for the bend angle curve in region II and region III has also been presented in this work. For the region II the Equation 2.11 is used and for the region III which is on the roller surface, following relation between θ and longitudinal distance w exists.

$$w=\sqrt{\frac{a^2\cos^2\theta}{\cos^2\theta_2}+2aR_1\frac{\sin(\theta_2-\theta_1)}{\cos(\theta_2)}-a^2} \quad (2.14)$$

where a is the flange length, R_1 is the roll base radius, θ_1 and θ_2 are the bend angles at the beginning and end of the pass.

In a later study, Panton et al. [13] investigated the deformation features of roll-forming process. In this study a small element taken from the flange of a sheet is considered and four main deformation types are studied with this element (Figure 2.6).

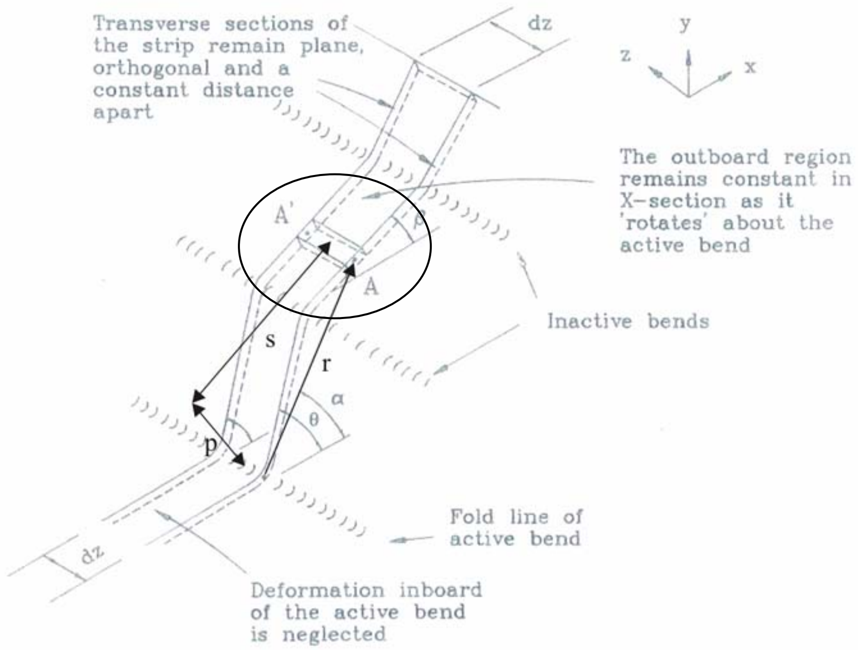

Figure 2.6 Small element investigated under different deformation types [13]

Longitudinal stretching: Longitudinal engineering strain is given as;

$$e_l=\frac{1}{2}r^2\left(\frac{d\alpha}{dz}\right)^2 \quad (2.15)$$

where r is the distance to the fold line and α is the bend angle. The longitudinal strain expression is exactly the same with the one found by Bhattacharrya [11].

Shear: Since AA' is not perpendicular to the mid-thickness line in the *xy*-plane in Figure 2.7, shear strain exists. It is showed that shear strain is equal to;

$$|\gamma| = r\sin(\alpha - \beta)\frac{d\theta}{dz} \tag{2.16}$$

where β is the angle between the side of the investigated element and the *x*-axis

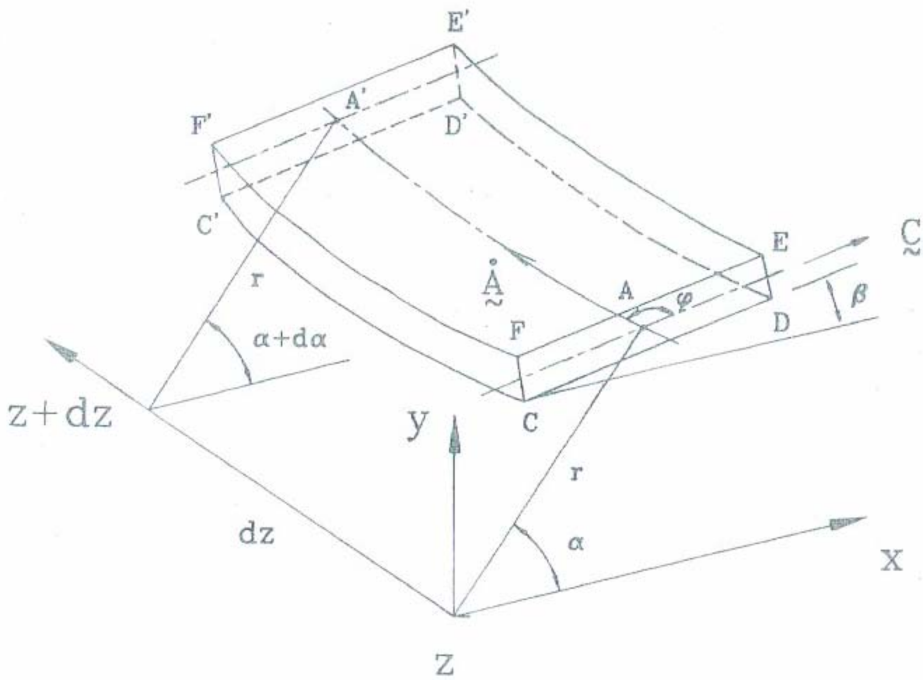

Figure 2.7 Small element in shear [13]

Longitudinal Bending: In roll-forming process, bending is also observed in the longitudinal direction. This bending is given as;

$$\varepsilon_{lb} = h\left(-p\left(\frac{d\theta}{dz}\right)^2 + s\left(\frac{d^2\theta}{dz^2}\right)\right) \tag{2.17}$$

where

$$p = r\sin(\alpha - \beta)$$
$$s = r\cos(\alpha - \beta)$$

with h is the distance from the mid-plane.

Transverse Bending: In this analysis only circular elements are considered to experience strain due to transverse bending. The transverse bending strain for a circular arc is given by the well-known expression:

$$\varepsilon_t = \frac{h}{r_0} \tag{2.18}$$

where h is the distance from the neutral axis and r_o is the radius to the neutral axis.

In this study, work expressions associated with each of the deformation types are also given. It is seen that work expressions are directly related with the sectional properties of the geometry. These sectional properties are;

***J*:** Polar second moment of area of the section outboard of the active bend about an axis through the active bend.

$$J = \int_A r^2 dA \tag{2.19}$$

***K*:** Perpendicular polar first moment of area of the section outboard of the active bend about an axis through the active bend.

$$K = \int_A p dA \tag{2.20}$$

***L*:** Parallel polar first moment of area of the section outboard of the active bend about an axis through the active bend.

$$L = \int_A s dA \tag{2.21}$$

The parameters *p*, *r* and *s* can be seen in Figure 2.6. A summary of the outcomes of that study can be seen in Table 2.1.

Table 2.1 Strain and work expressions for four deformation types, [13]

Deformation Type	**Strain**	**Work Done per Unit Lenght**
Longitudinal Streching	$\varepsilon_l = \frac{1}{2} r^2 \left(\frac{d\alpha}{dz}\right)^2$	$\frac{JY}{2}\left(\frac{d\theta}{dz}\right)^2$
Shear	$\lvert\gamma\rvert = r\sin(\alpha-\beta)\frac{d\theta}{dz}$	$\frac{KY}{2}\left(\frac{d\theta}{dz}\right)$
Longitudinal Bending	$\varepsilon_{lb} = h\left(-p\left(\frac{d\theta}{dz}\right)^2 + s\left(\frac{d^2\theta}{dz^2}\right)\right)$	$\frac{Yt}{4}\left(L\left(\frac{d^2\theta}{dz^2}\right) - K\left(\frac{d\theta}{dz}\right)^2\right)$
Transverse Bending	$\varepsilon_t = \frac{h}{r_0}$	$\frac{Yt^2}{4}(\theta-\theta_1)$

2.4 Numerical Studies on Roll-Forming

Studies by Kiuchi [2] on roll-forming of circular tubes establishes a mathematical theory to numerically study the deformation of sheet metal during the process. The deformed curved surface of metal sheet between two roll stands is expressed by the following sinusoidal shape functions.

$$
\begin{aligned}
&X = X(x, y)\\
&Y = Y_1(y) + \left[Y_2(y) - Y_1(y)\right] \cdot S(X)_y\\
&Z = Z_1(y) + \left[Z_2(y) - Z_1(y)\right] \cdot S(X)_z\\
&S(X)_y = \sin\left\{(\pi/2) \cdot \left(X^*/L\right)^{n_y}\right\}\\
&S(X)_z = \sin\left\{(\pi/2) \cdot \left(X^*/L\right)^{n_z}\right\}\\
&L = X_2 - X_1 \qquad X^* = X - X_1
\end{aligned}
\tag{2.22}
$$

where X_1, Y_1, Z_1 and X_2, Y_2, Z_2 are the coordinates of a point on the sheet in the first and second roll-sets respectively.

The geometry of the rollers is considered as boundary conditions of these functions. Once the surface is generated, it is divided into elements in longitudinal and transversal directions (Figure 2.8). From these elements strain and stress are obtained. Integrating stress and strain over the whole sheet energy of deformation is found. By varying the parameters, n_y and n_z, in the sinusoidal shape functions, the total power of deformation of the metal sheet between two roll stands is minimized in an iterative way. Therefore, the analysis is based on energy method. The numerical results have been verified with experimental studies.

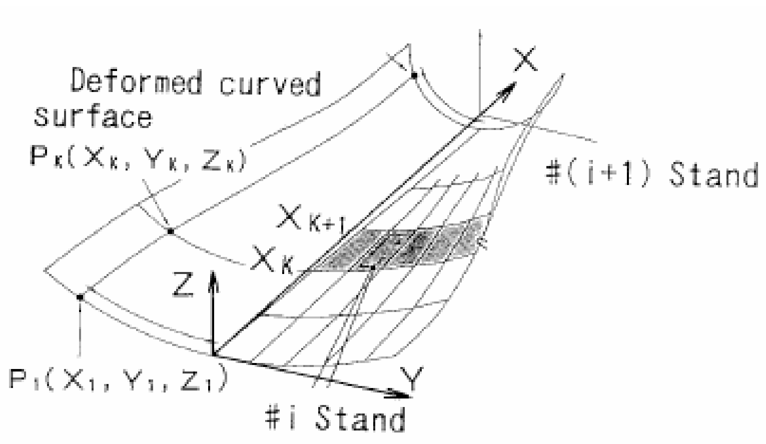

Figure 2.8 Sheet between two successive stands [2]

Based on the mathematical model presented by Kiuchi, finite difference method has been used to develop a program, RFPASS, by Duggal et al. [14] and it is compared with the experimental results. It is concluded that RFPASS will assist the engineers at least for simple sections.

Heislitz et al. [15] simulated roll-forming with the explicit finite element code PAM-STAMP. Authors fully modeled the process by using 8 node brick elements for the sheet and rigid dies. Since accurate rotation of the rolls is not possible in PAM-STAMP, the line speed which is the result of the rotation of the rolls and friction was approximated by a velocity field defined at the sheet-roll interface (Figure 2.9).

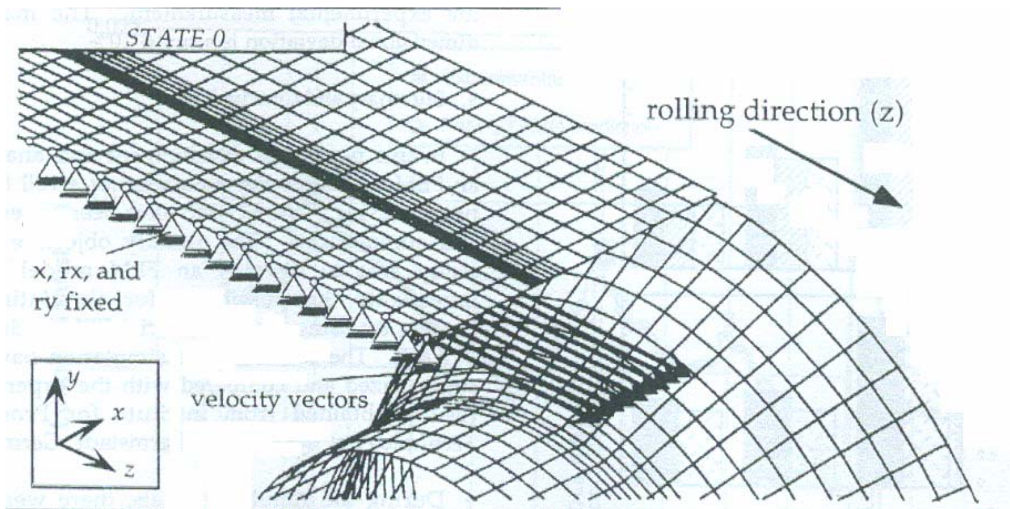

Figure 2.9 Undeformed sheet and the velocity field imposed to the nodes [15]

To optimize the simulations a parametric study has been performed to reduce the required computation time of the explicit code. Therefore proper element types and sizes, mass density and sheet speed is found. Also adaptive mesh refinement is found to be successful in reducing the CPU time.

The procedure followed to simulate roll-forming of a U-channel is as follows;

- Front end of the sheet is bent by moving the rollers vertically.
- The sheet is pulled through the first roll set until the second roll set is reached.
- The sheet is stopped and the rollers are moved vertically again to grab the sheet and bend the front end.
- The sheet is pulled again through both of the roller sets.
- This procedure is repeated until the sheet is pulled through all roll sets.

In this study, it is concluded that strain values obtained from PAM-STAMP are within 10% of the experimental strain gauge measurements. It is seen that simulation of roll-forming by PAM-STAMP is not efficient because of two main reasons: computation time and limitation to simple sections such as U and V channels.

Livatyali et al. [16] investigated roll-forming of pre-coated roof panels to eliminate crack formation occurring in the coating during the manufacturing stage. Both PAM-STAMP and DEFORM-2D have been utilized in the computations. In PAM-STAMP, 3D simulations are performed. In these simulations, the roll-forming operation is not simulated fully, instead, process is simulated by just moving the rollers in the vertical direction and making them grab the sheet in between. Therefore, there is no rolling motion. However, the critical roll set for the crack to be formed is identified with these simulations.

2D implicit simulations have also been performed by using DEFORM-2D and utilizing plane strain assumption. Four quadrilateral elements are used in the thickness direction and it is reported that these elements simulate local deformations in the thickness direction much better than the shell elements. In 2D plane strain simulations, rollers are modeled as rigid straight lines, and rolling operation is modeled by vertical movement of bottom roller to the upper roller (Figure 2.10).

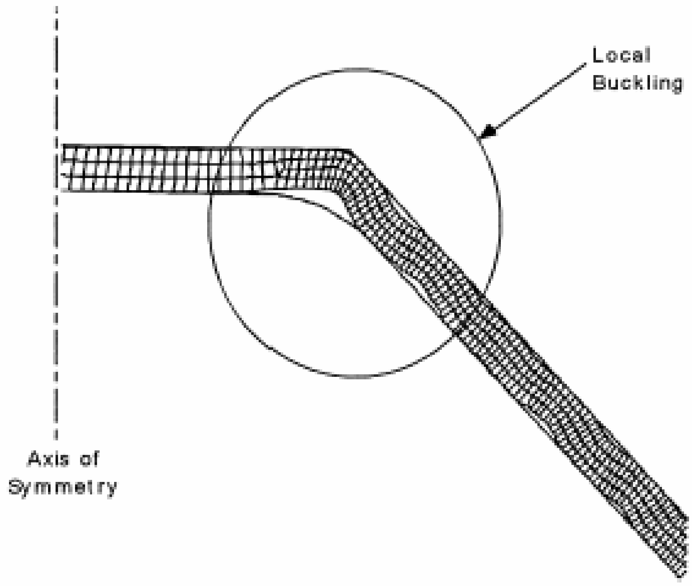

Figure 2.10 Plane strain simulation of roll-forming by vertically moving dies [16]

It is concluded that plane strain simulation is a valid approximation of the bending and stretching occurring in the cross-section and 2D plane strain analysis can be used more effectively than a full 3D analysis because of the computation time problem of 3D simulations.

Han et al. [17] studied the roll-forming process by the B-spline finite strip method. Deformed sheet between two progressive stands is named as "stage" and it is the main research object in this study. The research object is divided into *i* finite strips in the longitudinal direction and every finite strip is divided into *j* B-splines in the transverse direction (Figure 2.11).

The deformation between the upper and lower dies is modeled by moving the upper roll onto the lower roll. In every stage deformation is divided into displacement increments. The displacement functions consist of two parts: the transverse Hermitian cubic polynomials and longitudinal B-spline functions. Whole deformation of the sheet is simulated stage by stage. The stress, strain and geometry of the sheet after one stage are considered as initial state of the following stage.

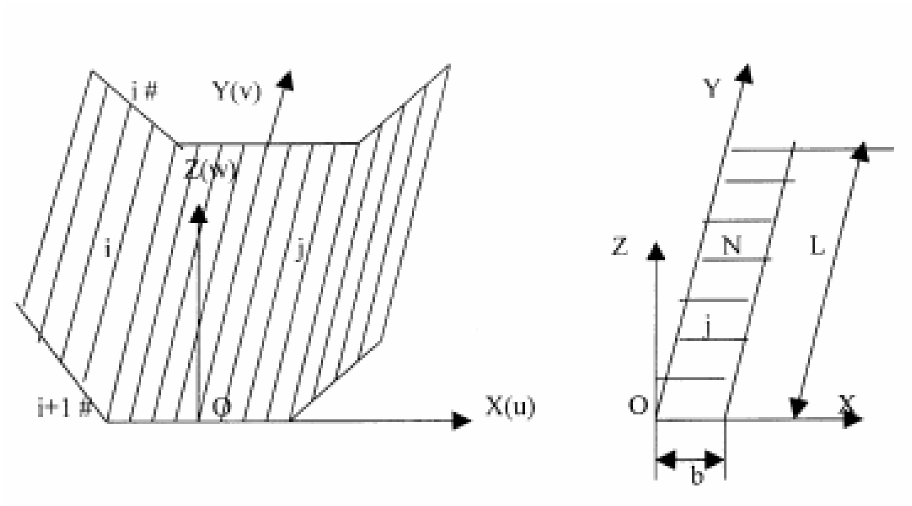

Figure 2.11 Stage is divided into finite strips and B-splines [17]

Kim and Oh [18] used polynomials to represent the deformed sheet surface in their study. The workpiece is divided into several cross-sections in the rolling direction. 2D plane strain simulations are performed at each cross-section to guess the deformed shape at the roll exit. Sixth order polynomials with undetermined coefficients are used as streamlines to generate 3D mesh over the guessed shapes (Figure 2.12). The coefficients are determined in such a way that the total deformation energy is minimized. The total deformation energy consists of 3 parts; plastic energy, volumetric energy and friction energy. Conjugate gradient method is utilized in finding the polynomial coefficients by minimizing the total energy.

Having obtained the 3D mesh system rigid viscoplastic finite element method is used to obtain the velocity field over the sheet. The results are compared with the experiments and it is concluded that the proposed simulation method computed the thickness distribution and strain correctly although some dissimilarity in magnitude exists.

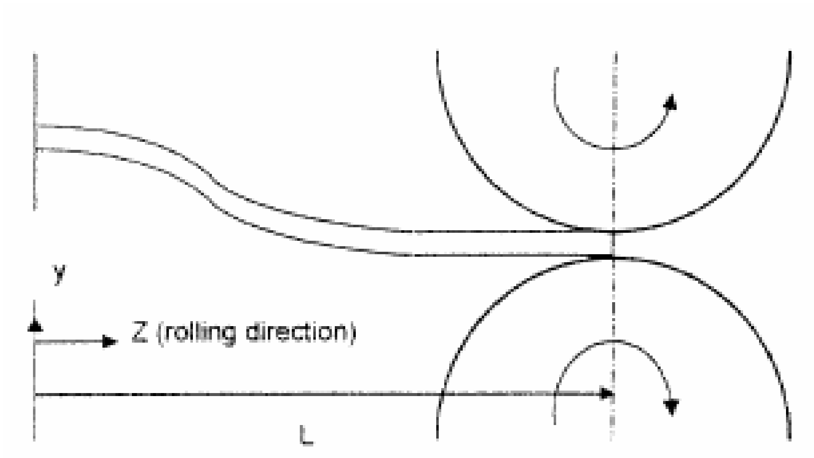

Figure 2.12 Streamline of strip entering the roll set [18]

Brunet et al. [19] simulated roll-forming process by a combined 2D and 3D simulations. The modeling technique is defined as a "master" 2D cross-section analysis with a "slave" 3D shell analysis between two or four successful stands. In the first master analysis, the action of the rotating rolls on the sheet is replaced by continuously moving rigid surfaces from one roll set profile to the next profile (Figure 2.13). Plane strain shell elements are used in the 2D analysis.

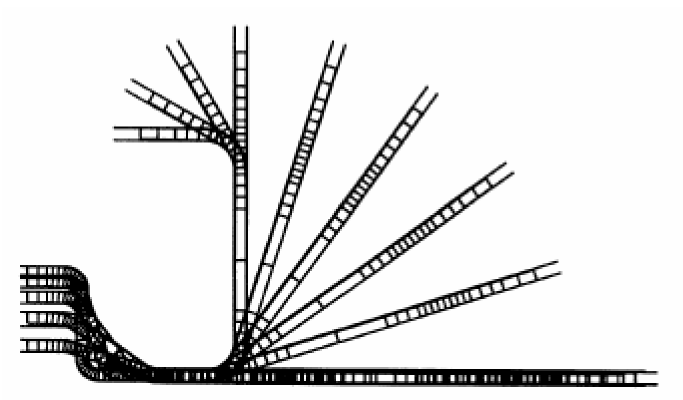

Figure 2.13 Deformed meshes of 2D cross-section analysis [19]

The second 3D phase is performed simultaneously with the first 2D phase. In this stage, the deformation of the sheet between successive roll sets is simulated. 3D mesh is constructed from the results of the 2D plane strain simulations by using sinusoidal functions. Again shell elements are utilized in the 3D simulations but with a less refined mesh (Figure 2.14). This algorithm is implemented in a program called PROFIL and the results have been verified with the experimental measurements.

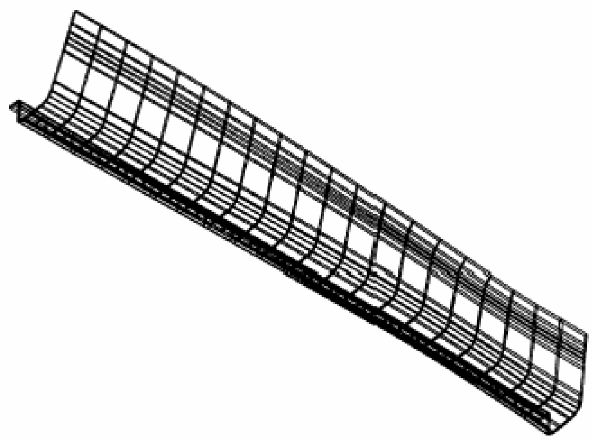

Figure 2.14 3D mesh generated from the 2D results shown in Figure 2.13 [19]

2.5 Effect of Roll-Forming Process on the Final Product

Abdel-Rahman and Sivakumaran [20] performed studies on the cold formed steel members and tried to include the effect of manufacturing processes in the simulations of these members under loads.

In order to obtain strain hardening data of the roll-formed section tensile test coupons are cut from different parts of the cross-section. These parts include the flat parts of the web and flange, curved parts of the bent regions and parts near the bent regions (Figure 2.15).

a)

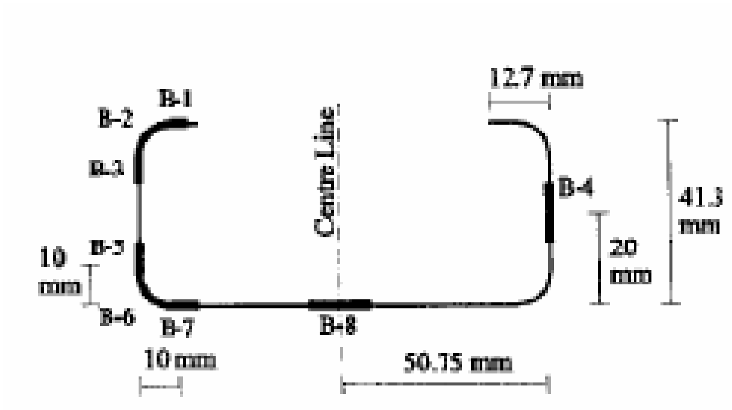

b)

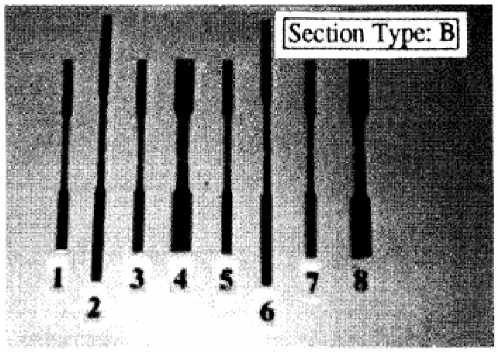

Figure 2.15 a) The roll-formed steel member and regions that the tensile test coupons are cut from **b)** Tensile test coupons taken from the cross-section [20]

At the end of the tensile tests it is observed that the coupons taken from the flat regions have approximately the same flow curve with the undeformed sheet. However, obvious changes in the material behaviour are observed in the coupons taken from or around the curved regions as a result of large plastic deformations occurred in roll-forming operation. It is seen that corner specimens have increased yield strength. On the other hand these are observed to have a decrease in the elongation in fracture (Figure 2.16).

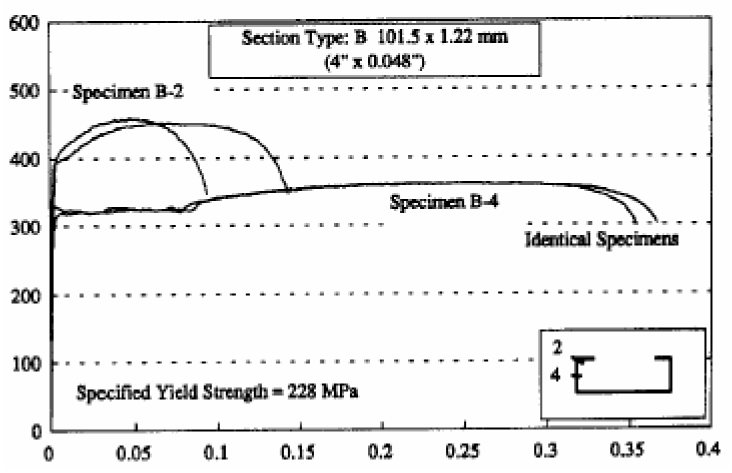

Figure 2.16 Sample tensile test results of specimens cut from flat and curved regions of the cross-section [20]

Based on the yield strength data obtained from the tensile tests an idealization is proposed. Different average yield strength values are assigned to the flat and curved parts of the cross-section to be used in the finite element simulation of the whole roll-formed member under loads. For the flat parts yield strength of the undeformed part is used and for the curved regions approximately 1.2 times the virgin yield strength is assigned. This idealization can be seen in Figure 2.17.

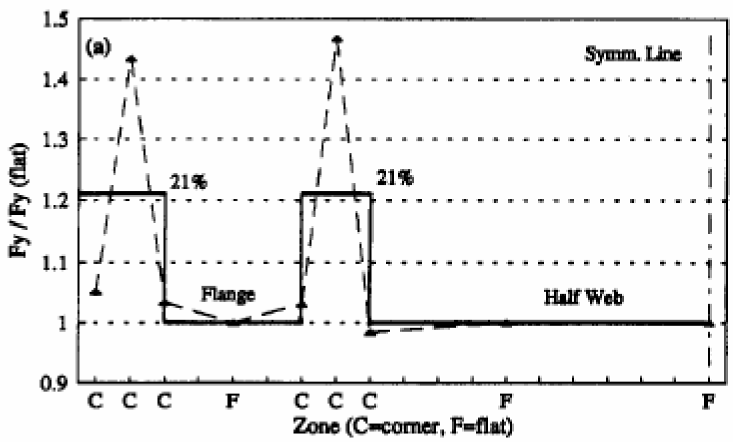

Figure 2.17 Idealization of the yield strengths for the flat and curved parts [20]

In order to determine the residual stresses, surface strains are released by slicing the sections into strips using electrical discharge machining (EDM), and the strains are measured using electrical resistance strain gauges. Strain gauges are mounted on both the inside and outside surfaces of the section along the longitudinal direction. From the measured strain values residual stresses are obtained.

It is noted that tensile residual stresses are recorded on the outside surface and compression on the inside. The highest magnitudes are found to occur at the web area around the curved corners. Another observation is that the magnitude of the residual stresses on the outside surface of a section is very close to the measurements taken from the inside surface, but with an opposite sign. From the rosetta type strain gauges principal strains are obtained and it is seen that difference between the first principal strain and the longitudinal strain at that location is less that 1%. Therefore, it is concluded that the principal residual stress direction of a roll-formed section is the longitudinal direction.

Again residual stresses for flat and curved parts of the section are idealized according to the measurements. Flat zones in the flange and web area are assigned with approximately 0.2 times of the yield strength and for the corners 0.4 times of the yield strength is used (Figure 2.18).

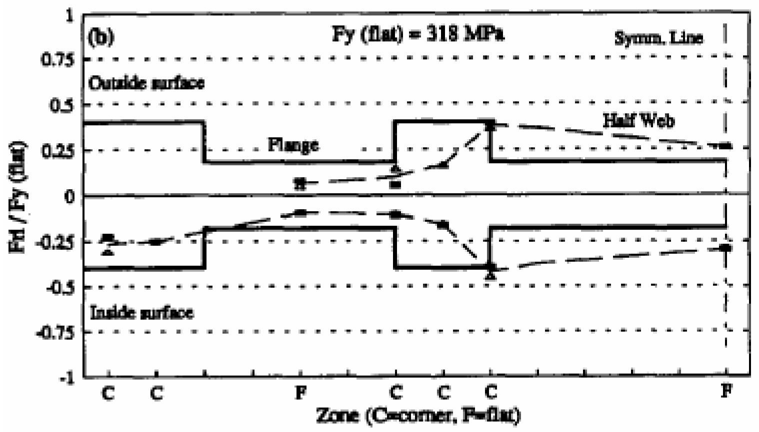

Figure 2.18 Idealization of the residual stress for the flat and curved parts [20]

Experiments involving the compression of the considered steel member are performed and force displacement data is obtained. 3D simulations of the experiment are also performed with and without the manufacturing effects. In the simulations without the manufacturing effects (F.E. (1) in Figure 2.19) material data of the undeformed material is used and for the simulations with the manufacturing effects (F.E. (2) in Figure 2.19) yield strength and residual stress idealizations are used combined with the undeformed material data. When the results are compared it is seen that both models predicted the material behaviour before yielding successfully. In addition, both models predicted similar maximum loads that are in agreement with the experimental measurements.

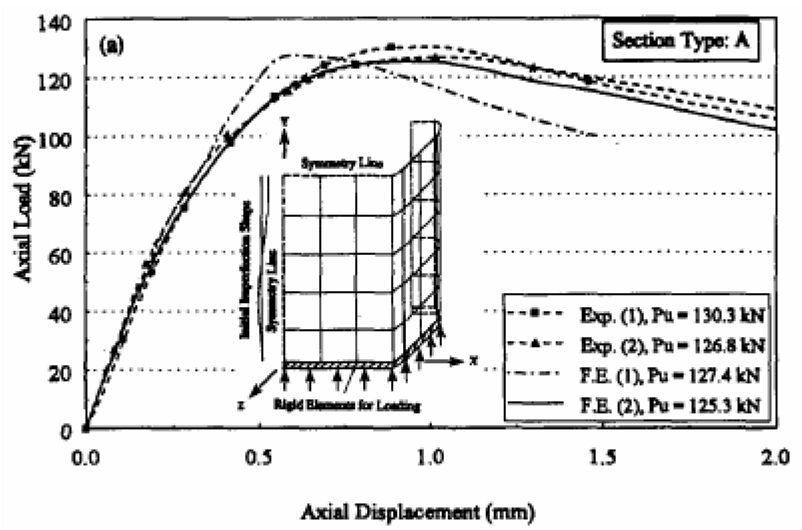

Figure 2.19 Comparison of two finite element models with the experiment [20]

However, there is a significant difference between the models after yielding. Model without the manufacturing effects is not successful in predicting the gradual yielding of the material since it resulted with 60% of the experimental axial displacement at the maximum load level. On the other hand, the model including the manufacturing effects is consistent with the experiments.

It is concluded that prediction of behaviour of cold-formed steel members necessitate correct representation of material properties and the proposed material model can successfully obtain deformation and stress distribution across a cold roll-formed section.

2.6 Relation between the Vickers Hardness Number and the Yield Stress

In order to validate the results of the numerical simulations, a trustful tool is needed. Vickers Hardness Tests can be used in that way since various authors have investigated the relationship between Vickers hardness and the yield stress of material.

In Vickers Hardness Testing, a square based pyramid shaped tool is forced onto the surface of the material (Figure 2.20). Standard forces such as 1 kg, 5 kg, 10 kg up to 120 kg can be used in the measurements depending on the test material. Vickers hardness number is defined as;

$$HV = \frac{\text{indenter force in kg}}{\text{surface area of the imprint in mm}^2} \tag{2.23}$$

The surface area of the imprint is found by measuring the diagonals by the help of a scaled microscope or an image processing software.

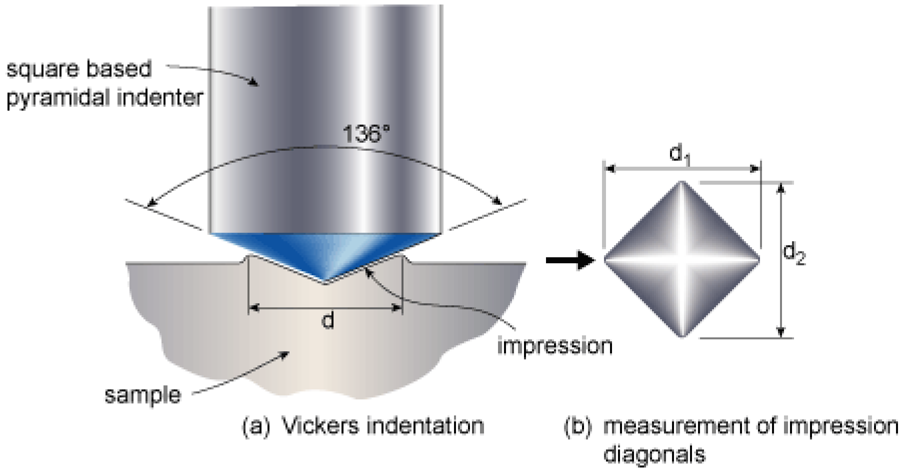

Figure 2.20 Vickers Hardness Indenter

From basic geometry it can be found that;

$$HV = \frac{2F\sin\left(136^\circ/2\right)}{d^2} \qquad (2.24)$$

where d is the arithmetic mean of the diagonals, d_1 and d_2, of the imprint.

A review of the first results regarding the relation between Vickers Hardness number and the yield stress is covered by Tabor [21]. Tabor found that constant yield stress Y is related to the Vickers Harness number in the following way;

$$HV = 2.9\ Y \text{ to } 3.0\ Y \qquad (2.25)$$

For strain hardening materials, Tabor [22] suggests a similar expression evaluated at a representative engineering plastic strain:

$$HV = 2.9\ Y \text{ (at an engineering strain of 0.08)} \qquad (2.26)$$

To analyze the effect of work-hardening material, Tabor performed upsetting tests and measured the hardness values of these specimens and correlated these values to the yield stress of the specimen, which was assumed to be constant. This approach involves errors because the hardness and hence yield stress distribution of the upsetting specimen is rather inhomogeneous due to friction.

The relationship between hardness number and yield stress related to metal forming is investigated by Ramaekers [23], Wilhelm [24], Dannenman et al. [25] and Srinivasan & Venugopal [26]. In all these studies, however, the error in correlation was around 20%.

Some modifications on Tabor's correlation have been performed by Tekkaya [27, 28] for the relationship between Vickers hardness number and the yield strength of the material. Tekkaya repeated Tabor’s experiments numerically by means of the finite element method. During virtual experiments; material behaviour is taken as elasto-plastic type. Although after cold forming it is known that materials show more or less anisotropic behaviour, isotropic hardening mode is assumed. Considering low tool velocity during indentation, it is assumed that deformation is temperature and velocity independent. No frictional effect is put on the indentation process, and common three-dimensional Vickers indentation process is replaced by a cone indentation process, so that virtual experiments have become axisymmetrical. Equivalent cone angle is selected such that the displaced volume of material for the same depth of penetration is the same for pyramidal and conical indenter.

For the analysis, mesh shown in Figure 2.21 is used and test is conducted with commercial software MSC/Marc.

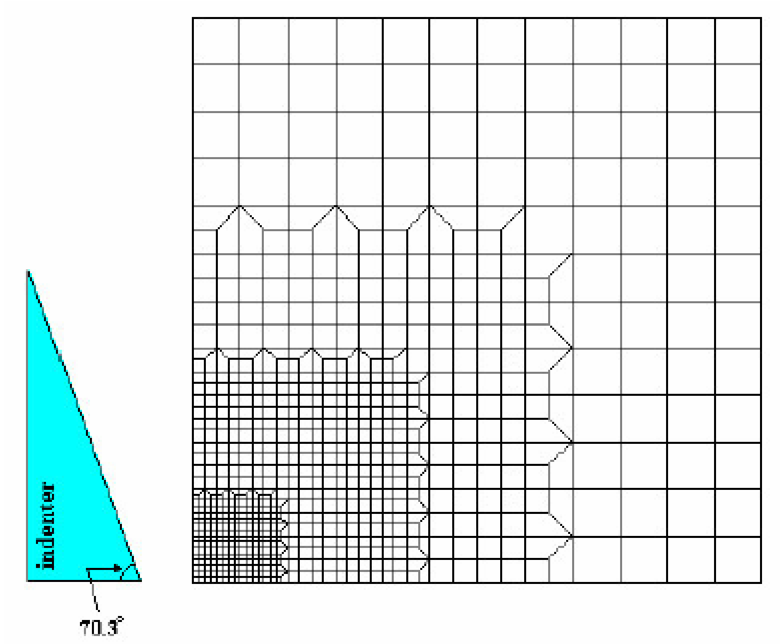

Figure 2.21 Finite element mesh and conical indenter used in Vickers Hardness simulations [27]

Computed Vickers hardness numbers for 5 different materials (CuZn40, C10, Ck15, St38, C35) with respect to prior plastic strain is unacceptably scattered. Optimizing the representative offset strain to minimize scattering in various hardness-flow stress pairs results with equivalent plastic strain: 0.112.

To find yield stress of the cold formed material, Tekkaya suggests obtaining the flow curve of the workpiece material up to high plastic strains as accurately as possible. Hardness measurements must be taken at specified location at least 10 times and average of them should be calculated. Representative flow stress in MPa at that specified location is calculated as:

$$\mathrm{Y}_{\mathrm{rep}}(at\ \varepsilon^{*}_{pl}) = 9.81 \cdot HV / 2.475 \tag{2.27}$$

From the flow curve of the material, plastic strain value is found corresponding to the representative yield stress. Actual yield stress of the material is found from the flow curve by reading the yield stress at the strain $\varepsilon^* - 0.112$ (Figure 2.22).

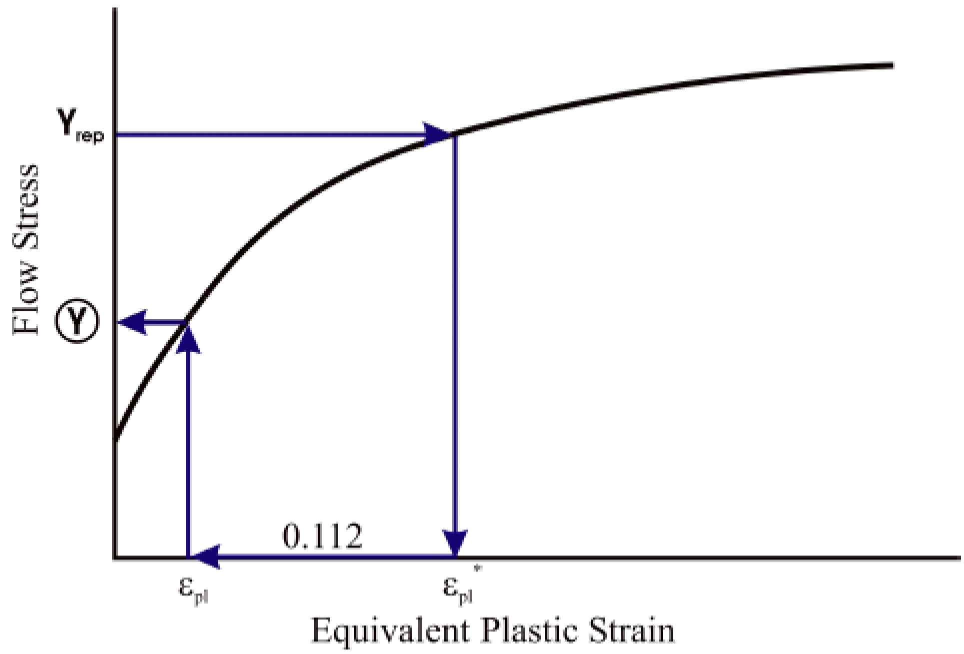

Figure 2.22 Procedure to find the actual yield stress of the material

Tekkaya and Yavuz [29] repeated a similar work with 10 different materials to obtain the hardness numbers in the strain-hardened states. The hardness values for non-hardened case have been analyzed separately, and the below relation is given

$$HV = 3.04 \cdot Y \text{ (at an offset strain of 0.03)} \tag{2.28}$$

Linear approximation analysis for the test results obtained from the strain hardened cases have been done by using different offset strains. Unlike the Tekkaya's relation, maximum regression value is obtained with the offset strain of 0.120 and the new relation is observed as following:

$$HV = 2.527 \cdot Y \text{ (At an offset strain of 0.120)} \tag{2.29}$$

To understand the effects of the strain-hardened states on the correlation, the numerical results have been divided into to two parts such as the equivalent plastic strain values lie between 0.00 and 0.50, and, greater than 0.50. Following relations are obtained:

$$
\begin{aligned}
&HV = 2.528 \cdot Y \text{ (At an offset strain of 0.130) for } 0<\varepsilon_{\mathrm{pl}} < 0.5 \\
&HV = 2.520 \cdot Y \text{ (At an offset strain of 0.230) for } \varepsilon_{\mathrm{pl}} > 0.5
\end{aligned}
\qquad (2.30)
$$

Another work has been done to analyze the influences of the strain-hardening exponent (n) in the Ludwik type representation of the flow curves by Tekkaya and Yavuz [29]. In this work, three relations were found for the given interval of n as followings:

$$
\begin{aligned}
&HV = 2.50 \cdot Y \text{ (At an offset strain of 0.018) for } 0.00<n<0.10 \\
&HV = 2.52 \cdot Y \text{ (At an offset strain of 0.016) for } 0.10<n<0.20 \qquad (2.31) \\
&HV = 2.54 \cdot Y \text{ (At an offset strain of 0.135) for } n>0.20
\end{aligned}
$$

CHAPTER 3

FINITE ELEMENT SIMULATION OF ROLL-FORMING PROCESS

3.1 Introduction

This chapter focuses on three implicit finite element models which can be used to simulate roll-forming process. The investigated models are 3D model with solid elements, 3D model with shell elements and 2D model with plane strain formulation.

Since roll-forming is an incremental process, a careful study of parameters such as contact tolerance and step size becomes more important. This is because of the fact that nodes touch the roller, move following the roller profile and separate from the roller one by one. Therefore a mischosen step size or contact tolerance may lead to development of artificial field variables due to the excessive displacement of nodes especially during the beginning or ending of contact with the roller surface. In addition, the error in field variables does not concentrate on a single region, instead it will spread all along the sheet metal because of the steady state nature of the problem. Hence, the models are studied from various aspects including the main parameters of the finite element method and the results are compared with both the experimental findings and the theory.

3.2 Experimental Procedure

The channel section considered in this study is shown in Figure 3.1. Also shown is the location of the strain gauges used in the experimental work of Bhattacharyya and Smith [30].

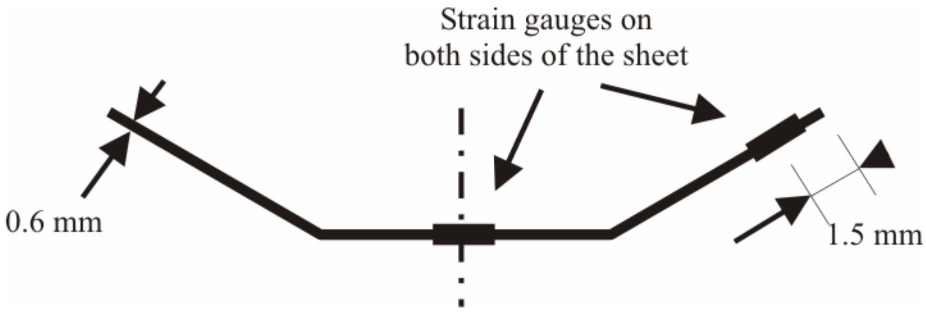

Figure 3.1 Investigated channel section and the locations of the strain gauges

Experiments were performed on an industrial roll-forming machine with stations spaced at 145 mm. All rollers have the same base diameter of 106 mm. The lower rollers are the main shaping rollers, whereas the upper rollers are flat (Figure 3.2). The formed sheet is a mild steel strip of 0.6 mm thickness, 40 mm width and 1200 mm length. The initially flat strips were formed into a symmetrical channel section having a nominal web width of 20 mm. Electrical resistance strain gauges were bonded to both upper and lower surfaces of the strip 1.5 mm away from the flange end and on the centerline of the web as shown in Figure 3.1. The strain gauges have been read continuously as a function of the longitudinal position. The resulting average longitudinal strain has been obtained by averaging the upper readings and the lower readings. The experiment has been repeated for four fold angles 20°, 30°, 40° and 50°.

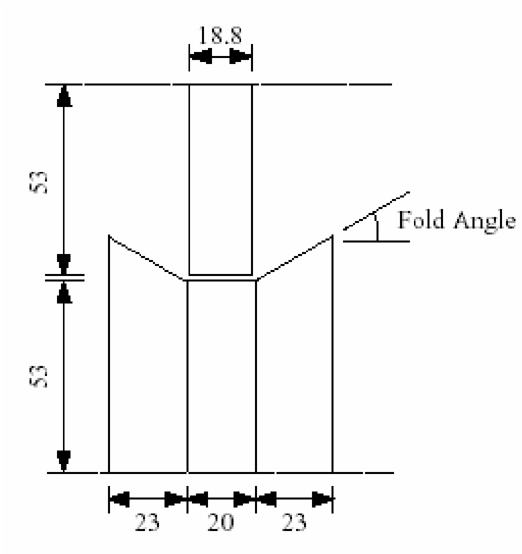

Figure 3.2 Geometry of the rollers

In the thesis work only the experiments with the 20° fold angle is used. The main reason for this choice is the simplicity of the process. As the fold angle increases the severity of forming also increases making the simulations hard to converge. However, the main aim of the study is to compare the three mentioned implicit formulations regardless of the bend angle or the roller geometry. Therefore, it is convenient to select the simplest one. The results of the average longitudinal engineering strain measurements of the 20° bended sheet can be seen in Figure 3.3.

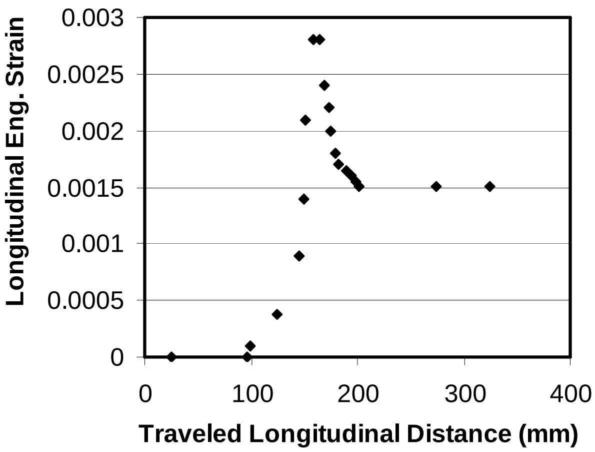

Figure 3.3 Longitudinal engineering strain measurement results for the 20° bend angle

The results are consistent with the former experimental and theoretical works. Longitudinal engineering strain in the flange remains at zero until the forming length is reached. Once the flange starts to bend, strain also increases and reaches its maximum just before the roller axis. This point corresponds to the point where the sheet gets in contact with the roller for the first time. This maximum is followed by a steep decrease and strain values remain constant but does not return back to zero, indicating plastification of the material. The theoretical background of this behavior is explained in Section 2.2 of Chapter 2.

3.3 3D Finite Element Model of Roll-Forming

Nearly the same model is used in the 3D simulations with solid and shell elements. The only difference is the boundary conditions used in the computations. Therefore, majority of the explained model is valid for both of the 3D element types. The difference is considered in the Boundary Conditions Section.

3.3.1 Geometry of the Model

Two roll-sets are used in the model. Roll-set zero in Figure 3.4 consists of the feeding rollers. These rollers have a flat profile and their main duty is to prevent the end of the sheet to oscillate in the vertical direction at the beginning of the simulation. Therefore, these rollers have no prescribed vertical or rotational speed. Roll-set one consists of the main forming rolls. As in the experiments, the lower roller is the shaping roller and the upper roller has a flat profile. Since the sheet is symmetric, only half of the sheet in width is modeled. In the experiments 1200 mm long sheet has been used. However, during computations it is seen that 300 mm length of sheet is enough to obtain steady properties developing in the sheet. Therefore, sheet dimensions used in the computations are 0.6 mm thickness, 20 mm width (symmetry) and 300 mm length.

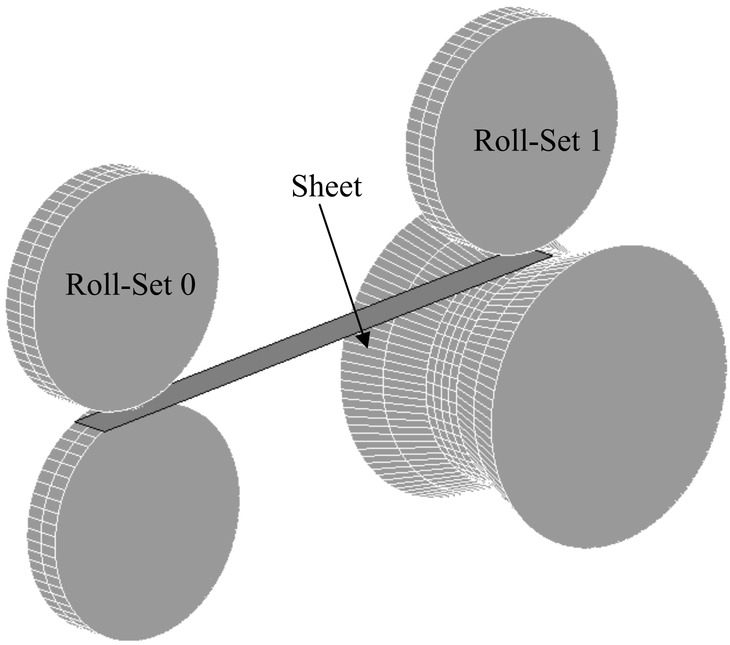

Figure 3.4 Geometry of the model

3.3.2 Forming Operation

At the beginning of the process the lower roller is located a distance below the sheet. Therefore, at the beginning the lower roller is not in contact with the sheet. However, the upper roller contacts the sheet on its base diameter. At this point the leading edge of the sheet is on the plane defined by the two axes of the rollers as in Figure 3.5-a. The forming operation is modeled in two steps. First, the lower shaping roller moves vertically up to grab the sheet between the rollers (Figure 3.5-b). At the end of this step, the distance between the base surfaces of the rollers is equal to the sheet thickness. Next, both rollers start to rotate about their axes with the same rotational speed but in reverse directions. By this way, the sheet is pulled throughout the roll-set with the help of friction (Figure 3.5-c).

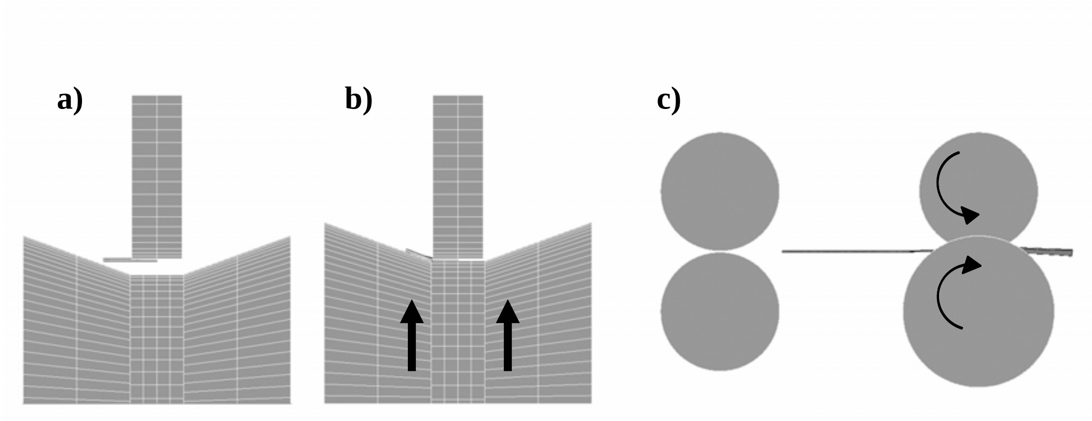

Figure 3.5 Forming sequence in computations

3.3.3 Boundary Conditions

Constant shear friction factor of 0.2 is assumed throughout the simulations. This value is recommended in reference [31] in order to simulate cold roll-forming.

Solid elements have only translational degree of freedom at their nodes. For the symmetry to be valid in simulations using solid elements, the displacements of nodes normal to the symmetry plane are fixed to zero. Shell elements have additional rotational degree of freedom at their nodes. Therefore, in simulations using shell elements the rotations on that plane are also fixed to zero.

The nodes lying at the end of the sheet are fixed in vertical direction in order to prevent the end of the sheet to move in vertical direction. This adds additional stiffness to the sheet and simplifies the computations in terms of convergence. However, this necessitates the end of the sheet not to enter the deformation zone. Otherwise, the nature of the deformation changes and additional strain occurs in the sheet due to the vertically fixed end of the sheet. There is no boundary condition on the sheet along the longitudinal direction. The boundary conditions are summarized in Figure 3.6.

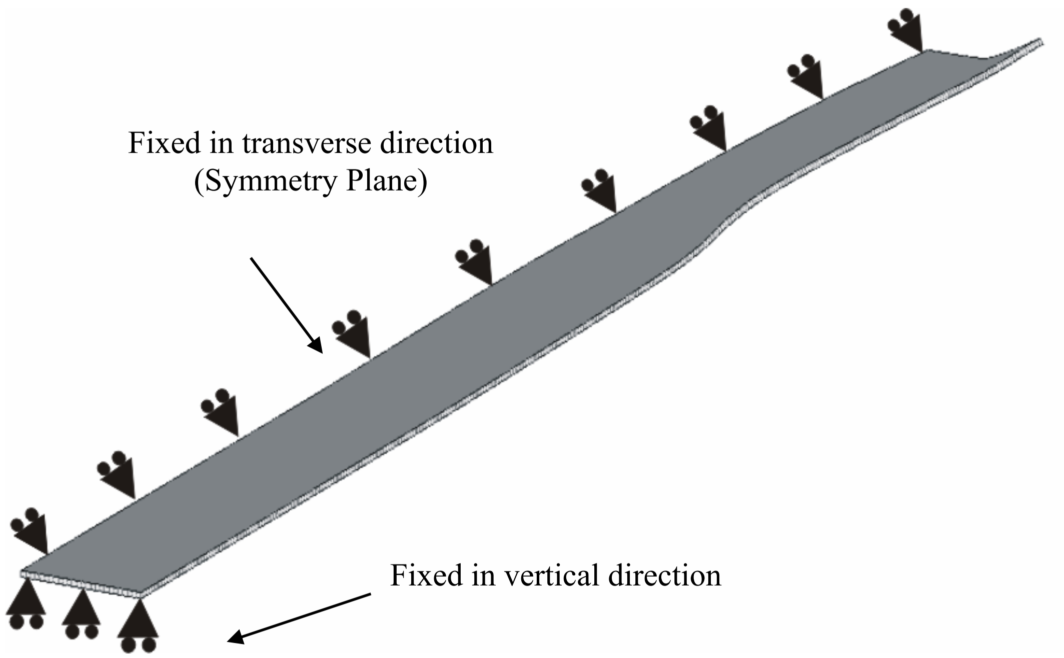

Figure 3.6 Boundary Conditions

3.3.4 Material Properties

In Bhattacharyya and Smith's [30] experiments a strip of mild steel has been used. As a typical representation of the properties of this material, data for SAE 1020 steel has been utilized in the simulations. Elastic-plastic material model is used in the simulations. The flow curve for this material obtained from the data supplied in Reference [31] is shown in Figure 3.7. Piecewise linear flow curve is defined in the simulations by the help of that flow curve. The Elastic Modulus of the material is given as 207 GPa and the Poisson's Ratio is assumed as 0.3.

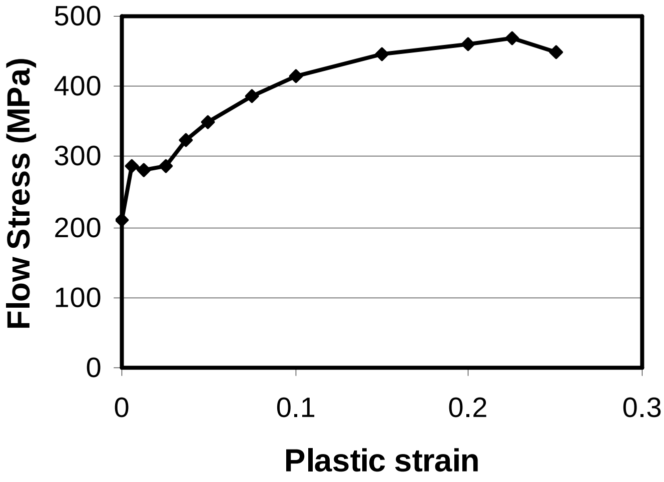

Figure 3.7 Flow Curve of SAE 1020 steel

3.4 Method Followed In Interpreting the Results of the 3D Simulations

In comparison of the results, three major measures have been taken into account. The first one is the longitudinal engineering strain. In the experimental work, strain gauges are mounted on the sheet 1.5 mm away from the flange end and the average of the two gauges is supplied with respect to the longitudinal traveled distance. In computations with solid elements, the average longitudinal engineering strain values are calculated from the displacements of the upper and lower surface nodes that are 1.5 mm away from the flange end. In the analyses with shell elements, the top and bottom layers of the node that lies in the mentioned location are used. Again, these values are plotted with respect to the longitudinal displacement of the nodes.

The second measure used in interpreting the results is the equivalent plastic strain on the upper surface of the sheet, measured in transverse direction from web center to flange end. This data is only calculated at the end of the process. Therefore, it does not give any clue about the development of strain through the process but reveals the hardening on the surface of the sheet at the end of the process.

The last measure is the equivalent plastic strain through the thickness in the bended region at the end of the process. In solid elements, the number of calculated strain values through the thickness depends on the number of elements used across the thickness and this number is generally limited because of increased computation durations. However, shell elements output strain values at all layers enabling a better capture of strain distribution through the thickness. Therefore, these equivalent plastic strain vs. thickness plots are mainly used in the simulations with shell elements.

As mentioned before roll-forming can be thought as an incremental process. Whole process is governed by repeatedly touching and separation of nodes. This mechanism can be seen in Figure 3.8. A node approaching the roller surface starts to contact the surface according to the contact tolerance assumed in computations. Then this node follows the roller profile staying in contact. Finally, the contact ends according to the contact tolerance again. This deformation pattern applies to all nodes in a row one by one.

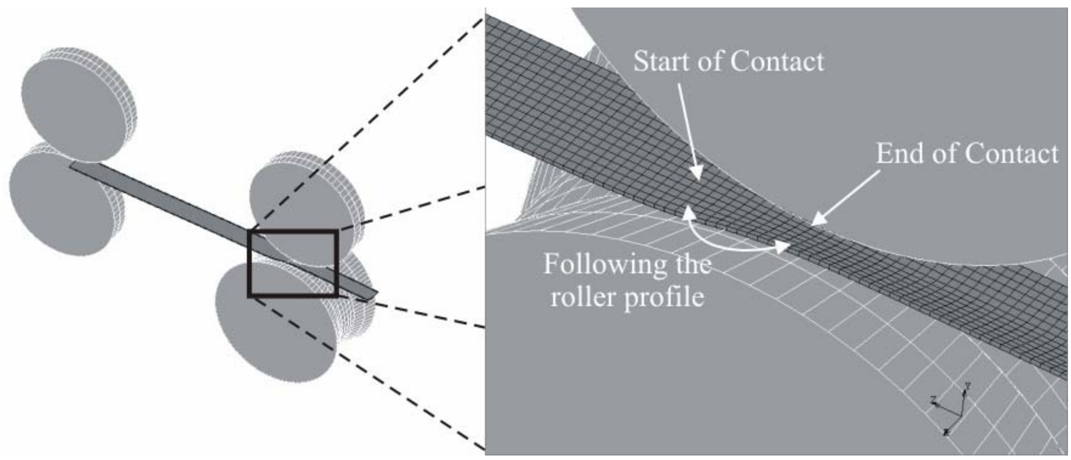

Figure 3.8 Deformation behavior of the nodes

That kind of behavior of the nodes affects the results of the 3D simulations. When the longitudinal engineering strain curves of consecutive nodes are analyzed, an oscillation of the results is observed as in Figure 3.9-a. The difference between the maximum and minimum values is 30% of the minimum value. However, this oscillation mainly depends on the mesh density. As the mesh is refined, the oscillations reduce and the difference between the maximum and minimum observed values come out to be 5% of the minimum value (Figure 3.9-b). This oscillation can be said to be negligible.

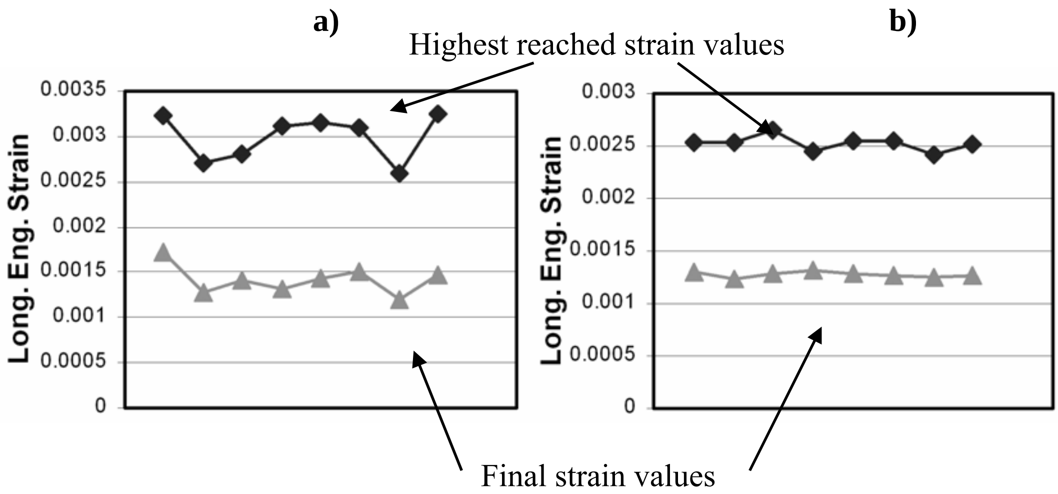

Figure 3.9 Oscillations in results a) with coarse mesh b) with fine mesh

Hence, in interpreting the results of 3D simulations with large oscillations, average of the values obtained from consecutive nodes are used. However, in simulations with smoother results the values obtained from a node are used directly without any averaging.

Another oscillation phenomenon in the results is observed in particular regions of longitudinal engineering strain curves. Figure 3.10 shows a characteristic longitudinal eng. strain vs. longitudinal traveled distance curve. The marked regions of the curve show sudden rises and drops in strain values. The different oscillation patterns observed in these regions are within an engineering strain band of 0.0005. For two neighbor nodes with a distance of 1.5 mm in between, which is the largest distance used in the study, this strain value is reached when the elongation is 7.5×10^{-4} mm. Therefore, these oscillations can be disregarded since such a small value of elongation or contraction can occur even because of numerical issues.

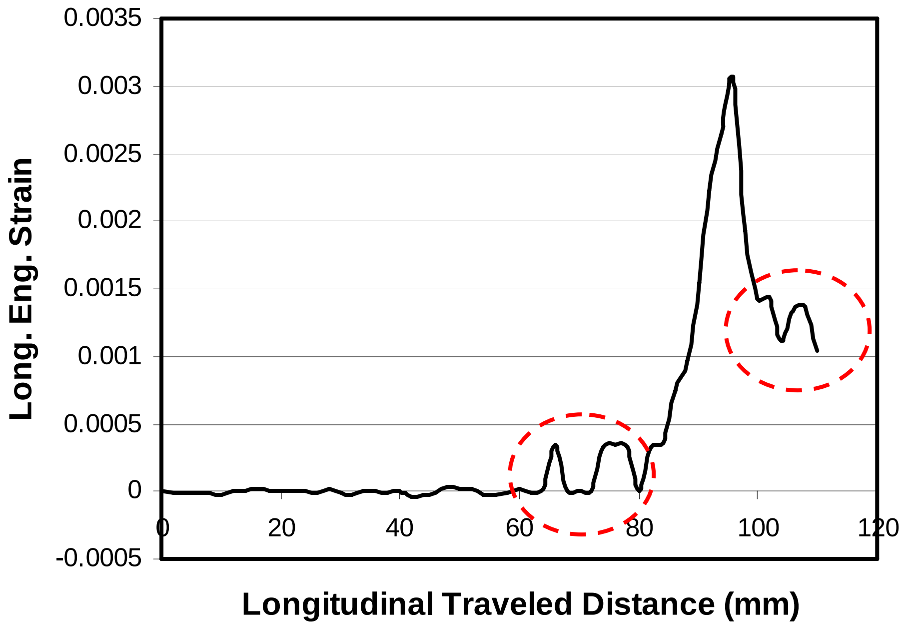

Figure 3.10 A sample longitudinal engineering strain curve

3.5 Simulation of Roll-Forming with 3D Solid Elements

Three dimensional, isoparametric, arbitrary hexahedral shaped elements with eight nodes are utilized in this section. Important parameters of the finite element method are investigated. The details of this study can be found in Appendix A. For completeness, the results of the parametric study are tabulated in Table 3.1. Having decided on the values of the parameters, mesh densities are varied and a suitable mesh density for the simulation of roll-forming is selected regarding the computation durations and convergence of the results. The use of assumed strain formulation is also discussed in Appendix A.

Table 3.1 Results of the parametric study

Relative force and displacement convergence tolerance	0.1
Contact Tolerance	8% of the thickness
Step Size	1.2 mm/step
Solver	Direct sparse

3.5.1 Investigated Mesh Densities

Four mesh densities are investigated for the simulation of roll-forming with solid elements. The first three mesh densities are uniform meaning that all the elements have the same dimensions. In the last mesh, small elements are concentrated in the bend region, where as larger elements are used in the flange. These mesh densities are tabulated in Table 3.2 together with the relative computation durations with respect to the fastest simulation.

Table 3.2 Four investigated mesh densities and relative computation durations

		Dimensions (mm)			Number of Elements	Relative Durations	Figure
		Thickness	**Length**	**Width**			
CASE 1		0.6	1.5	1.5	2600	1	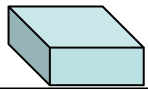
CASE 2		0.6	0.75	0.75	5200	3	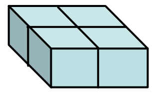
CASE 3		0.3	0.75	0.375	10400	7	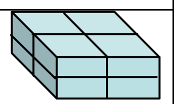
CASE 4	**MIN**	0.15	0.5	0.15	41600	202	-
	MAX	0.6	0.5	0.6			-

When Figure 3.11 is analyzed, the method followed in mesh refinement can be better understood. In Case 1 and Case 2, there is only one element through the thickness. The refinement for Case 2 is performed by dividing the elements into four elements in longitudinal and transverse directions. In Case 3, the elements in Case 2 are divided into two in thickness direction. Therefore, there are two elements in thickness in Case 3. Lastly in Case 4, the mesh is non-uniform. Four elements through the thickness are utilized in the bend region, two elements are used in the regions adjacent to the bend region and only one element is used at the end of the flange.

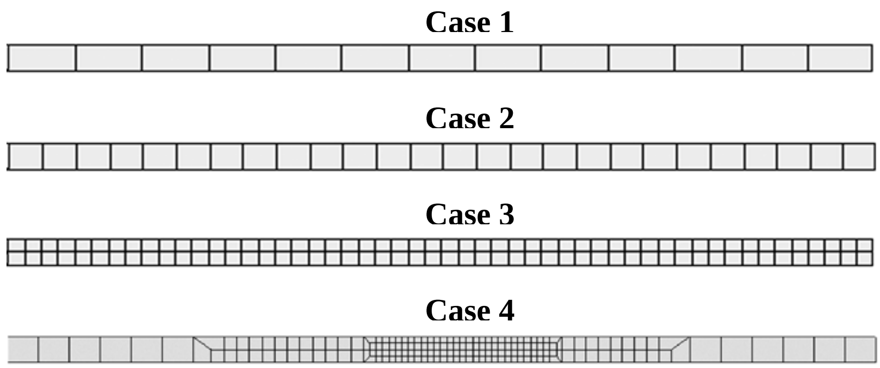

Figure 3.11 Cross-sections of the sheet with different mesh densities

3.5.2 Results of the Simulations with Four Mesh Densities

The longitudinal engineering strain development in four mesh densities can be seen in Figure 3.12. It is seen that the coarsest mesh gives the highest strain. As the mesh is refined, the maximum reached strain value decreases and converges to a value. This is because of the fact that, in coarse mesh nodes have to move a larger distance on the roller surface compared to the finer meshes. In other words, a large displacement of a node in coarse mesh is represented by smoother and shorter displacements of several nodes in fine mesh. That is why the maximum reached longitudinal engineering strain values drop as the mesh is refined. In Case 3 the solution can be said to converge since the difference between the maximum reached strain values of Case 3 and Case 4 is less than 5%. The strain values at the end of the process are nearly the same in all mesh densities. This means that the level of plastification is the same in all simulations. This can also be seen in Figure 3.13.

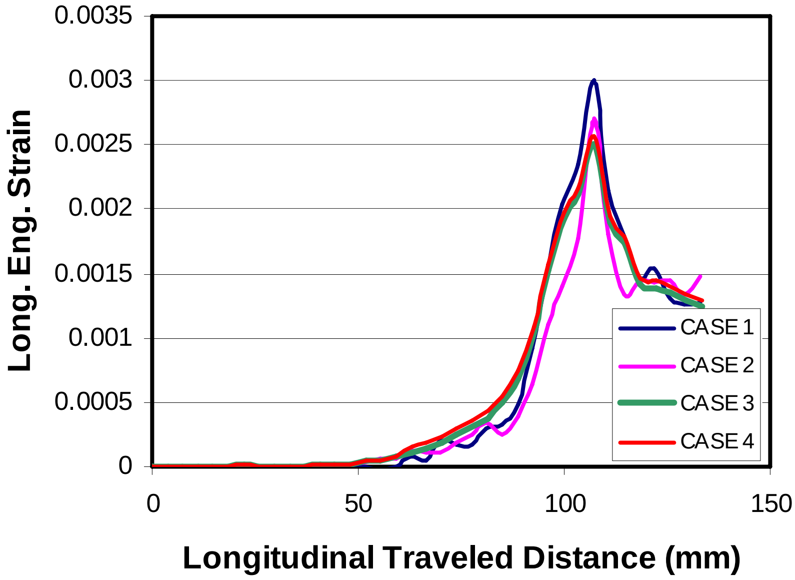

Figure 3.12 Longitudinal strain development with four mesh densities

When the equivalent plastic strain on the sheet surface in Figure 3.13 is analyzed with the four mesh densities, it is seen that the values are not highly affected by the mesh refinements. The main difference is that the results with the coarse mesh densities can not represent the hardening distribution in detail. However, the fine meshes give the results in a finer detail. This is mainly seen in the bend region of the sheet. Since there is a high variation of strain along the bend region, the coarse meshes are not able to represent this change. Again, it is seen that as the mesh is refined the solution converges.

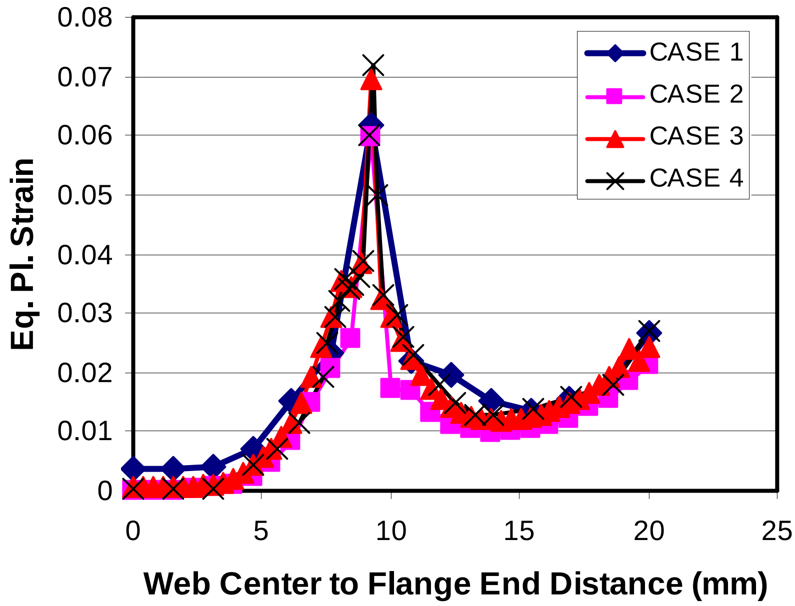

Figure 3.13 Strain hardening on the sheet surface along the transverse direction

When the computation durations are investigated together with the convergence of the results Case 3 is selected to be the suitable mesh density for the simulation of roll-forming.

3.6 Simulation of Roll-Forming with 3D Shell Elements

Four node thick shell elements with global displacements and rotations as degrees of freedom are employed in this analysis. Shell elements are preferred when one dimension of the modeled geometry is small compared to the other two dimensions. In this case, the thickness of the sheet is small compared to the length and width of the sheet. Shell elements solve the field variables in thickness direction in their layers.

Parametric study of important parameters of the finite element method is performed and the details can be found in Appendix B. The results of the parametric study are tabulated in Table 3.3.

Table 3.3 Results of the parametric study with shell elements

Number of Layers	7
Relative force and displacement convergence tolerance	0.1
Contact Tolerance	8% of the thickness
Step Size	1.2 mm/step
Solver	Direct sparse

The same method followed in simulations with solid elements is applied to the simulations with shell elements. Different mesh densities are investigated and an appropriate mesh density is selected regarding the computation durations and convergence of the results.

3.6.1 Investigated Mesh Densities

Three mesh densities are examined for the shell elements case. The details of the meshes can be seen in Table 3.4 together with the relative computation durations. All three meshes are uniform, that is all the elements in a mesh have the same dimensions.

Table 3.4 Examined mesh densities and relative computation durations

	Dimensions (mm)			Number of Elements	Relative Computation Durations	Figure
	Thickness	Length	Width			
CASE 1	0.6	1.5	1.5	2600	1	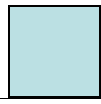
CASE 2	0.6	0.75	0.75	10400	12	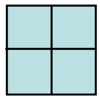
CASE 3	0.6	0.75	0.375	20800	62	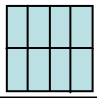

The elements in Case 2 are created by dividing the elements in Case 1 into four in longitudinal and transverse direction. Case 3 is generated by dividing the elements in Case 2 in to two in the transverse direction. As tabulated in Table 3.3, 7 layers are used in all cases and the thickness of the elements is equal to the thickness of the sheet which is 0.6 mm.

3.6.2 Results of the Simulations with Three Mesh Densities

The longitudinal engineering strain history of the process can be seen in Figure 3.14. It is seen that as the mesh is refined both the maximum reached strain values and the final strain values converge. The difference between the maximum reached strain values of Case 2 and Case 3 is less than 3% of the value in Case 3.

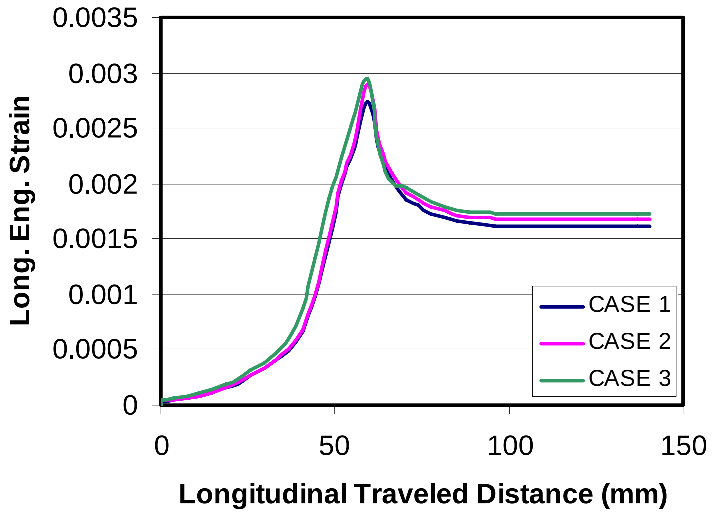

Figure 3.14 Long. eng. strain development in simulations with shell elements

Final strain hardening on the sheet surface is presented in Figure 3.15. The convergence in Case 2 is more significant in this case. The mesh density of Case 1 is incapable of computing the equivalent plastic strain distribution in the required resolution especially in the bend region. Therefore, Case 2 is selected to be the appropriate mesh density that can be used in the simulations of roll-forming with shell elements.

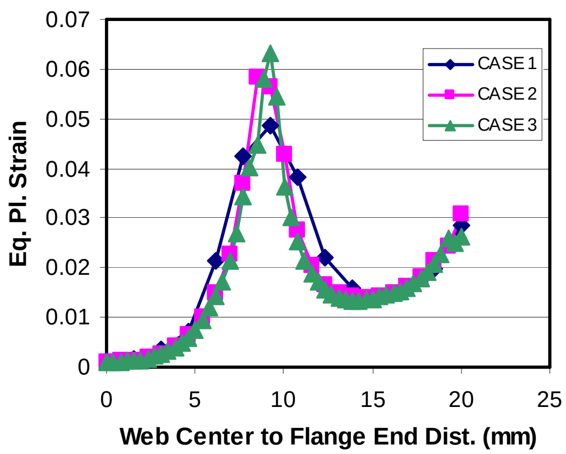

Figure 3.15 Equivalent Plastic Strain distribution on the sheet surface

3.7 Comparison and Verification of the 3D Simulation Results

The selected mesh densities for the 3D simulation of roll-forming are Case 3 for the solid elements and Case 2 for the shell elements. The longitudinal engineering strain development for these cases and the experimental result are plotted in Figure 3.16.

The results show that both element types follow a similar strain curve at the beginning. However, after a point the results start to differ and simulation with solid elements gives a lower maximum strain value. The results of the simulation using shell elements are in agreement with the experiments. The strain values at the end of the process that are obtained from both of the simulations differ from the experiment.

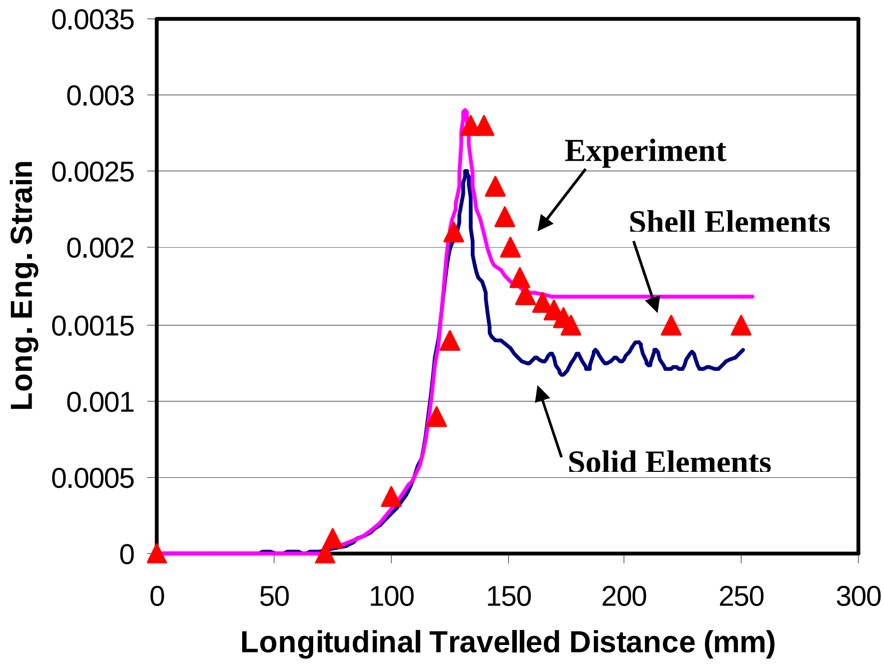

Figure 3.16 Long. eng. strain development in simulations and experiment

The numerical representation of the simulation results and the experiment results are tabulated in Table 3.5. Since the simulation using shell elements give better results both in the maximum reached value and the final reached strain, shell elements are selected to be convenient for the simulation of roll-forming processes.

Table 3.5 Numerical representation of the longitudinal engineering strain plots

	Experiment	**3D Solid Elements**	**3D Shell Elements**
Peak strain	0.0028	0.0025 11% error	0.0029 4% error
Final strain	0.0015	0.00125 17% error	0.0016 7% error

The deformation of the sheet can be plotted by the angle change of the flange end with respect to the longitudinal distance. This curve is called the bend angle curve. The length of deformation which is the total length that sheet deforms can be easily calculated from this plot. There is a theoretically derived formula for finding both the deformation length and the bend angle curve for a given sheet and roller geometry. These are given as the equations 2.11 and 2.14 in Chapter 2. According to these formulas the bend angle curve for the investigated sheet and the deformation length are calculated and compared with the simulation results using shell elements in Figure 3.17.

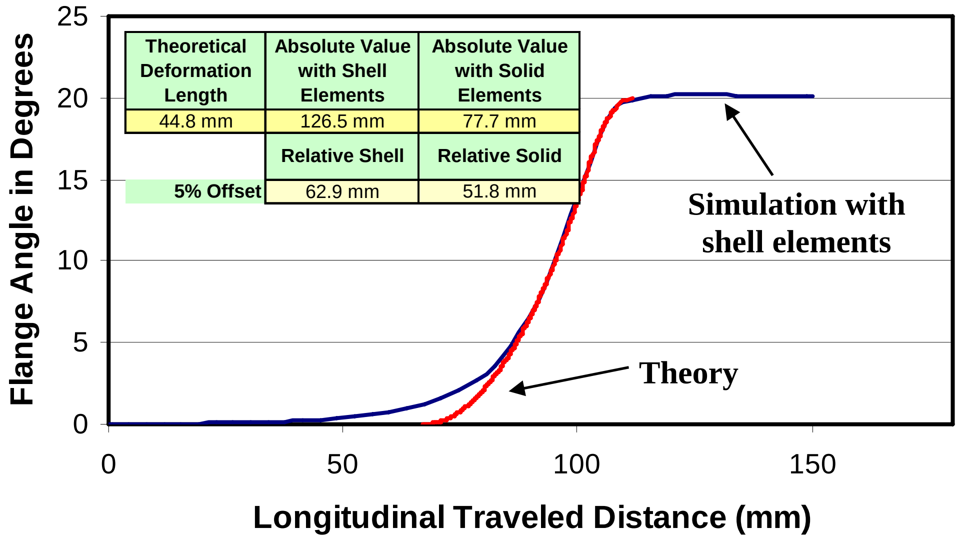

Figure 3.17 Theoretical and numerically found bend angle curve and the deformation length of the sheet

In the calculation of the numerical deformation length, the deformation is assumed to start when the angle change of the flange end equals 5% of the total angle change which is 20°. From the Figure 3.17 it is observed that the theoretical deformation length is shorter than the numerically found one. However, the theory predicts the mid and final part of the curve with a good agreement with the simulation result. The theoretical longitudinal strain is found by the equation 2.15 in Chapter 2. This equation involves the differentiation of the bend angle curve with respect to the longitudinal coordinate and multiplication of the result with the already known quantities. Therefore, once the bend angle curve is obtained the longitudinal engineering strain curve is also obtained. The theoretical and numerical longitudinal engineering strain curves are plotted in Figure 3.18 together with the experimental results.

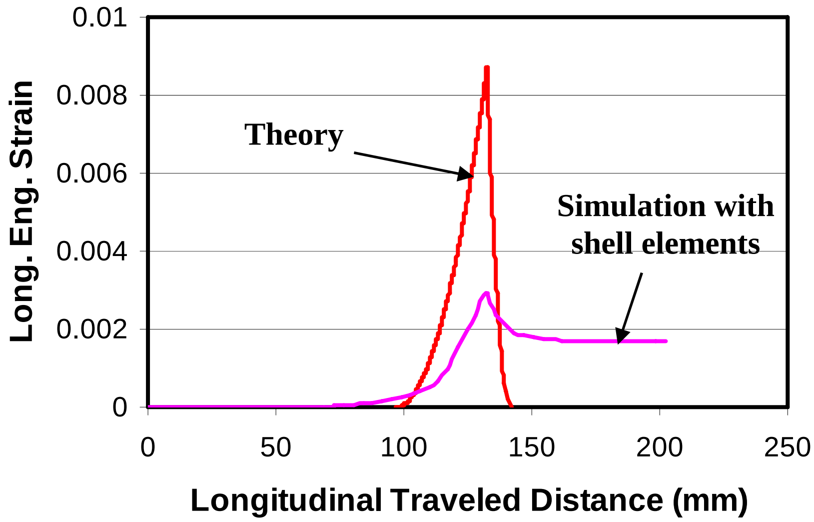

Figure 3.18 Theoretical, experimental and numerically found longitudinal engineering strain curves

The difference in the values is immediately seen. The theory overestimates the strain especially around the location of the roller axes. Theory predicts the maximum reached strain as three times the experimental result. Moreover, theory predicts that the longitudinal engineering strain will drop back to zero after the sheet passes the roller. However, this is not the case. There is plastification occurring in the flange related to the longitudinal strain. Theory is not capable of predicting this plastification. Therefore, theoretical relations can be used to obtain the bend angle diagrams or the deformation length to some extent. However, it is for sure that longitudinal engineering strain prediction of the theory is useless. The main reason behind this fact is the assumptions lying under the theory and these are discussed in Chapter 4.

3.8 Plane Strain Simulation of Roll-Forming and Comparison with the 3D Simulations

Roll-forming process of the investigated sheet is simulated under plane strain assumption. In fact, during roll-forming, sheet takes a complex 3D shape and both the stress and strain state is three dimensional. However, plane strain formulation assumes that there is no strain in one of the dimensions. Therefore, the problem is solved in two dimensions. In this study, the applicability of the plane strain assumption to the roll-forming process on separate regions of the sheet such as web, bend region or flange will be investigated.

3.8.1 Plane Strain Model

In the plane strain model four node, isoparametric, arbitrary quadrilateral elements are utilized. Bending of the sheet is modeled by a rotating rigid die around a fixed axis as seen in Figure 3.19. Web of the sheet is fixed between two rigid dies. Because of symmetry only one half of the sheet is modeled. Therefore used sheet dimensions are 0.6 mm in thickness and 20 mm in width. The same material model in the 3D simulations is used for the plane strain simulations. The nodes in the symmetry plane are fixed in the transverse direction in order symmetry to be valid. In the 3D simulations friction is needed to pull the sheet throughout the rollers. However, in plane strain simulations there is no such a need. Therefore, friction is assumed to be zero.

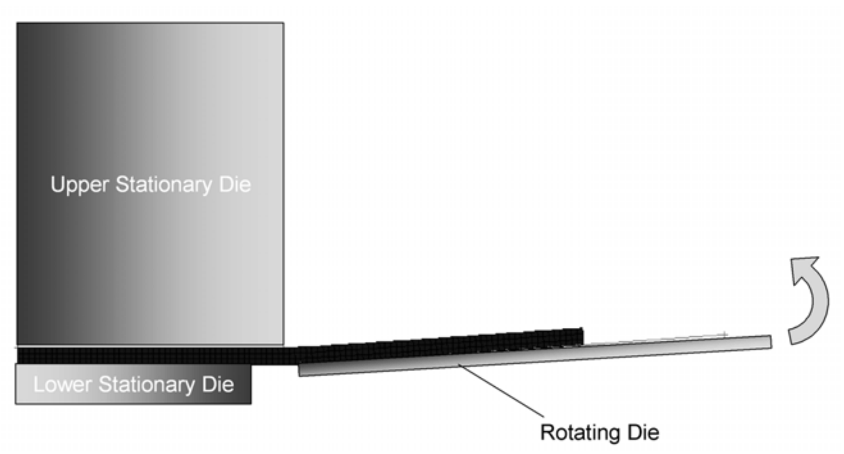

Figure 3.19 Plane strain model of the roll-forming process

3.8.2 Examined Mesh Densities

Four different cases of mesh densities have been examined in plane strain simulations. The details of the mesh densities can be seen in Table 3.6. The computation durations in plane strain simulations are relatively shorter than the 3D simulations. Therefore, it is possible to use more elements across the thickness. In addition, since the durations are short, uniform meshes are used in the analyses. There is no need to use concentrated mesh in the bend region and coarse mesh in the flange in order to lower the total number of elements.

Table 3.6 Details of the examined mesh densities

	Dimensions (mm)		Number of Elements	Number of Elements Through the Thickness	Relative Computation Durations
	Length	Width			
CASE 1	0.2	0.2	300	3	1
CASE 2	0.1	0.1	1200	6	4
CASE 3	0.05	0.05	4800	12	17
CASE 4	0.025	0.025	19200	24	84

The equivalent plastic strain distribution of the four cases through the thickness can be seen in Figure 3.20. The values are calculated at the bend region. Except the Case 1 the results are quite similar. In Case 1 there are three elements through the thickness. That is way the strain distribution is captured with a low detail especially in the mid-surface of the sheet. The results can be said to converge starting from the Case 3. The maximum difference between the Case 3 and Case 4 is observed at the upper surface of the sheet which is 5% of the Case 4. Therefore, Case 3 is selected to be the appropriate mesh density for the plane strain simulation of the roll-forming process.

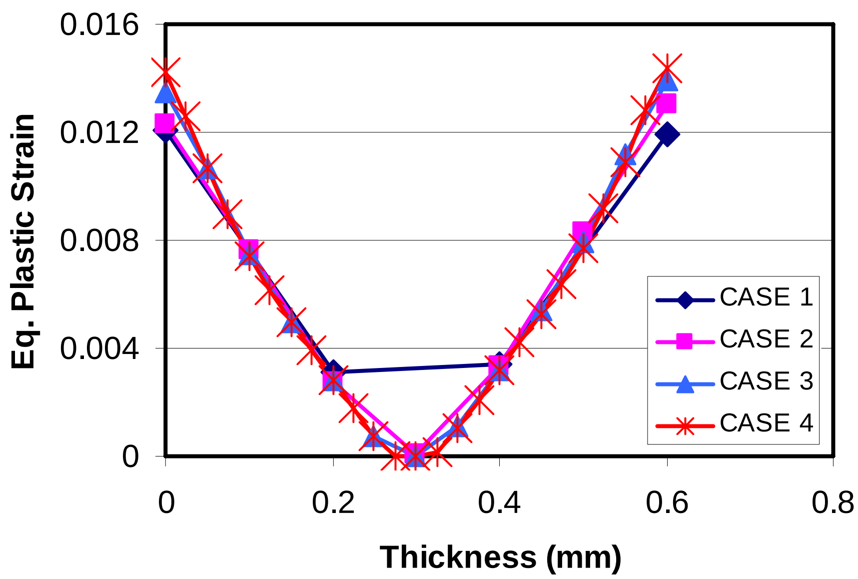

Figure 3.20 Equivalent plastic strain distribution through the thickness

3.8.3 Comparison of the Plane Strain Results with the 3D Simulation Results

In order to better understand the deformation behavior in roll-forming the strain development and final equivalent plastic strain in different regions of the sheet are investigated. As 3D simulation results, the results of the simulation with shell elements is used which is the Case 2 of the simulations with shell elements. The points that the strains are calculated can be seen in Figure 3.21. There is one point in the web area named P_w, two points in the bend region named B_1 and B_2, and one point in the flange named as P_F.

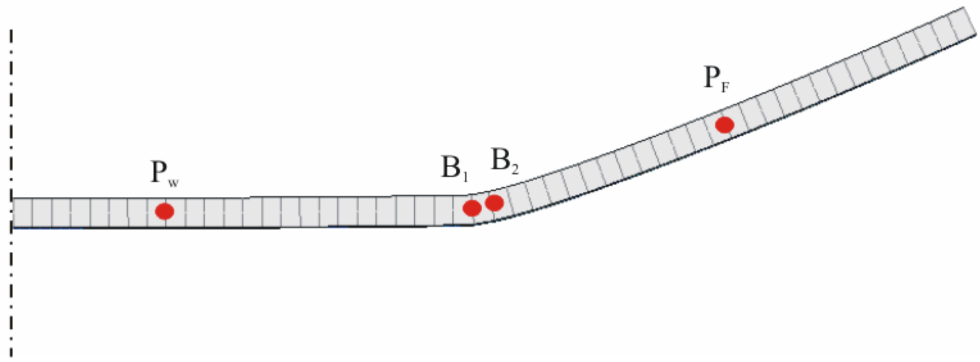

Figure 3.21 Locations of the strain calculations

Figure 3.22 shows the final equivalent plastic strain values through the thickness of the sheet at the mentioned locations. At the point P_w, plane strain simulations predict no strain hardening through the thickness. However, 3D simulation results show that there is plastic strain development in the web area with a maximum value of 0.0026. At point B_1, the plane strain results start to be in agreement with the 3D results and at point B_2 the results almost overlap with an error in the mid plane. At point P_F, again the plane strain simulation outputs zero plastic strain through the thickness, where as the 3D simulation predicts some strain hardening in the flange.

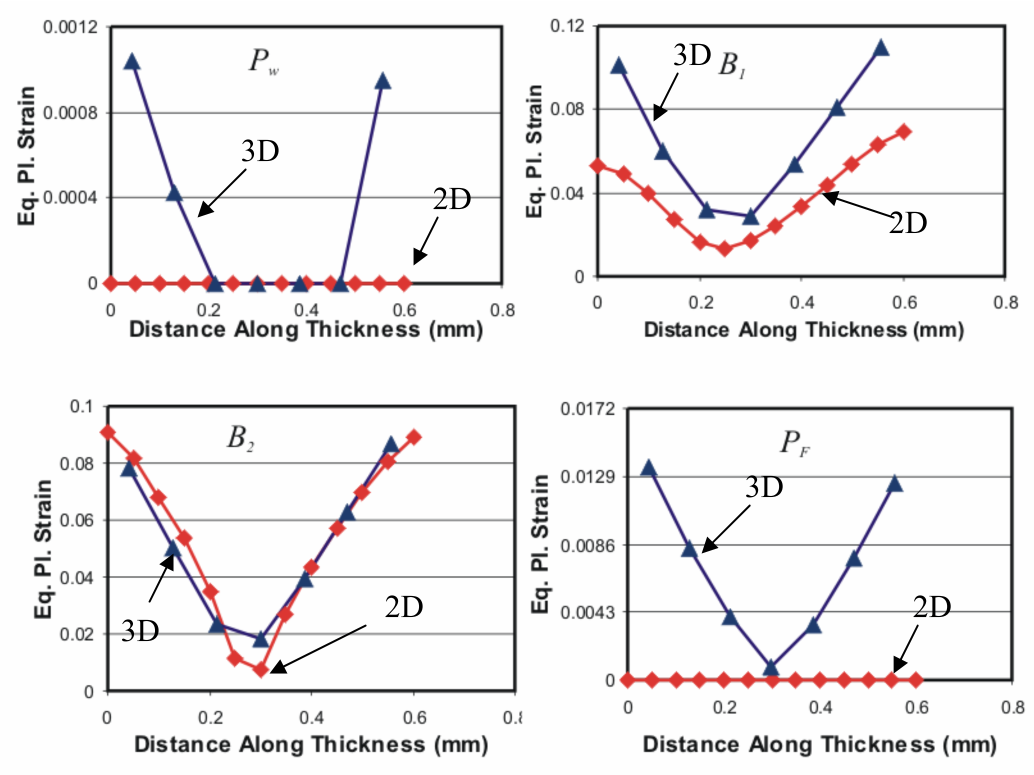

Figure 3.22 Equivalent plastic strain through the thickness at selected locations

Figure 3.22 reveals the fact that plane strain simulations can predict the strain hardening in the bend regions with a good agreement with the 3D simulations. Other than the bend region, plane strain simulations predict zero strain since there is no deformation in these regions. Web area remains undeformed between the two rigid dies and flange region only undergoes a rigid body rotation around the corner. In plane strain simulations, the only deforming part is the bend region.

To explain this result, the plastic strain tensor histories of the points B_2 and P_F in the 3D simulation are plotted. The directions of tensor components are presented in Figure 3.23. In 3D simulations, direction "1" is the transverse direction, "2" is the longitudinal direction and "3" is the thickness direction. Since there is no longitudinal strain in plane strain simulations only directions "1" and "3" can be seen.

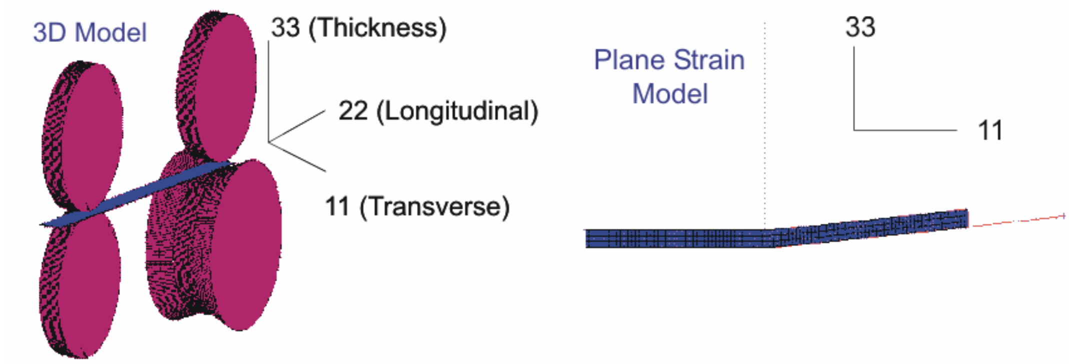

Figure 3.23 Directions of the tensorial notation

In studying the plastic strain components the values and the signs of the components is not important. The aim of the study is to reveal the dominant strain components. Therefore, some rules are followed in plotting the strain histories. These are:

- Absolute values of the plastic strain components are plotted.
- Only the components that exceed the 10% of the highest reached strain value are plotted.
- The strain components are normalized according to the highest reached strain value. Therefore, all strain components are plotted between zero and one, where zero means zero strain and one means the highest value reached by any of the components.

In Figure 3.24, plastic strain histories of the point P_F calculated at the upper, mid and lower layers of the 3D simulation can be seen. The dominant strain components in all of the layers are "22", "12" and "11". As mentioned before direction "2" is the longitudinal direction and it is not taken into account in the plane strain formulation. Therefore, the reason why the plane strain simulation can not predict strain in the flange is revealed: there is a considerable deformation in the flange along the longitudinal direction which can not be calculated under the plane strain assumption.

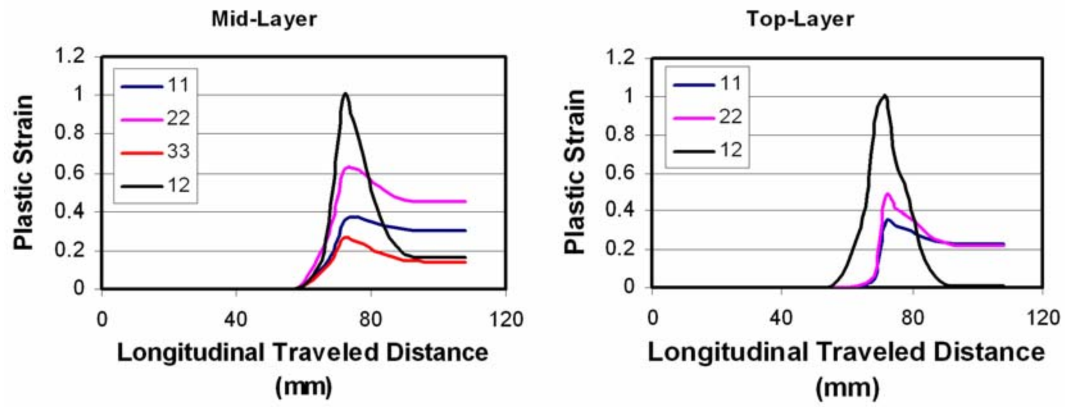

Figure 3.24 Plastic strain tensor component histories in 3D simulation with shell elements at point P_F

Figure 3.25 presents the histories of strain components of point B_2. At this point, the equivalent plastic strain values obtained by the 3D simulation and plane strain simulation have been shown to overlap in Figure 3.22. The reason for this overlap can be explained by the fact that the dominant strain components are "11" and "33" in all layers and these are the directions that strain values can be calculated in plane strain simulations. In other words, since the deformation in the bend region is not mainly governed by the longitudinal deformations, plane strain simulation is successful in predicting the strain in these regions.

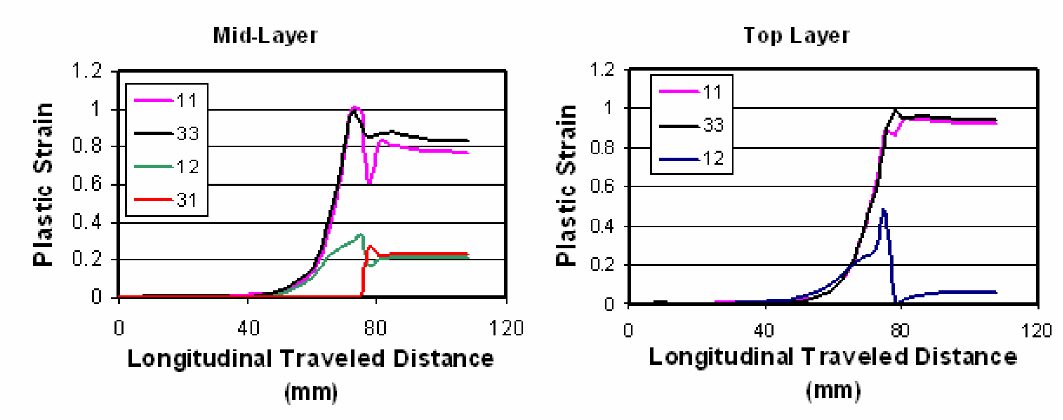

Figure 3.25 Plastic strain tensor components histories in 3D simulation with shell elements at point B_2

3.9 Outcomes of the Chapter 3

To summarize the chapter, conclusions derived from the study of the simulation of roll-forming process are listed below.

- Proper values for the parameters of the finite element method that are important in roll-forming analysis are found for 3D simulations using either solid or shell elements.
- 3D simulation of roll-forming process with solid and shell element are examined including the effect of the mesh densities and it is concluded that shell elements are more suitable in terms of experimentally verified results and computation durations.
- The theoretical longitudinal strain and bend angle curves are compared with the experimental and numerical results. It is concluded that the bend angle curves can be predicted by the theory to some extent. However, the longitudinal engineering strain prediction of the theory is found to be weak.
- Plane strain simulation of the roll-forming process is proposed and the weak and strong sides of application of plane strain formulation to the

simulation of roll-forming process are discussed. It is concluded that plane strain simulations can predict the plastic strain in the bend region with a good agreement with the 3D simulation results. However, the plastic strain development in the web and flange regions of the sheet can not be computed with plane strain simulations because of the longitudinal effects.

CHAPTER 4

FEATURES OF DEFORMATIONS OBSERVED IN ROLL-FORMING

4.1 Introduction

During roll-forming sheet takes a complex 3D shape resulting in a 3D strain state. The deformation is mainly influenced by the geometric parameters of the sheet and the rollers. This section identifies the main parameters of roll-forming and studies the effects of each parameter. In order to clarify the effects of the parameters, the deformation behaviour in different parts of the sheet is investigated and dominant straining mechanisms are revealed for each distinct part. The deformation occurring under the examined parameters are compared with the theoretical knowledge and the main assumptions lying behind the theory are discussed. Finally, convenient set of parameters, which enables application of the proposed plane strain simulation of the roll-forming process, are presented.

4.2 Study of the Geometric Parameters of Roll-Forming

Roll-forming is governed under the effects of several parameters. These are;

- Thickness of the sheet, t
- Base diameter of the forming rollers, d
- Angle change, $\Delta\theta$
- Length of the flange, L_f

- Material of the sheet
- Number of steps to form the sheet through an angle of $\Delta\theta$, n

Among these parameters, material of the sheet only affects the portion of the deformation that occurs in the elastic region. In other words, deformation of the sheet is prescribed by the geometrical features of the sheet and the rollers. Material of the sheet sets the degree of plastification on the sheet. The last parameter, which is the number of steps, does not help on the investigation of the deformation of the sheet during roll-forming. The main deformation pattern of the sheet that is bent from $0°$ to $\theta_1°$ or from $\theta_1°$ to $\theta_2°$ is the same for both cases. Therefore, in order to analyze the deformation of the sheet, the first four of the listed parameters are examined namely, thickness of the sheet, base diameter of the rollers, angle change and length of the flange. These parameters are also presented in Table 4.1.

Table 4.1 Selected parameters of roll-forming

Thickness	
Angle Change	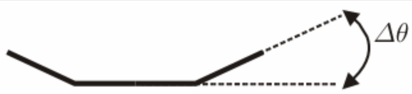
Base Diameter	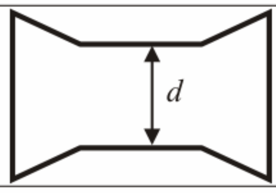
Flange Length	

In the analysis of the deformation of the sheet, mainly two measures of the deformations are dealt with. The first one is strain hardening through the thickness of the sheet. This is measured by reading the equivalent plastic strain values through the thickness in different locations of the sheet. The second measure is the components of the total strain tensors calculated at different locations of the sheet. By the help of the mentioned measures both the total hardening of the sheet and main directions of the hardening at distinct parts of the sheet are analyzed regarding the geometrical parameters of the sheet and the rollers.

4.2.1 Finite Element Model

In Chapter 3, the convenient element type to simulate a 3D roll-forming process has been given as shell elements. The proper mesh density that should be used in the analyses has also been discussed. The model used in the current chapter uses the same type of elements, assumptions and the boundary conditions as the described model in Section 3.3.1, Section 3.3.2 and Section 3.3.3 of the Chapter 3. The only difference is the geometry of the sheet and rollers that are varied in order to reveal their influences. The selected mesh density in Chapter 3 is the CASE 2 of Table 3.4. Same mesh density is used in the current models. Therefore, the elements have the dimensions of 0.75 mm of length and width. The thickness equals the thickness of the sheet. As the sheet gets larger, elements with the same dimensions are added to the mesh in order to preserve the density. The web length of the sheet is kept constant at a value of 10 mm. The total length is 300 mm.

Table 4.2 Values of the geometrical parameters

	Values
Thickness, t	0.5 mm - 1 mm - 2 mm - 4 mm
Angle Change, $\Delta\theta$	5° - 10° - 20°
Roller Diameter, d	60 mm - 80 mm - 100 mm
Flange Length, L_F	10 mm - 20 mm

The variation of the geometrical parameters is listed in Table 4.2. All combinations of the parameters are modeled and computed giving the total number of simulations as seventy two (4 thickness × 3 roller radii × 3 angle change × 2 flange length).

C15 steel is selected as the material of the sheet. This is a low carbon steel widely used in metal forming industry representing a general mild steel. Flow curve for the C15 steel is plotted in Figure 4.1. The yield stress of C15 steel is 297 MPa and its elastic modulus is 213 GPa. Poisson's ratio is assumed to be 0.3. The same material is used in all of the models.

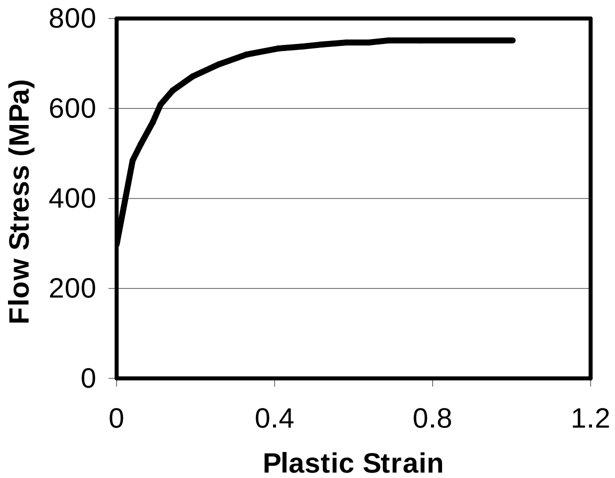

Figure 4.1 Flow curve of C15 steel

The numerical parameters of the finite element method that are used in the analyses are tabulated in Table 4.3. The selection of these parameters is explained in Appendix A and they have also been referred for the simulations of Chapter 3.

Table 4.3 Numerical parameters of the models

Number of Layers	7
Relative Force and Displacement Convergence Tolerance	0.1
Contact Tolerance	8% of the thickness
Step Size	1.2 mm/step
Solver	Direct sparse

4.2.2 Effects of the Geometric Parameters

The effects of the variables will be illustrated on the sheet with the short flange length since the effects are similar in the short and long flange lengths. The locations of the strain measurements on the short sheet are shown in Figure 4.2.

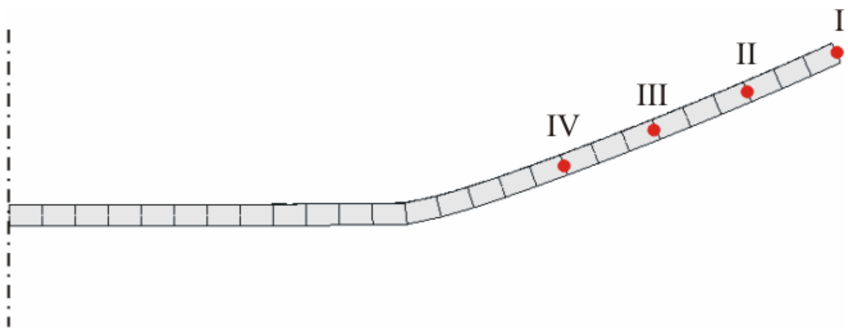

Figure 4.2 Locations of the strain measurements

In Chapter 3, it has been shown that the deformation in the bend region is mainly governed by the pure bending of the sheet and the longitudinal strain is low. Therefore, in the analysis of the effects of the geometric parameters, strain development in the flange is dealt with. Figure 4.3 presents the results of the strain values through the thickness of the sheet at the specified locations with respect to the different sheet thicknesses at a constant angle change of 5°.

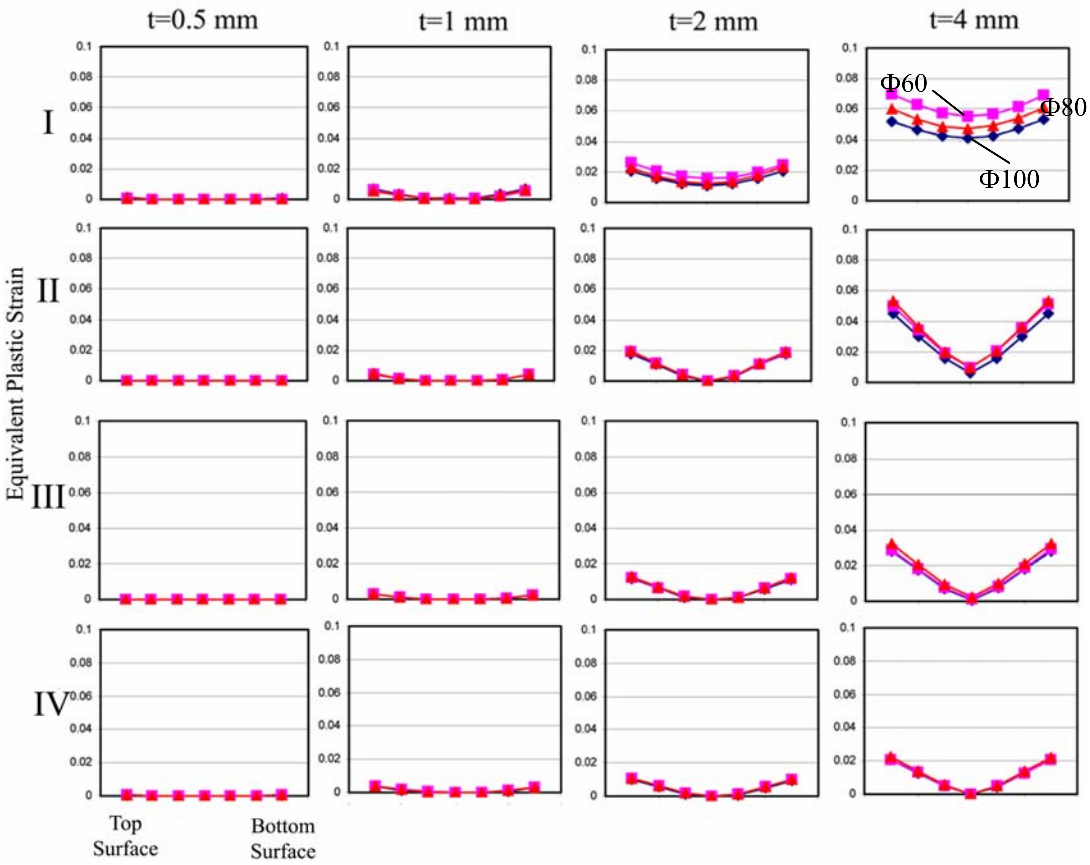

Figure 4.3 Effect of roller diameter

It is seen that roller diameter has a slight effect on the hardening of the sheet except the flange end. The effect in the flange end increases as the sheet gets thicker. This result is also the same for the sheet with the long flange. In addition, increasing angle change $\Delta\theta$ does not change the response. There is only a slight effect that is observed at large thicknesses at the end of the flange where the sheet contacts the roller surface. The maximum difference in the results is less than 10% of the smaller value. The main effect of the roller diameter is on the deformation length of the sheet. With large diameters the sheet starts to bend earlier giving rise to a larger deformation length.

As a result, the roller diameter is found to have a negligible effect on the hardening of the sheet. From this point on, the roller diameter will not be regarded as a geometrical parameter affecting the strain hardening of the sheet.

The effect of angle change $\Delta\theta$ and thickness t of the sheet is shown in Figure 4.5 at the prescribed locations of the flange for a roller diameter of 100 mm. For the small values of $\Delta\theta$, thickness change has a considerable effect on the strain values. As the thickness of the sheet increases, the strain values also increase. The difference in the results for different thicknesses increases towards the flange end. Another increase in the difference of the results is seen towards the increasing $\Delta\theta$ value. To give an example, increasing the thickness from 2 mm to 4 mm raises the flange end strain value at the top surface of the sheet by 0.25 at an angle change of 5°. This value turns out to be 0.5 when the angle change is 20°. As a general rule, it can be said that as the severity of forming increases the effect of thickness of the sheet increases.

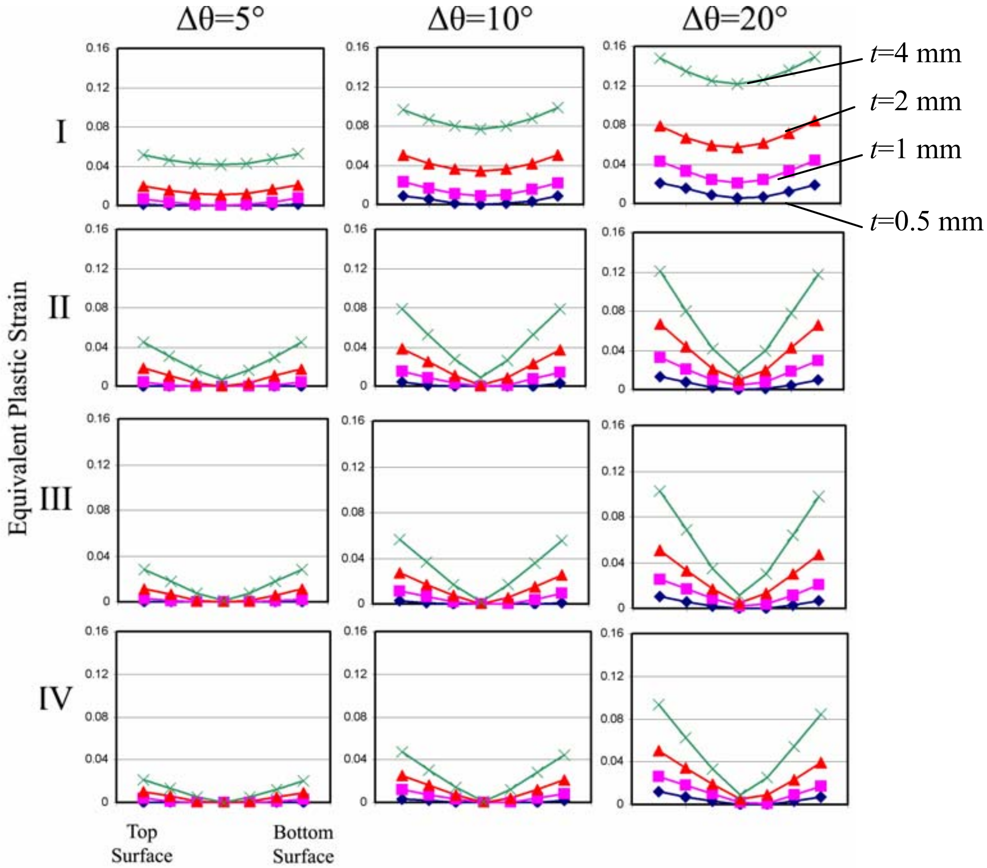

Figure 4.4 Effects of *Δθ* and *t*

The plastification along the flange can also be observed with the Figure 4.4. At the flange end high strain values are observed in comparison with the rest of the flange. Another important point is that strain values do not drop to zero at the sheet mid-surface except the thinnest sheet. Strain values decrease gradually from flange end to the web. The strain values in the nearest point to the web are roughly the half of the strain values at the flange end. To illustrate the general plastic strain distribution from flange end to web center, a general characteristic strain distribution is plotted in Figure 4.5 for a 20° bend angle and 4 mm sheet thickness.

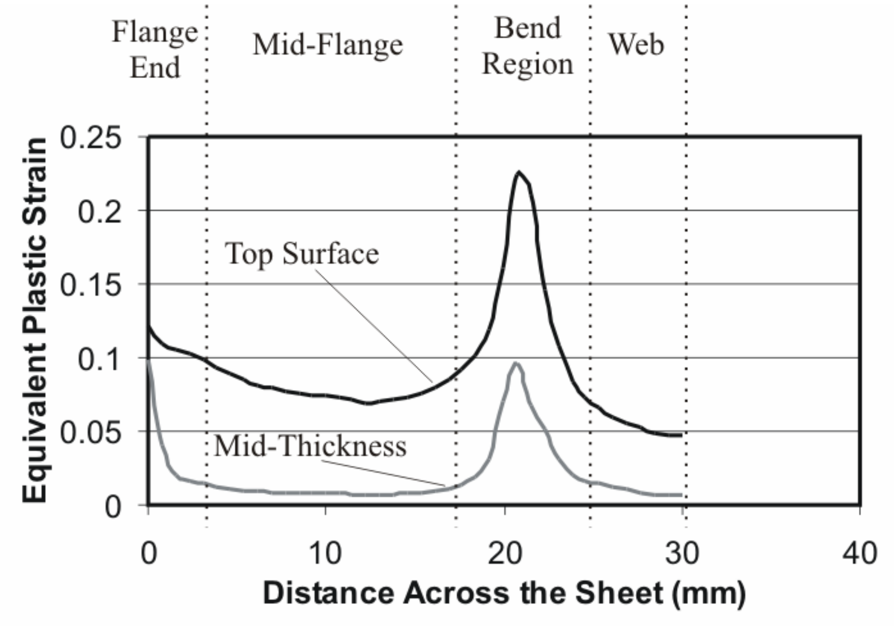

Figure 4.5 Plastic strain distribution on the sheet from flange end to web center

The plot in Figure 4.5 can be divided in to four distinct regions as flange end, mid-flange, bend region and web. The highest plastic strain values are observed in flange end and in bend region. There is a steep decrease of strain values after the flange end. This decrease is followed by a nearly constant strain values in the mid-flange. As the bend region is approached, the plastic strain values start to increase again and reach the highest value in the middle of the bend. Finally, strain values decrease again to end up with lower strain values in the web. This distribution of plastic strain is common for all combinations of geometrical parameters. The change is observed in the relative strain values of the distinct regions. The top and bottom layers give the same results for the plastic strain. That is why only the top layer is plotted.

The plastic strain distribution across the sheet for the thickest and thinnest sheets with three flange lengths are plotted for a 20° bend angle in Figure 4.6. It is seen that flange length increase does not the effect the plastic strain values in the bend regions. This is true for both thick and thin sheets. Increasing flange length lowers the plastic strain values of the outer surfaces in the flange including the flange end and mid-flange regions. As the flange length increases through the values 10-20-30 mm the lowest strain values reduce through 0.1-0.75-0.5 respectively. However, mid-thickness strain values remain unchanged with respect to the increasing flange length.

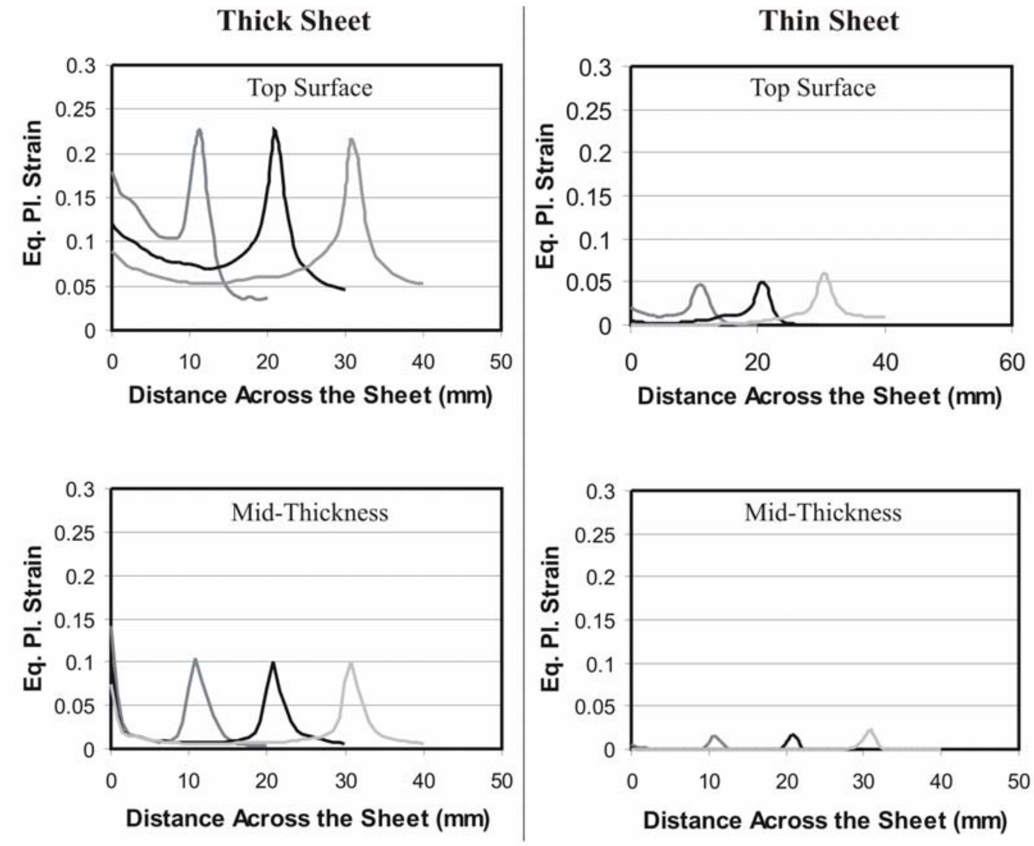

Figure 4.6 Plastic strain distribution across the sheet for thick and thin sheets for flange lengths of 10 mm, 20mm and 30 mm

4.2.3 Types of Deformations in Roll-Forming

The foregoing section presented the effect of the geometric parameters on the equivalent plastic strain values. This section focuses on the types of deformation on different parts of the sheet. This will be governed by the help of the development of the true strain tensor components at specific locations of the sheet. By this way, the deformation of the sheet can be visualized and the main straining directions can be distinguished. In plotting the strain tensor components a guideline is followed in order to obtain simplified and clear plots. The rules of the guideline are:

- Absolute values of the plastic strain components are plotted.
- Only the components that exceed the 10% of the highest reached strain value are plotted.
- The strain components are normalized according to the highest reached strain value at the studied location. Therefore, all strain components in a plot are plotted between zero and one, where zero means zero strain and one means the highest value reached by any of the components at this specific location reached either on the top layer or on the mid-layer.

The calculation points are selected from the main parts of the sheet that has been mentioned in the former section. These points are named as P_F from flange end, M_1 and M_2 from mid-flange, P_B from bend region and P_W from the web. The locations of the true strain tensor calculations on the sheet are shown in Figure 4.7 and the directions of the tensor components are shown in Figure 4.8.

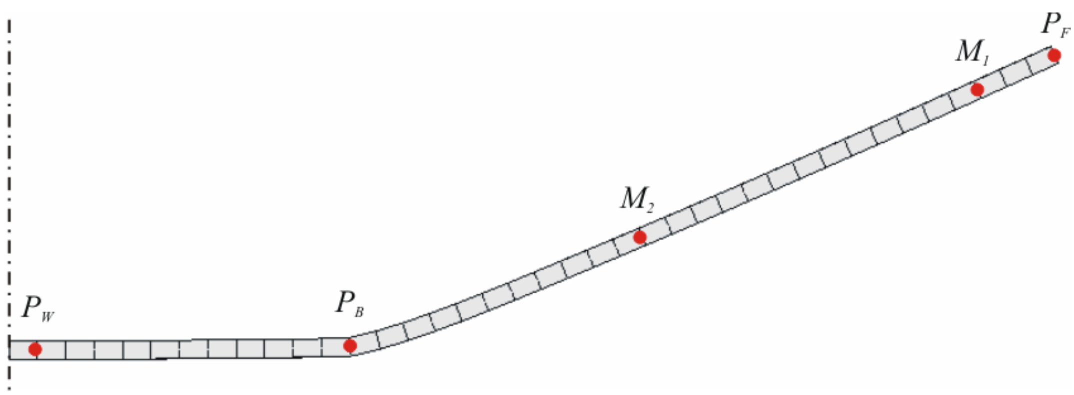

Figure 4.7 Locations of the true strain tensor calculations

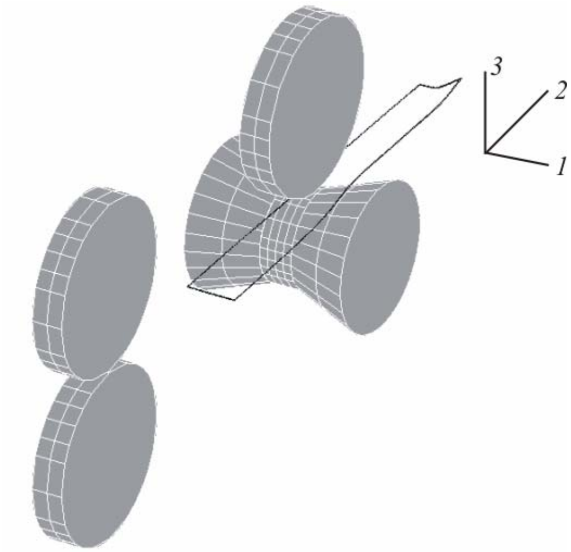

Figure 4.8 Directions of the tensorial components

The true strain tensors derived according to the mentioned rules are presented in Figure 4.9 for the sheet with 20 mm flange length, 4 mm thickness and 20° bend angle. The reason for the selection of the 20 mm flange length is that the distinct parts of the sheet can be identified clearly with the 20 mm sheet. In Figure 4.7, it is seen that flange end, mid-flange and bend regions are overlapping in the sheet with 10 mm of flange length. However starting with the 20 mm length flange, these regions are clearly separate.

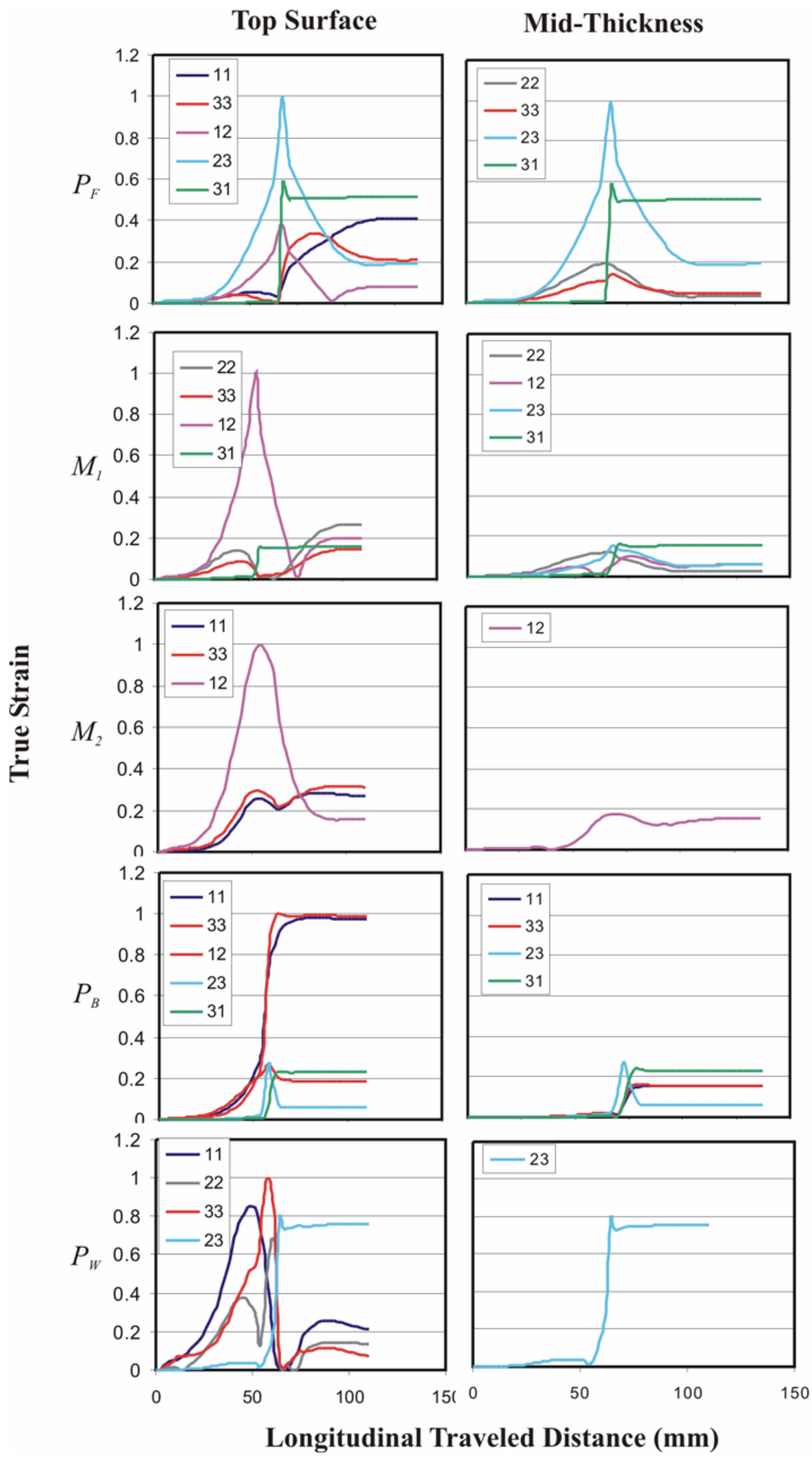

Figure 4.9 True strain values at the specified locations of the 4 mm thick sheet

At point P_F the strain state is complex. Almost all of the strain components are present in the flange end. This point contacts the roller and deforms along the roller according to the profile of the roller. That is why the flange end deforms into a complex 3D shape resulting in a complex 3D strain state. Same complexity is observed in the outer and mid surface of the sheet. However, shear strains are dominant on the mid-thickness of the sheet. At point M_1, the dominant strain component on the surface of the sheet is in "12" direction. It is observed that the other strain components can only reach to a value less than 25% of the highest value of the dominant strain component. The strain components on the mid-thickness of the sheet have again small values and a concept of dominant strain direction is not applicable.

Starting with the point M_2, bending effects of the corner becomes visible. The strain in "12" direction is again dominant as in point M_1 but strain values in "11" and "33" directions are also noticeable. As the bend region is approached, these components becomes more and more remarkable compared to the shear strain in "12" direction. When the point P_B is reached which lies at the center of the bend region, bending effects are clear. The deformation occurs in "11", "33" and "13" directions mainly. It is worth to note that "13" plane is the plane defined by the cross-section of the sheet. Therefore, in the bend area deformation is mainly governed in the cross-section plane. Same strain components are also present in the mid-thickness of the sheet.

At point P_W, there is a complex strain state as in the flange end. The strain component in "23" direction is common for both surface and mid-thickness of the sheet. In addition to this shear strain, normal strains in 11, 22 and 33 directions are also present on the surface of the sheet. The deformation of the web region is affected by two major factors. One is the bend region by the web area. The deformation of the bend region has an effect on the web region. As the bend region is approached, this effect becomes more visible. The other factor is the rollers. Web area of the sheet is always in contact with both the upper and lower rollers. The friction between the web region and the rollers has an effect on the deformation of the web.

In case of thin sheet, the results differ from the thick sheet case. The true strain tensor components for the 0.5 mm thick sheet can be seen in Figure 4.10. At points PF and M1 the main strain directions are the 22 and 12 for both surface and mid-thickness of the sheet. In other words, the primary direction of deformation is longitudinal direction. As in the thick sheet case, at point M2 the bending effects starts to be visible by the introduction of the strains in 33 and 11 directions. At point PW the strain state is exactly the same with the thick sheet case having the dominant strains in 11, 33 and 13 directions. Finally, the strains at point PW are again similar to the thick shell case where the strain state is complex having the maximum deformation in 11 and 33 directions. The major difference in the results is the main directions of the strain components in the flange end and mid-flange. In case of thin sheet, longitudinal strain components are more noticeable than the thick sheet case.

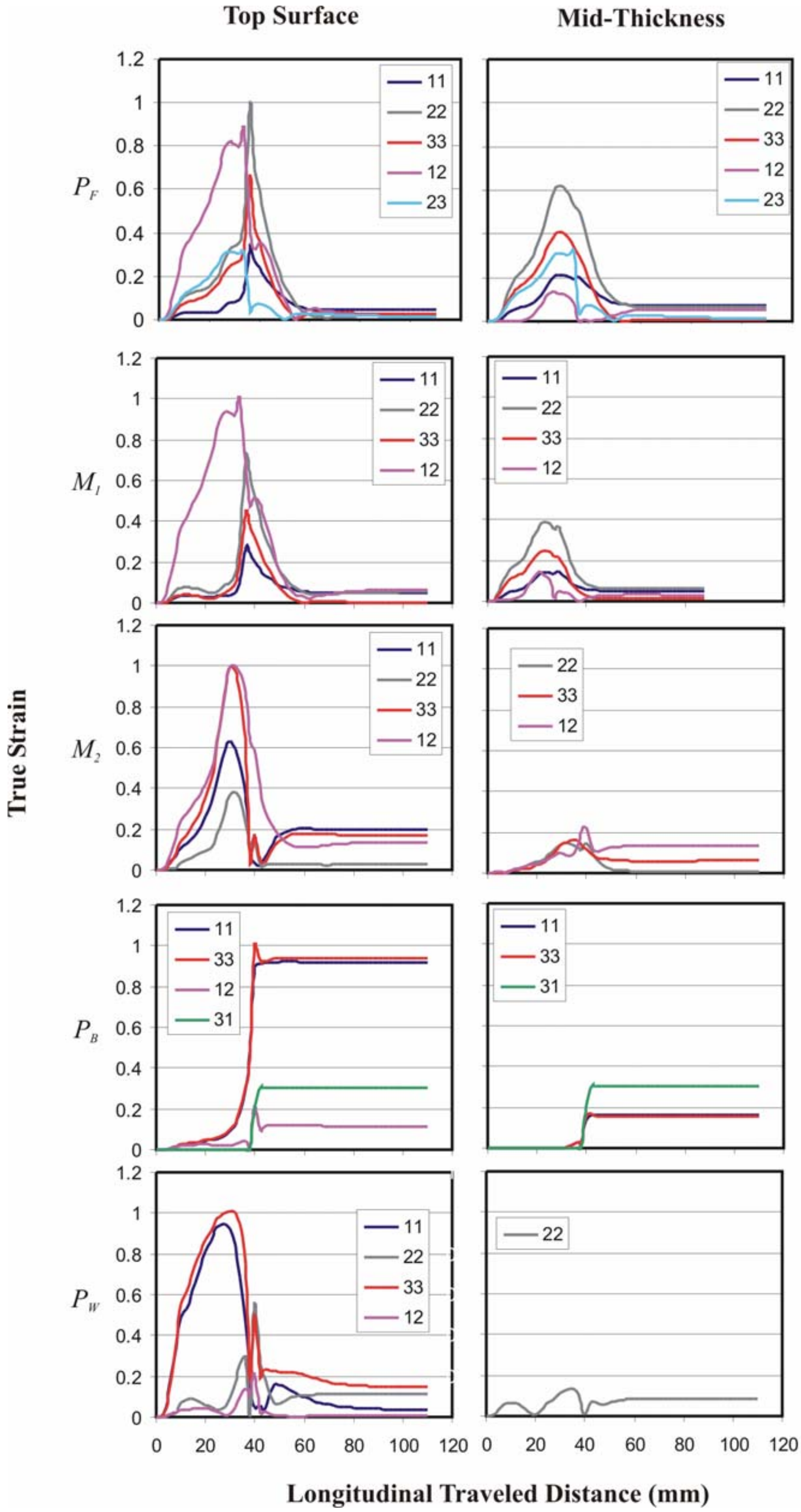

Figure 4.10 True strain values at the specified locations of the 0.5 mm thick sheet

4.3 Comparison of the Results with the Theoretical Knowledge

The theory formulizing the deformation in roll-forming is presented in reference [13]. Summary of the reference has been given in Section 2.2 of the Chapter 2. The theory is based on three basic assumptions. These are;

- The thickness of the strip is small compared with other sectional dimensions.
- Transverse sections of the strip remain plane, orthogonal and a constant distance apart at the mid-thickness surface during forming.
- Bending takes place only about the fold line of the active bend.

With these assumptions, four deformation types are formulized for roll-forming, namely, longitudinal stretching, longitudinal bending, shear and transverse bending. Among those deformation types longitudinal stretching and longitudinal bending creates longitudinal strains only, which is 2 direction in the simulations. Transverse strain is seen in the bend region in the plane of cross-section which is 13 plane and shear strain is observed in the 12 plane. According to the results of the study shear strains should be zero for the channel section that is examined in the last section. Therefore, the whole flange should only have longitudinal strains, the bend region should have bending strains only, and the web of the flange should have no strain.

From Figures 4.9 and 4.10 it is clearly seen that the predictions of the theory hardly coincides with the computed results. For the both sheet thicknesses, strain in the flange is not in the longitudinal direction only. In thin sheet case, the strain in the longitudinal direction is more apparent than the thick sheet case. Moreover, both of the sheets have deformation in the web area. The mismatch between the theory and the computation results is the result of the assumptions of the theory.

The first assumption of the theory necessitates the thickness of the sheet to be small compared to the other dimensions. In the simulations with 4 mm thick sheet, the width/thickness ratio is 7.5. For the 0.5 mm thick sheet, this ratio turns out to be 60. This is one of the reasons why the longitudinal strains are more apparent in the thin sheet case. According to the second assumption, transverse sections of the sheet should remain plane. Therefore, no warping should occur in order the theory to be valid. Figure 4.11 shows the geometry of the sheet between the rollers. It is clear that the sections do not remain plane. Sheet takes a complex 3D shape while passing through the rollers. The warpage of the transverse planes is seen clearly in the thick sheets but thin sheets have less warpage in their transverse sections. This is the second reason of the high level of mismatch between the thick sheet case and the theory.

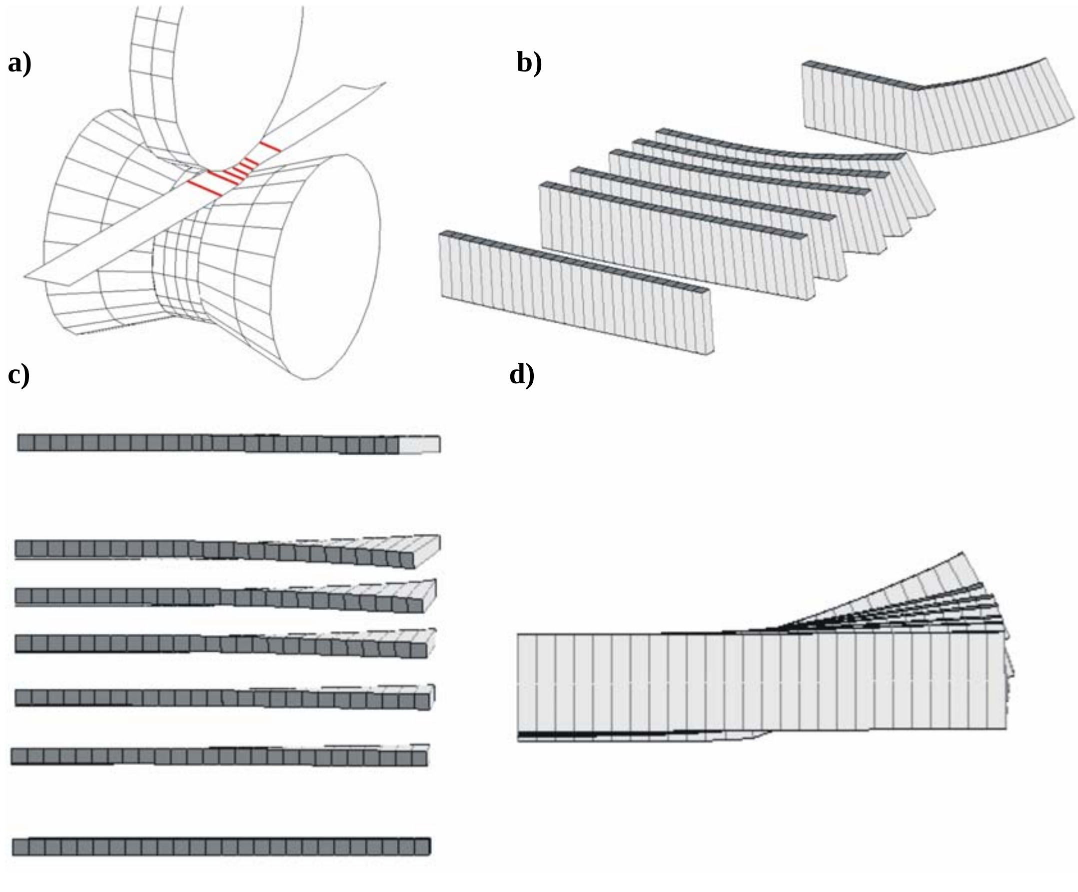

Figure 4.11 Geometry of the sheet passing through the roller. **a)** Examined sections **b)** Perspective view of the sections **c)** Top view **d)** Front view

4.4 Applicability of the 2D Plane Strain Formulation to Roll-Forming

In Section 3.8.3 of the Chapter 3 it has been shown that plane strain simulation results coincides with the 3D computation results at the bend region. The reason for this coincidence has been shown to be the low values of longitudinal strain in that region. The main deformation occurs in the cross-section plane, which can be studied under plane strain assumption.

In the current chapter, it is shown that this deformation mechanism is the same for all combinations of the geometrical parameters. In other words, deformation in the bend region occurs mainly in the cross-section plane regardless of the sheet thickness, flange length or bend angle. Hence, plane strain simulations can be used to predict strain hardening in the bend regions.

Another discussion can be made for the flange and web regions of the sheet. As mentioned in Chapter 3, plane strain simulations predict zero strain except the bend region. Web region remains undeformed between rigid dies and the flange undergoes a rigid body rotation around the bend region. However in all combinations of the geometrical parameters of roll-forming equivalent plastic strain is observed in the web and flange regions.

In Figure 4.7, it is seen that as the flange length increases the plastic strain in the flange decreases whereas the plastic strain in the bend region remains constant. In thin sheet case, the situation is the same but this time plastic strain values in the flange and web regions are already low compared with the bend region strains except the very end of the flange.

As a result, plane strain computations can be used for the following cases of roll-forming:

- Thin sheet thicknesses with a considerable error at the very end of the flange
- Thick sheet thicknesses with relatively long flange lengths. The longer the flange length, the lower the plastification in the flange with respect to the bend region.

CHAPTER 5

CASE STUDY AND EXPERIMENTAL VERIFICATION

5.1 Introduction

In this chapter, numerical analysis of roll-forming utilizing plane strain assumption will be assessed by the experimental findings. In addition, the effects of strain hardening occurring during roll-forming on the behaviour of the final product will be shown by the help of the finite element simulations and the experiments. A series of finite element simulations will be performed to obtain strain hardening on the cross-section and to examine the behaviour under the application of service loads and each step will be verified by the experiments.

As a case study a commercial roll-formed product is selected. The product is a channel having roughly square shaped cross-section (Figure 5.1). This channel is available with 3 m and 6m length choices with constant 3.5 mm wall thickness. The lateral holes are used to fix channels together. The main area of usage is the construction of structures that are designed for carrying heavy loads. The channel geometry is totally manufactured by roll-forming. At the end of the production line the two ends of the cross-section are joined by laser welding. Meanwhile the lateral holes are sheared off the channel. Finally the product is cut to the desired length and hot-dip galvanized against oxidation.

All Dimensions in mm

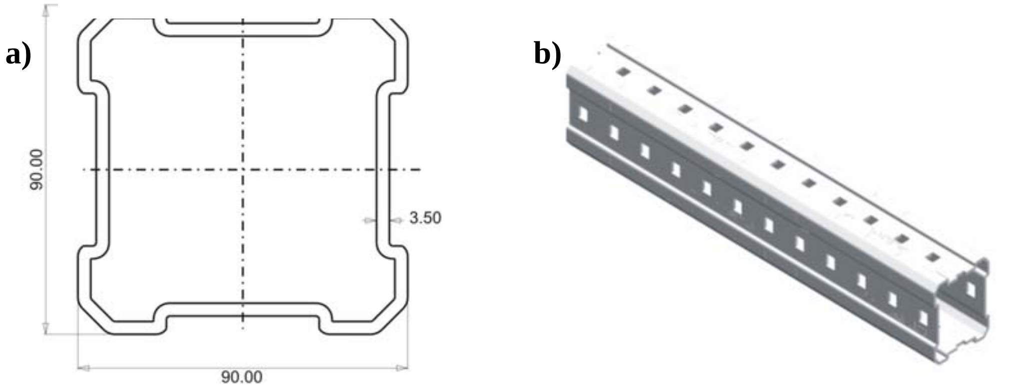

Figure 5.1 Case study product: a) Cross-section and b) Perspective view

5.2 Performed Experiments

Several experiments were performed for the characterization of the raw material and the final product. The experiments aim to obtain the flow curve of the material, strain distribution along the thickness and the behaviour of the final product under bending loads. Details of the experiments will be presented in this section.

5.2.1 Tension and Compression Tests

Since the raw material of the workpiece is prepared by rolling operation, several tension tests had to be performed in different orientations in order to take anisotropy into account. The orientations are namely;

0-degree: Along the rolling direction
90-degree: Transverse to the rolling direction
45-degree: Along the middle of the 0 and 90 degree directions

Therefore, for each direction four tension tests were performed and the results can be seen in Figure 5.2.

From the flow curves it is seen that anisotropy is negligible except the early parts of the curves. Hence, the one which extends to the highest strain is selected, namely, the 0-degree flow curve and the first studies are performed with this curve. However since large deformation processes are dealt with, necessity for extending the flow curve to large strains arises. For this reason, Ludwik equation is selected for the extrapolation of the curve. The utilized Ludwik equation is

$$\sigma_f = C \times \bar{\varepsilon}^n \tag{5.1}$$

where

C = 578 MPa and n = 0.134

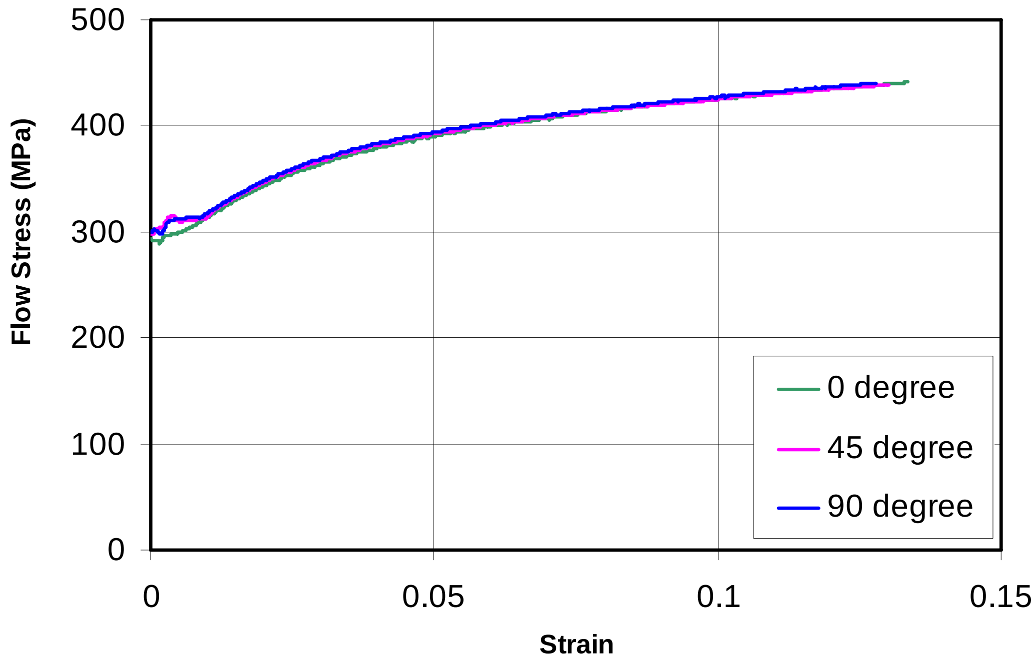

Figure 5.2 Tension flow curves in different orientations

The galvanizing process at the end of the roll-forming operation affects the flow curve of the material. Therefore, new tests are needed to get the flow curve. This time compression tests were performed on both the raw material and the galvanized product to see the difference clearly and to reach higher strains. Compression test results in Figure 5.3 shows that initial yield stress is the same for compression and tension tests and it is not affected by the galvanizing process. Up to the tension test strain limit of 0.13, tension test results are close to the compression test results before galvanizing. However, the extrapolated tension test results give 10% error according to the both compression test results.

Therefore, for roll-forming simulations, the compression flow curve before galvanizing and for service load application simulations, the compression flow curve after galvanizing is used.

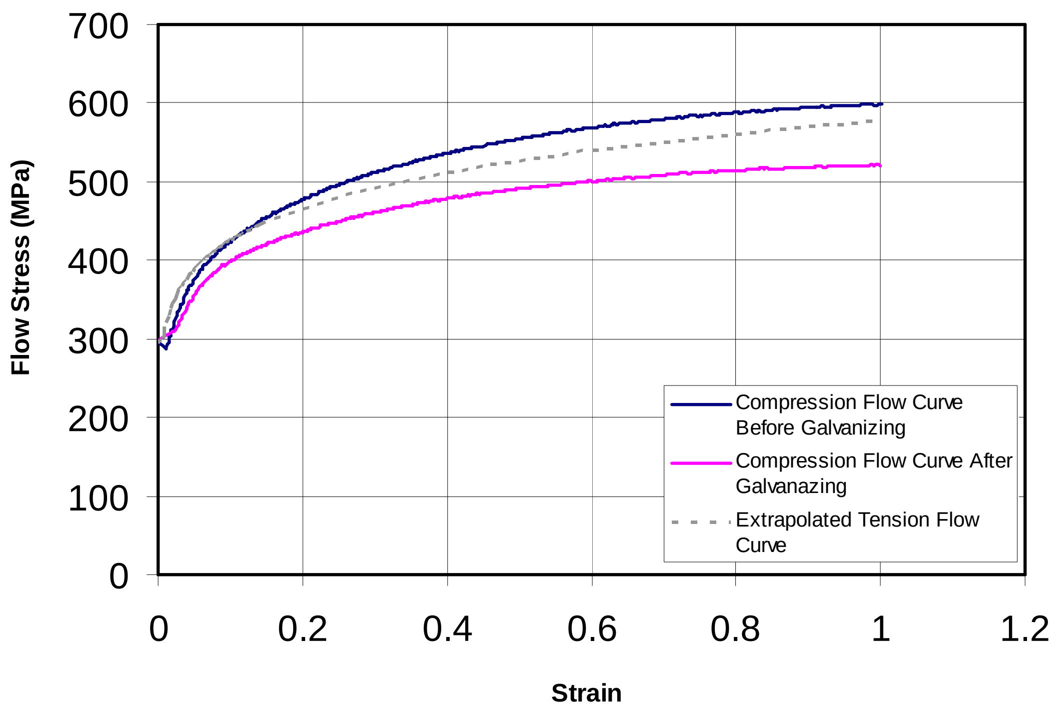

Figure 5.3 Compression test results and tension test results extended with Ludwik Equation

5.2.2 Hardness Measurements

Vickers Hardness measurements were performed on two different cross-sections of the final product to see how the product undergoes deformation during roll-forming (Figure 5.4). For this purpose, the relation between Vickers Hardness and yield stress proposed by Tekkaya is used [28]. This relation has been mentioned as equation 2.27 in Section 2.6 of Chapter 2.

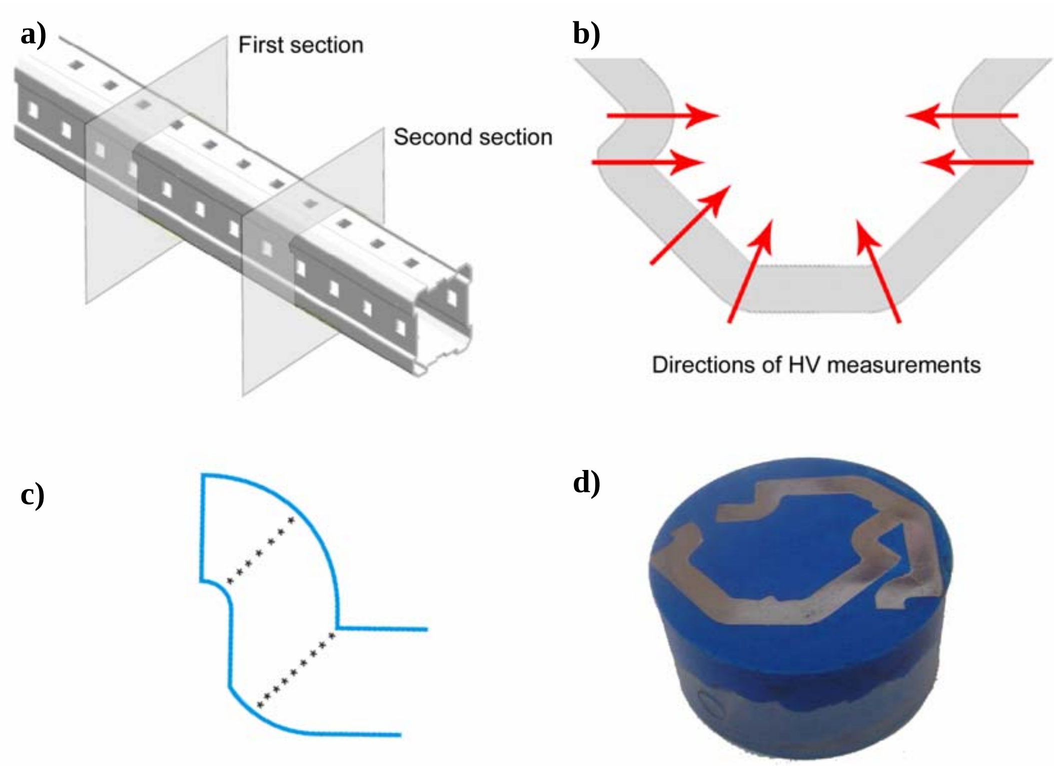

Figure 5.4 HV measurement locations: a) Two sections, b) Directions of the measurements, c) location of the measurements, d) HV Test specimen

The measurements were performed along the wall thickness of the product to calculate strain gradients on the section. Totally 800 measurements have been performed on the two sections and average values of a location are used to calculate the strain. These hardness values are used to verify the results of roll-forming simulation of the product. Equivalent strain values obtained from simulations will be compared with the values obtained from the HV measurements. The details and the results of these measurements will be discussed combined with the verification of roll-forming simulations in Section 5.4.2.

5.2.3 Bending Experiments

In order to observe the bending response of the final product, bending tests were performed on 5 different specimens with 1100 mm length supported between 2 supports that are located 50 mm away from each end (Figure 5.5).

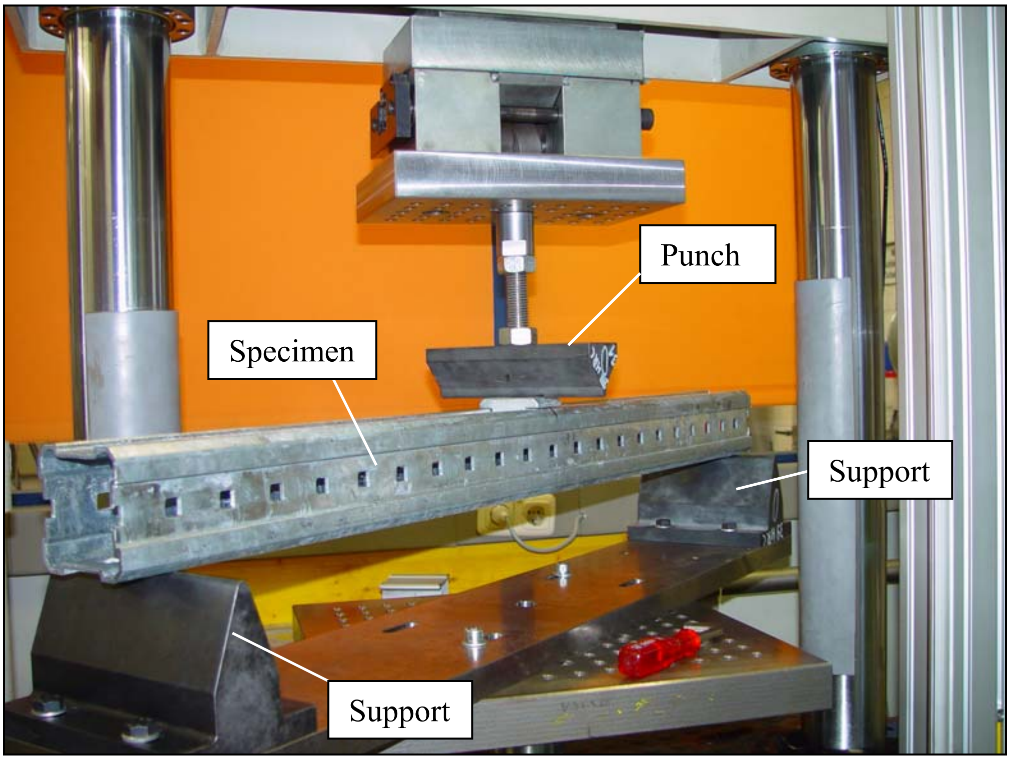

Figure 5.5 Bending experiment setup

The purpose of this experiment is to verify the simulations with service load applied on the product having roll-forming effects found from manufacturing simulations. In addition, the difference between the simulations using products without deformation effects and the experiments will be seen. Therefore, the error created by disregarding or underestimating roll-forming effects will be seen clearly.

The force vs. deflection curves obtained from the experiments have three different regions (Figure 5.6). The curves start with a slightly non-linear behavior (Region I), then continue with a linear part (region II) and followed by a highly non-linear region (region III). Interpretation of these behaviors will be presented in Section 5.3.6.

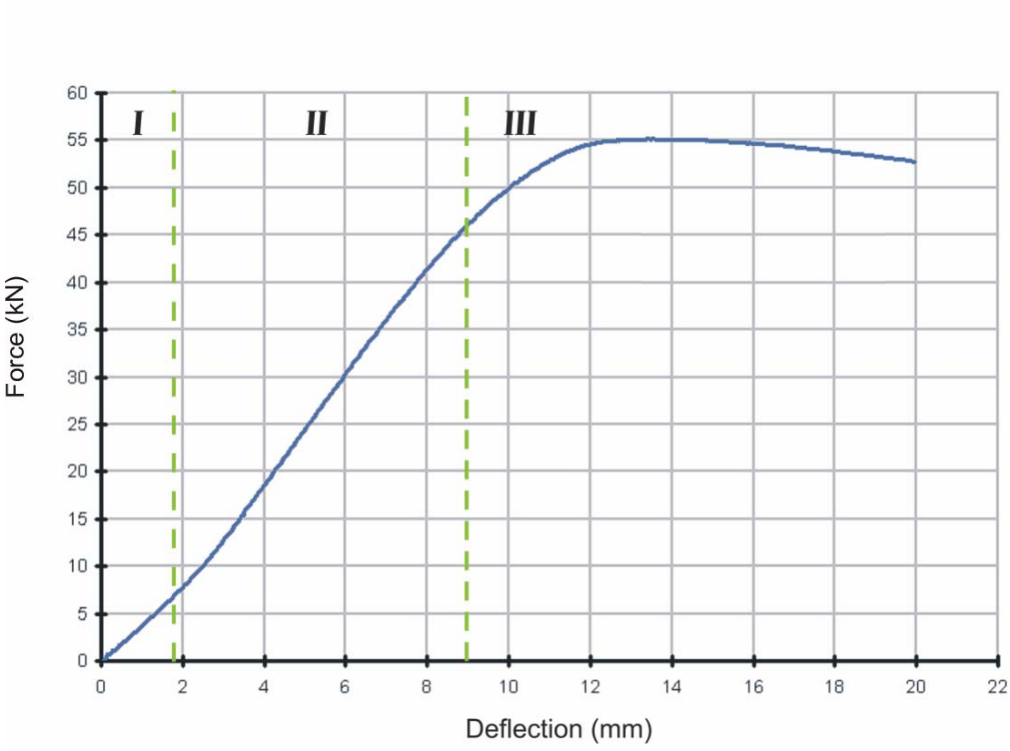

Figure 5.6 Bending experiment result

5.3 Bending Experiment Simulations without Deformation Effects

In this section, results of the bending simulations with the workpiece having the exact geometry of the technical drawings and without any initial strain or stress are presented. The aim is to compare the results with the experiments and hence to reveal the significance of the cold forming effects.

5.3.1 Preliminary Studies

The thickness of the workpiece is very small compared to the length of the product. This geometry forces the side length of the elements on the cross-section to be small. If aspect ratio of the elements is to be conserved, the total number of elements will be quite large since the side lengths in the longitudinal direction will be of the same order of magnitude of the cross-section side lengths. Therefore, a need to study the effect of aspect ratio of the elements arises. In order to investigate this phenomenon a simple cantilever beam problem is selected (Figure 5.7).

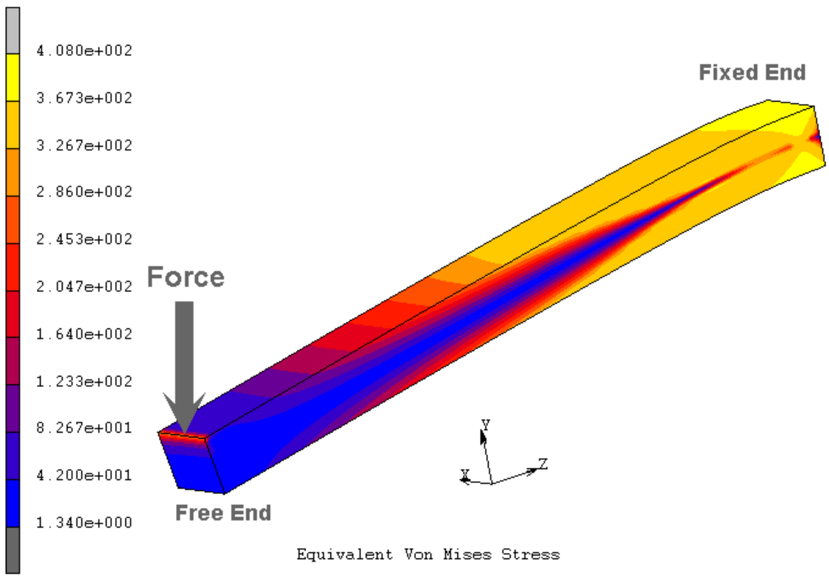

Figure 5.7 Selected cantilever beam problem

First a convergence study is performed. The details of the finite element model can be found in Table 5.1. In the convergence study the element aspect ratios are kept at 1:1:1:, that is all the side lengths of the elements are equal. In Figure 5.8 it is seen that at about 30000 elements with aspect ratio of 1:1:1 the solution converges with a relative percent error of 3.1%.

Table 5.1 Finite Element Model Data of cantilever beam problem

Cantilever Beam Dimensions in mm	32×12×150
Max. Applied Force in N	1,800
Analysis	Mechanical, elasto-plastic
Formulations	Large disp., large strain with additive decomposition
Number of Elements	6,000; 30,000; 58,000
Element Type	3D Brick elements
Remeshing	Not used
Convergence Criteria	Relative force and displacement residuals
Solver	Multifrontal sparse

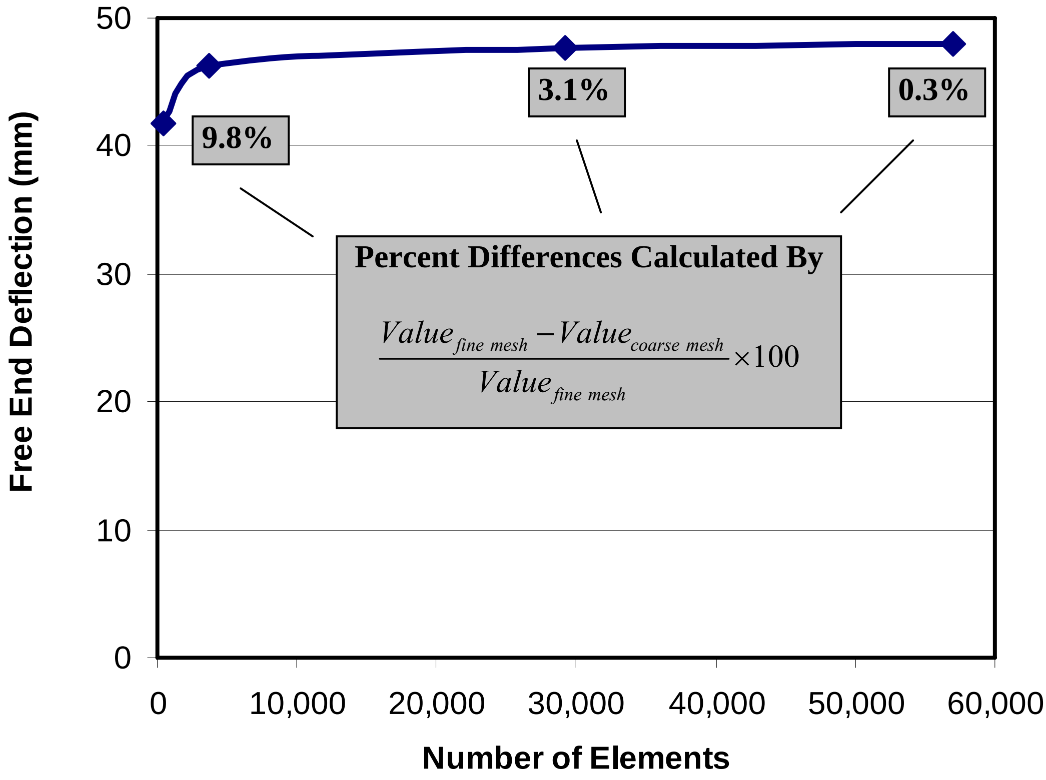

Figure 5.8 Result of the convergence analysis

Next, the aspect ratio of the elements is varied (Figure. 5.9). In this study, the aspect ratios are distorted only by changing the length of the element sides in longitudinal direction or in other words along the beam. This is because of the fact that in bending experiment simulations, mesh is created first by meshing the 2D cross-section and then extruding the elements on the cross-section to 3D brick elements along the whole beam. Therefore, having almost proper element geometries on the cross-section is rather simple. On the other hand, when these elements are extruded to form the whole geometry by keeping the 1:1:1 aspect ratio, total number of elements turn out to be a huge number that makes it inefficient to perform the simulations in terms of computation time.

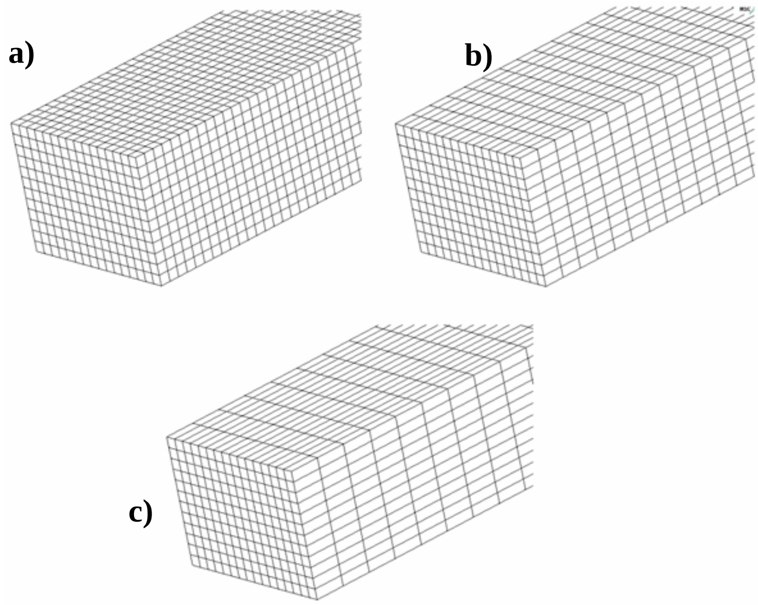

Figure 5.9 Meshes with different aspect ratios: a) 1:1:1, b) 1:1:2, c) 1:1:3

Figure 5.10 shows that all the models with different aspect ratios predict the deflection successfully in the elastic range. However, predicted deflections starts to differ in the plastic range. It is observed that up to aspect ratios of 1:1:3, the free end deflection of the elements does not change significantly. In addition, as the lengths of the element sides along the beam are increased, it is seen that the beam gets stiffer. The elements with the most distorted geometry give a less deflection with an error of 27% (Table 5.2). These results are benefited from in terms of decreasing the computation time of actual bending experiment simulations by using less number of elements along the beam. Therefore the aspect ratio of the elements will not exceed 1:1:3 throughout the study.

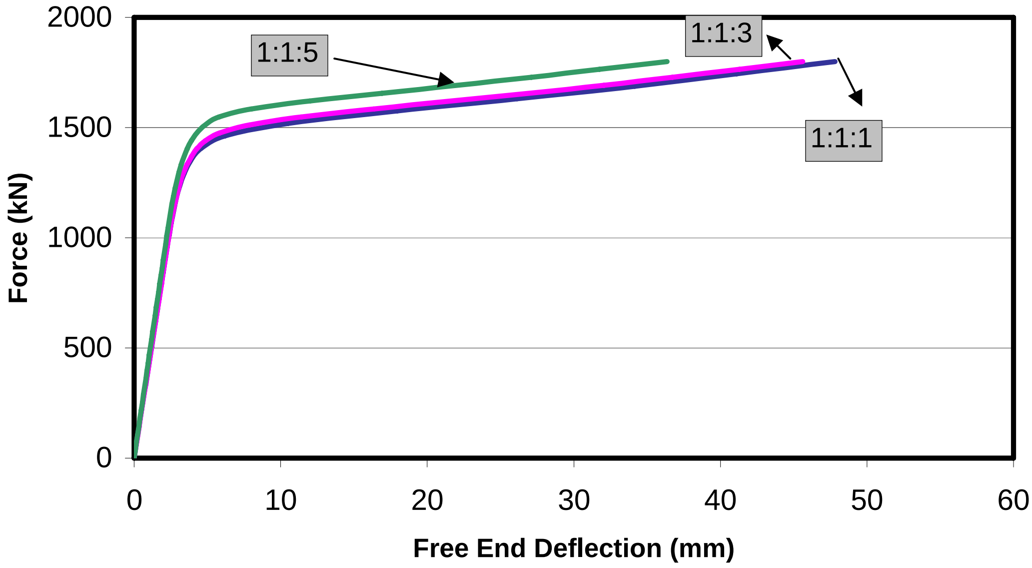

Figure 5.10 Effect of aspect ratio

Table 5.2 Effect of aspect ratio in terms of % error in deflection

Aspect Ratio	Deflection (mm)	% Error
1:1:1	47.82	-
1:1:1.5	46.35	2.4
1:1:2	46.28	2.6
1:1:3	45.63	4.1
1:1:4	40.54	15.3
1:1:5	36.36	27.5

The "assumed strain" formulation is also utilized in the simulations. In this formulation, "the bending behavior of 3-D brick elements is improved by replacing the standard bi- or trilinear interpolation functions with an enriched group that is able to represent pure bending behavior. This formulation results in improved accuracy for isotropic behavior, but it should be noted that the computational costs increase" [32].

To analyze the effects of the assumed strain formulation the same cantilever beam problem is solved again by using elements having aspect ratios of 1:1:1 and the results are compared with the simulations without the assumed strain formulation in Figure 5.11. It is observed that assumed strain formulation gives better results with the same number of elements when a coarse mesh is used and eventually the results starts to overlap after a critical mesh density is reached.

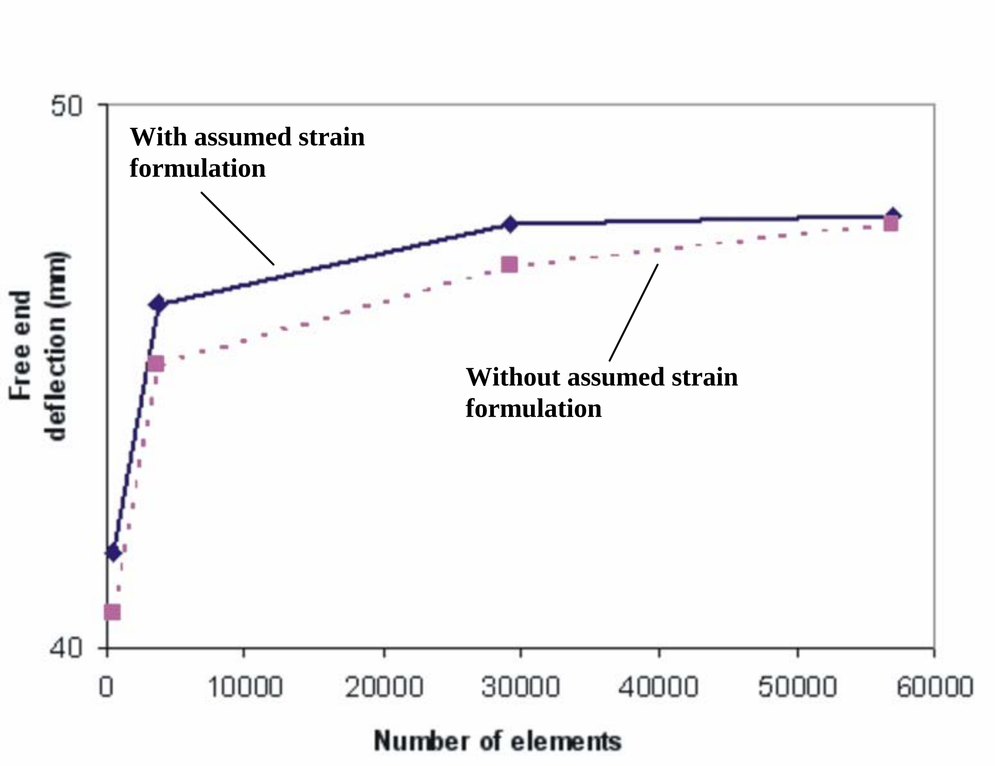

Figure 5.11 Significance of assumed strain formulation

To summarize this section, two remarkable issues are decided on with the preliminary study;

•Assumed strain formulation will be used in bending experiment simulations since the formulation enables convergence with fewer elements.

•Aspect ratios up to 1:1:3 can be used in bending experiment simulations without significant loss of information.

5.3.2 The Model and Simulations

Symmetry of the product is benefited from in the models. Therefore, ¼ of the channel is modeled in the simulations. The supports and the punch are modeled as rigid bodies. The model prepared for the workpiece with lateral holes is given in Figure 5.12. The FEM data of the bending experiment simulations can be seen in Table 5.3.

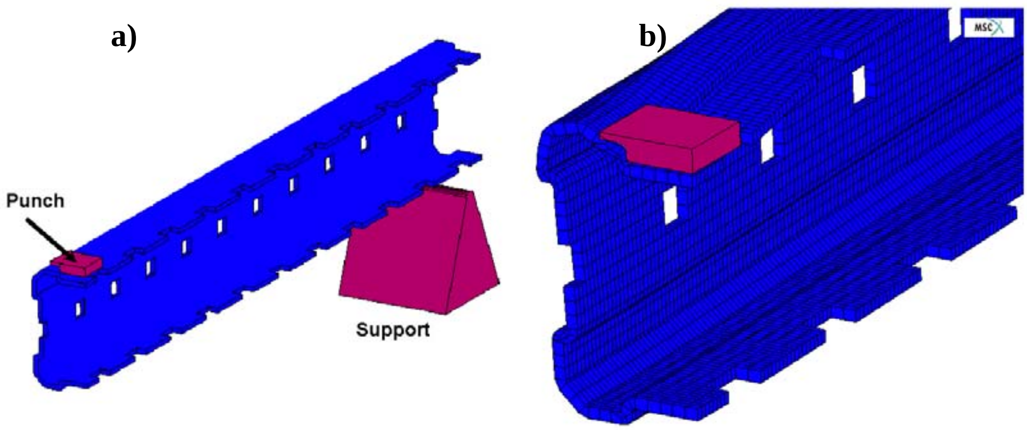

Figure 5.12 a) The model for the simulations with lateral holes **b)** Close view of the deformed region

Table 5.3 Finite Element Model data of the bending simulations

Modeled channel dimensions in mm	90×45×550 (t = 3.5)
Analysis	Mechanical, elasto-plastic
Formulations	Large disp., large strain with additive decomposition, assumed strain
Number of Elements	20000, 40000, 65000
Element Type	3D Brick elements
Remeshing	Not used
Convergence Criteria	Relative force and displacement residuals
Solver	Multifrontal sparse

A convergence analysis is performed to decide on the proper number of elements. As mentioned before the aspect ratio of the elements is not distorted more than 1:1:3. The convergence study needs to start with 20,000 elements because of the necessity of capturing the geometrical features of the cross-section. When the results in Figure 5.13 are investigated, it is seen that with 40,000 elements the solution can be accepted as converged. Therefore, 40,000 elements are used in the study.

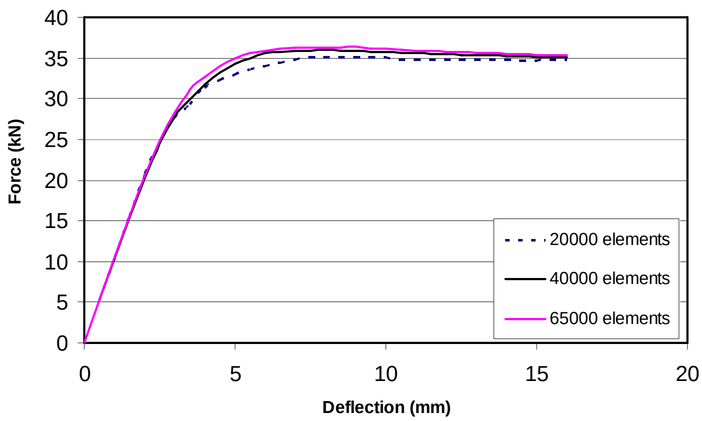

Figure 5.13 Convergence analysis according to number of elements

The results of the simulations with and without lateral holes compared with the experiment results can be seen in Figure 5.14. Here, the force and deflection stands for the punch force and punch displacement, respectively. There are two remarkable points in these results. First, existence of holes brings 13% difference of maximum force which makes lateral holes an important parameter for the simulations. Secondly, there is a significant difference between the simulations and the bending experiments in terms of maximum reached force and the slope of the linear parts of the curves.

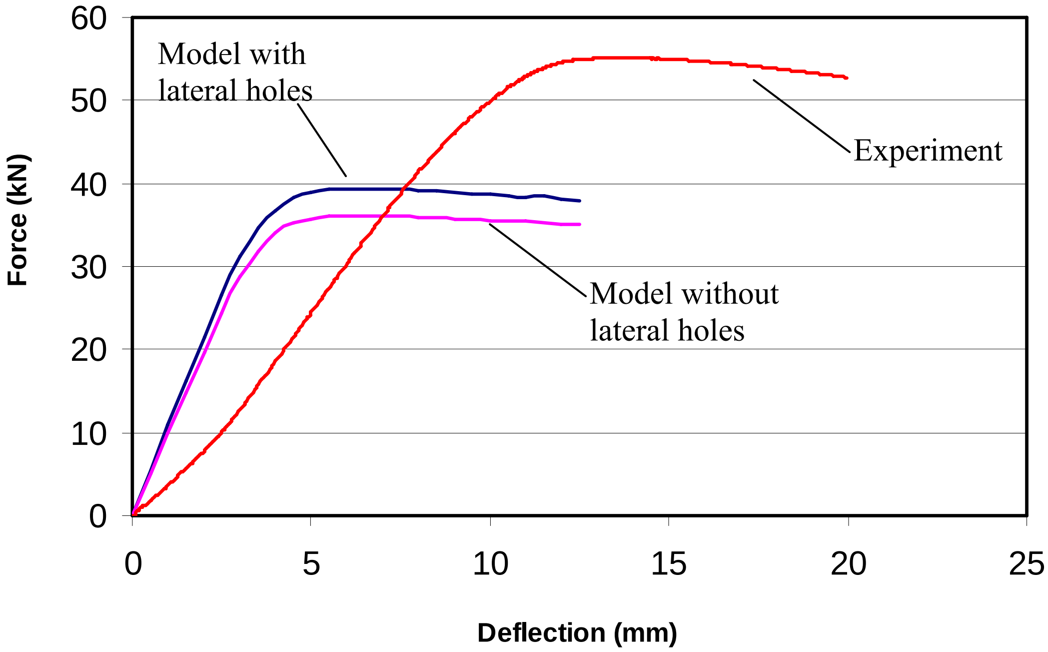

Figure 5.14 Punch force vs. punch displacement curves

Since there is a large difference between the simulations and the experiments, a parametric study of the both is needed to understand the process in depth.

5.3.3 Effect of Modulus of Elasticity

Difference in the slope of the curves brings in minds the possibility of using an incorrect modulus of elasticity for the material of the product. Therefore, simulations with different elastic modulii are performed (Figure 5.15). The effect of the elastic modulus can be regarded as negligible in the range of variation.

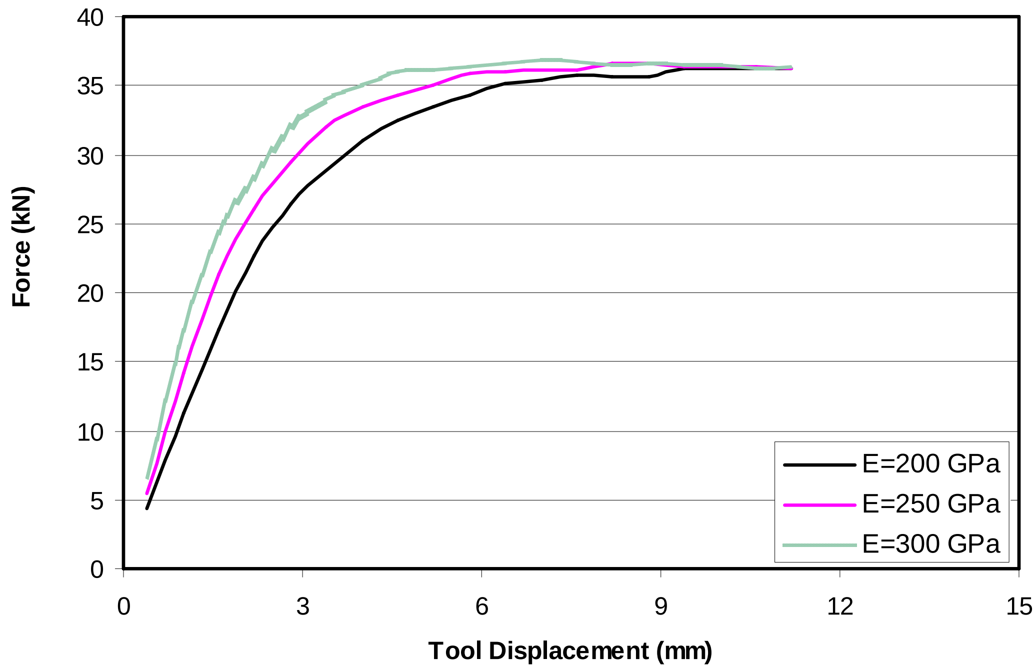

Figure 5.15 Elastic modulus effect

5.3.4 Effect of Equivalent Plastic Strain

In order to investigate the role of strain hardening in the material, simulations are performed with constant initial plastic strains artificially assigned to all elements. The assigned strain values are increased gradually to observe the effects clearly.

From the bending experiment simulation results, it is observed that, during bending a very small region of the profile which is just under the punch is plastified (Figure 5.17). Therefore, since most of the profile is in elastic region, assigning an initial plastic strain to all elements actually does not affect the elements except those near to the punch.

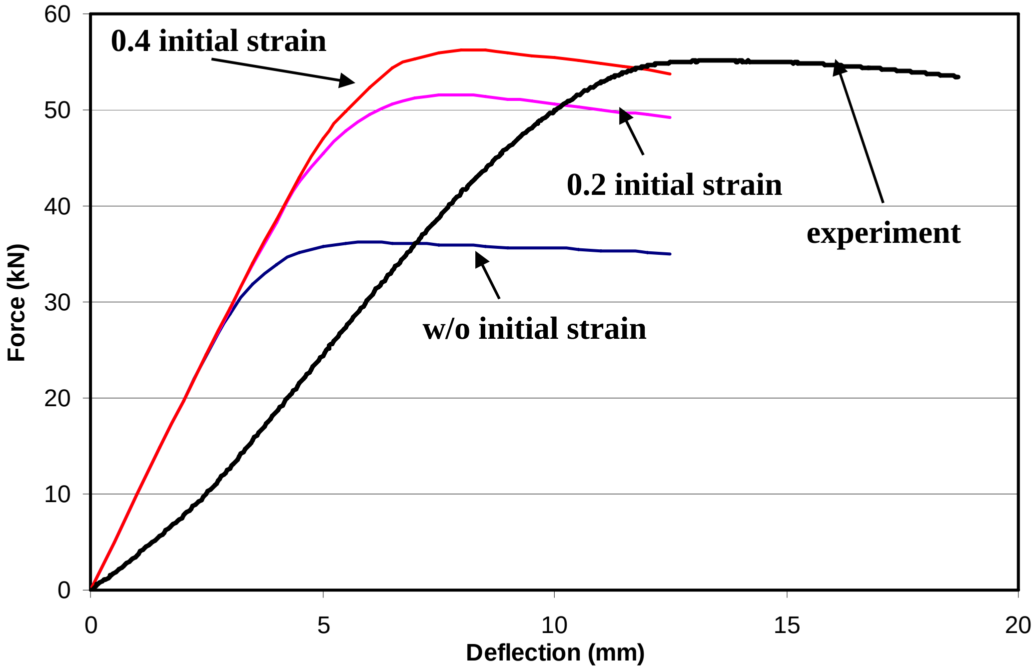

Figure 5.16 Effect of strain hardening

Effect of initial equivalent plastic strain can be seen clearly in Figure 5.16. First of all, initial plastic strain does not affect the slope of the linear part of curves. Second observation is that, with increasing strain values, change in the maximum reached force decreases and maximum force tends to converge to a value. For an initial strain value of 0.2, the difference between the experiment and the simulation is 6% and for a value of 0.4 the difference is 1%.

5.3.5 Local Deformation Effect

As mentioned before, the bending experiment takes place with local plastification and this region is located under and around the punch (Figure 5.17). To investigate this phenomenon the deflections of the profile from punch side (upper part) and opposite side (lower part) are compared by the help of simulations.

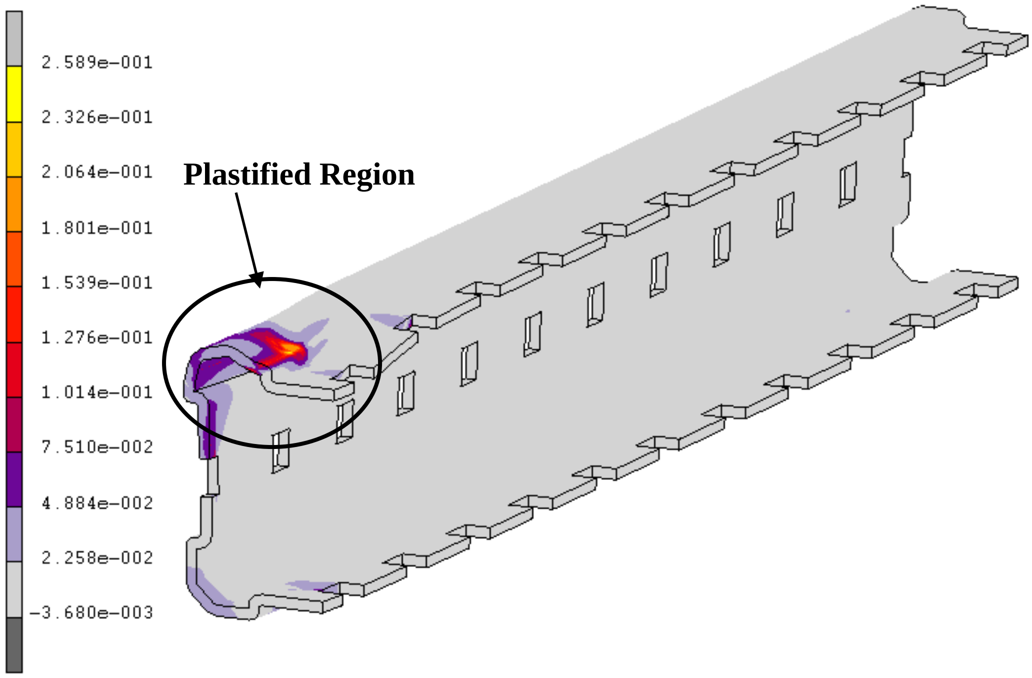

Figure 5.17 Equivalent plastic strain around the localized deformation region

Figure 5.18 shows that at the very beginning of the test, deflection is homogenous over the cross-section. Other than that part, deflections differ increasingly from upper part to lower part as the test proceeds. The dashed vertical line in Figure 5.18 shows the instance when the deflections start to differ. This instance also corresponds to starting point of non-linear part of the force deflection curve. These properties are also applicable to the simulations with initial plastic strain.

Therefore, most of the test is dominated with the locally deformed part around the punch. It can be thought that the rest of the profile does not add to the stiffness after that instance. So it can be visualized as the deformed part is supported between rigid surfaces and deforms under the punch.

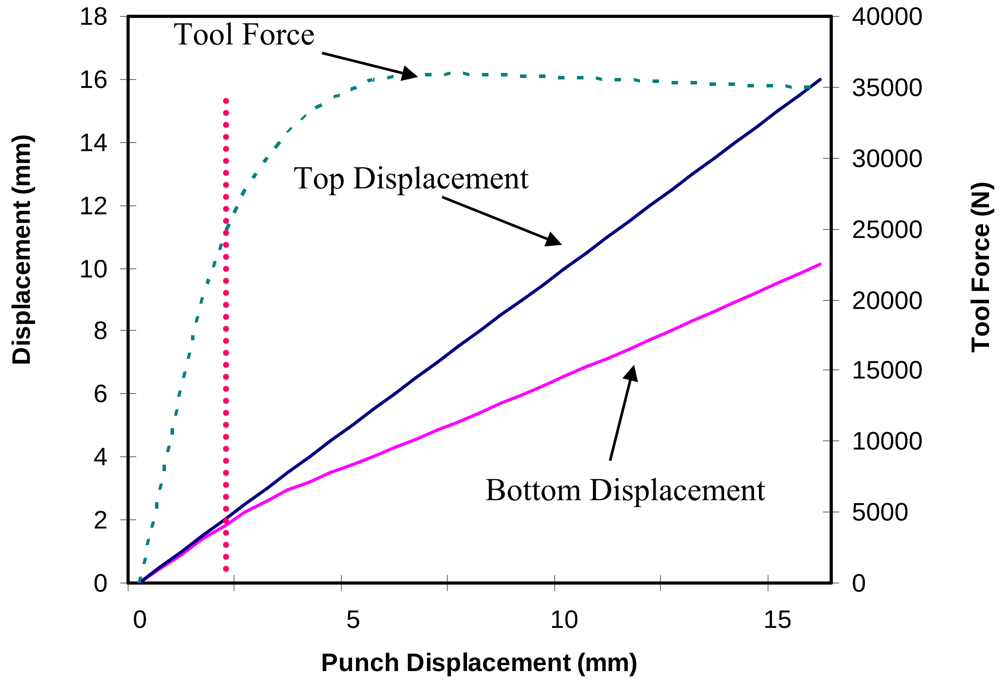

Figure 5.18 Deflection of upper and lower parts of MI-90

5.3.6 Experiment Data Modification

From the above studies it is observed that elastic modulus of the material and plastic strain does not affect the slope of the force-deflection curves. In addition in all simulations the same slope is observed. Therefore, it is concluded that there should be an error in the experiments. When the experiment results and the simulation results are compared it is seen that there are 2 types of errors in the experiments.

First one is the error in the slope of the experiments which is caused by the deflections in the frame of the experiment setup. Since these deflections are added to the actual deflections the resulting slope is eventually lower than the actual slope. The simulation and experiment results are also compared with the classical

(Euler-Bernoulli) Beam Theory and Figure 5.19 shows that the experiments also differ significantly from the theory. The calculation of the theoretical displacements can be found in Appendix B.

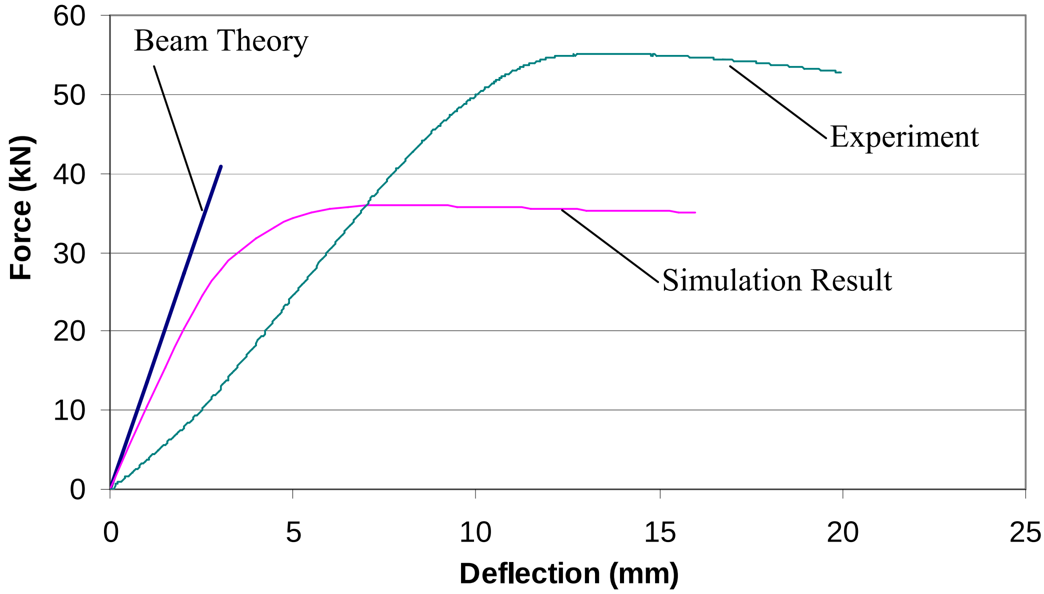

Figure 5.19 Comparison of theory, simulations and experiments

The second error is due to gaps or backlashes in the setup. Because of that error, there is a constant displacement error throughout the test except the very beginning. As seen in Figure 5.6, region I is not a linear region. This non-linearity is caused by the gradually closing gaps and decreasing backlash.

As a result, experiment results are modified with respect to these errors and the modified curve together with its modification formula is given in Figure 5.20. In the formula, the second term in the right-hand side stands for the frame stiffness error and the last term stands for the constant displacement error. Obviously, the part of the curve with negative deflection values will not be used.

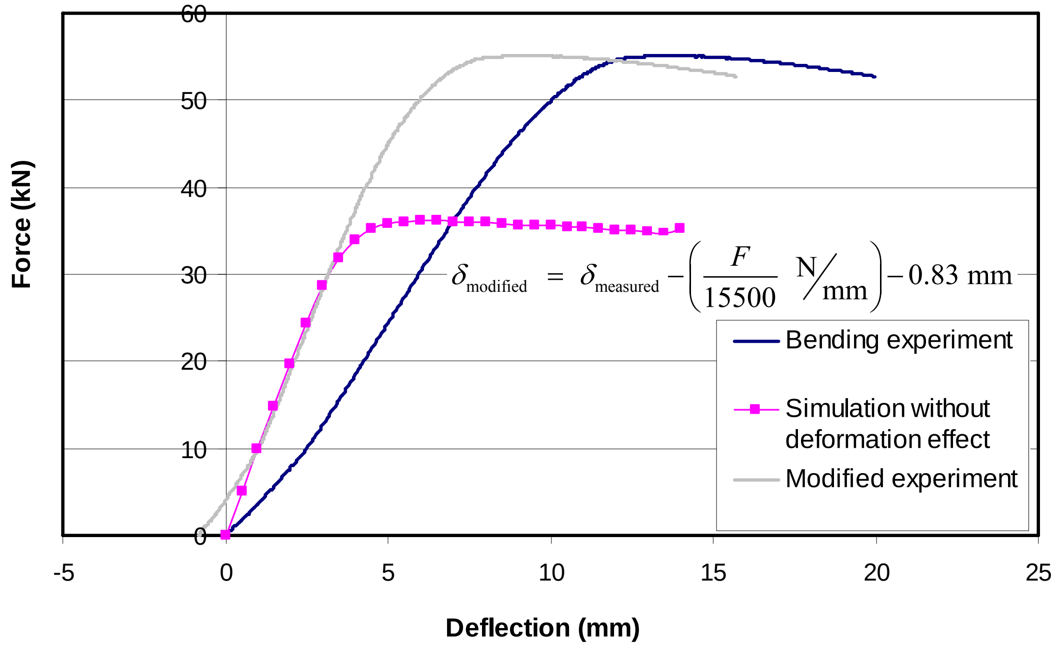

Figure 5.20 Modification of the bending experiment results

So, Figure 5.16 can be redrawn as in Figure 5.21. From this point on, the modified experiment data will be used throughout the studies.

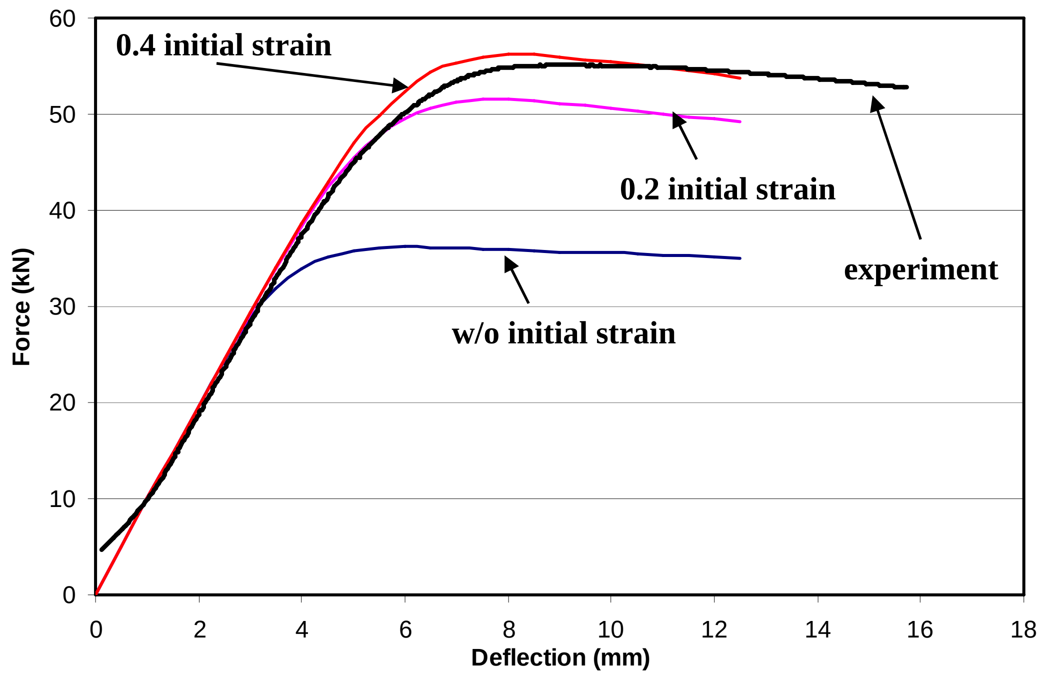

Figure 5.21 Modified experiment data and curves for different initial strain values

5.3.7 Outcomes of the Parametric Study

With the studies above, some important points are revealed that makes it easier to understand and visualize the bending test and that will guide throughout this chapter:

- Elastic modulus of the workpiece material does not affect the result of the simulations considerably.
- Initial plastic strain affects the force to bend the material but does not have an influence on the slope of the linear part of the force-displacement curves which is expected since this region is the elastic region.
- The test is dominated by local deformation of the region under the punch.
- Experiment setup has some defects which are compensated by modifying the displacement data.

5.4 Roll-Forming Simulations

The cold roll-forming sequence of the channel has been simulated to obtain the plastic strain and residual stress distribution across the cross-section after the manufacturing sequences. Strain distribution has been compared with the Vickers Hardness (HV) measurements. The resulting geometry has also been checked with the actual product geometry.

5.4.1 Finite Element Model

In order to obtain the stress and strain distribution, simulations have been performed utilizing the plane strain assumption. Dies are considered to be rigid with no friction and workpiece material is assumed to be elasto-plastic, meshed with quadrilateral plane strain elements. Only one half of the workpiece is modeled because of symmetry (Figure 5.22). Compression flow curve obtained before galvanizing process has been used as the material flow curve. The FEM data used in the simulations can be seen in Table 5.4.

Table 5.4 Finite Element Model data of plane strain roll-forming simulations

Modeled sheet dimensions in mm	3.5×180 mm
Analysis	Mechanical, elasto-plastic
Formulations	Plane strain, large disp., large strain
Number of Elements	200, 400, 1500
Element Type	4 noded quadrilateral elements
Remeshing	Not used
Convergence Criteria	Relative force and displacement residuals
Solver	Sparse

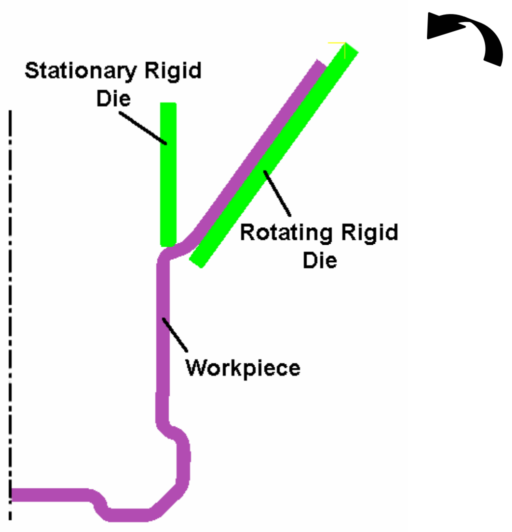

Figure 5.22 Model used to simulate roll-forming

In order to simulate all the bends in the half geometry, 12 successive simulations are needed (Figure 5.23). Having completed these simulations, a final model has been prepared to simulate the springback and residual stress development after the welding process. The effect of laser welding is simulated by applying fixed displacement boundary conditions to the nodes at the welded edge and removing all the dies. Last simulation is performed for 1 increment to reach the new equilibrium state without the dies.

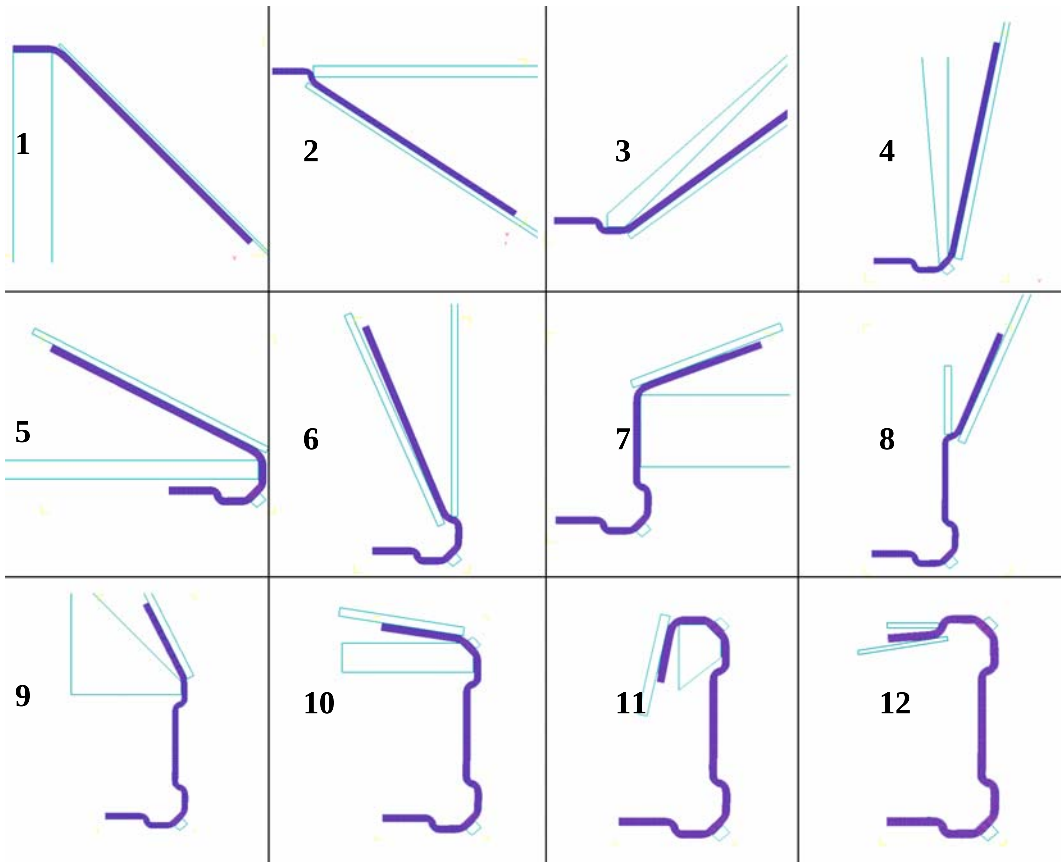

Figure 5.23 Forming sequence of the channel

Simulations have been performed with 3 different mesh densities, 200, 400 and 1500 elements. Equivalent plastic strain distribution gets a smoother gradient over the cross-section as the mesh is refined. The expected neutral surface occurring during bending can only be seen by using fine meshes. In addition, the final geometry of the workpiece can not have the small details when a coarse mesh is used (Figure 5.24). Therefore, mesh density plays an important role in the roll-forming simulations.

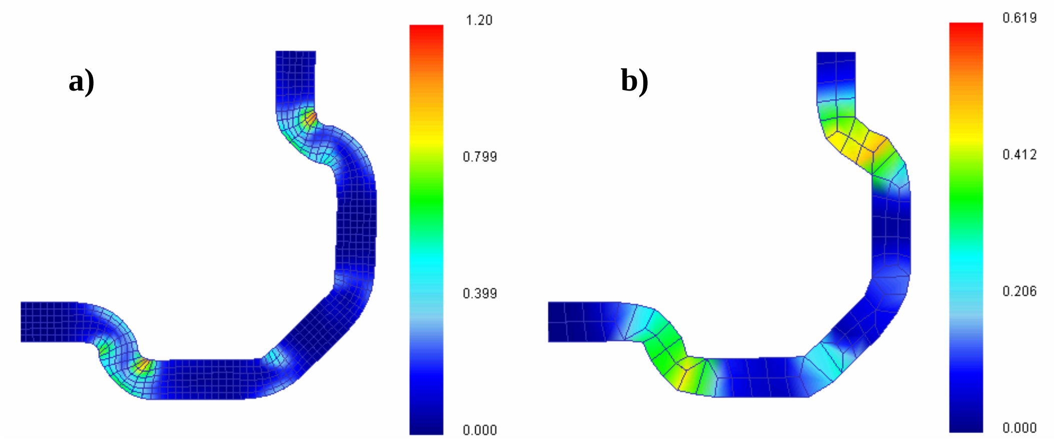

Figure 5.24 Equivalent Plastic Strain distribution and final geometry of simulations with a) 1500 and b) 200 elements

5.4.2 Validation of the Results

As mentioned in Section 5.2.2, HV measurements have been performed throughout the cross-section to verify the simulation results in terms of equivalent plastic strain. Measurements are focused on the two types of 90° bends that are repeated recursively on the cross-section (Figure 5.25).

Figure 5.26 and Figure 5.27 compare the simulation results and the HV measurements for the two types of 90° bends. The figures also show the boundary of the scatter of the strain values obtained from the HV measurements as dashed lines. In Figure 5.27, the strain distribution obtained from the HV results are not complete. That is because of the fact that most of the measurements from the Type-

2 90° bends give strain values that are out of the flow curve range, which is over 1.00. The same consideration applies to the boundary of measurement scatter curves.

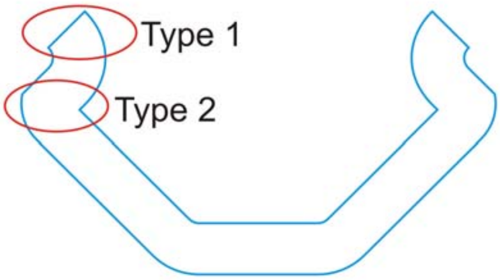

Figure 5.25 Types of the bends where HV measurements are focused

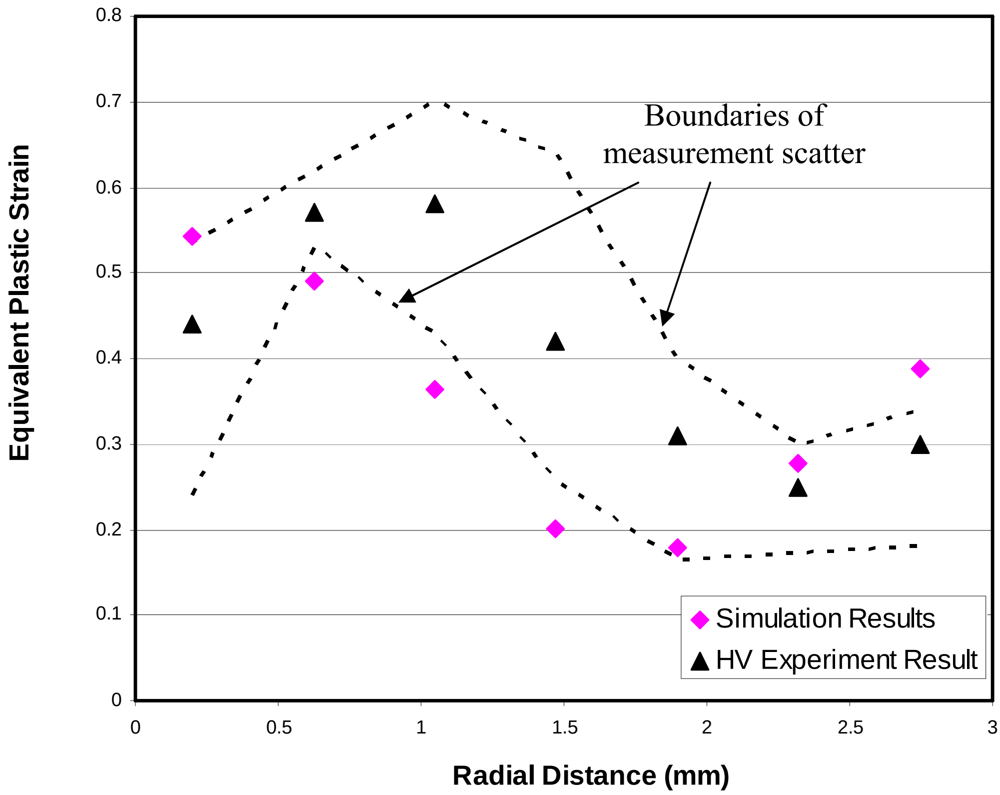

Figure 5.26 Strain distributions obtained from the simulations and HV measurements for the Type-1 90° bend

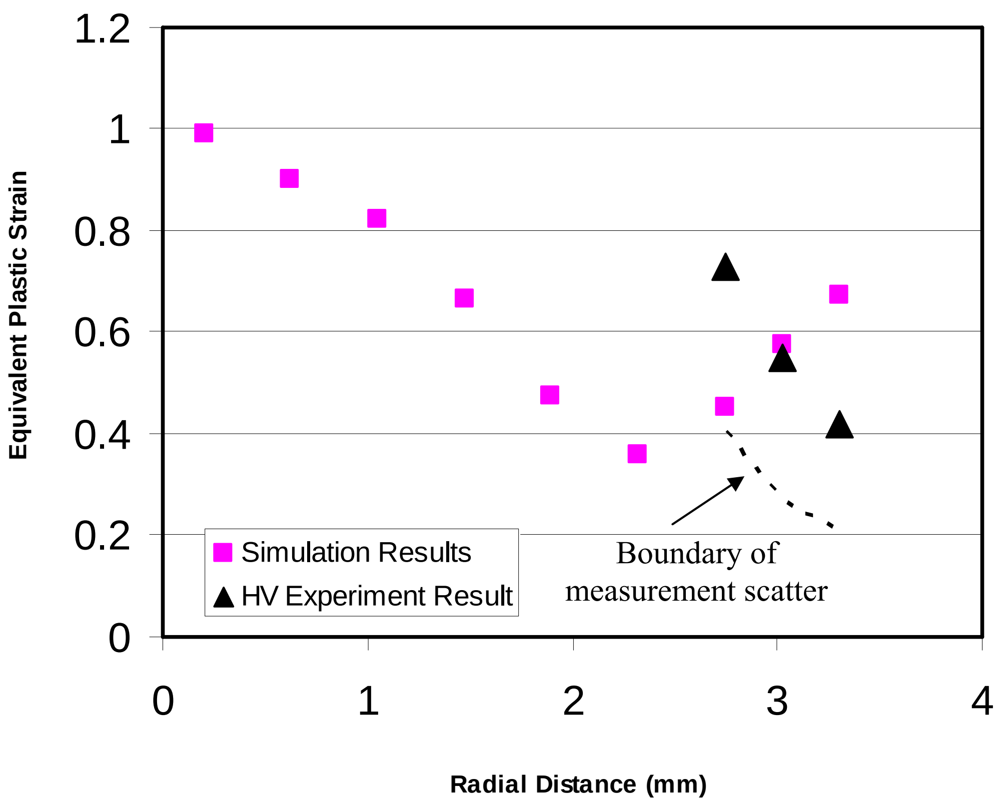

Figure 5.27 Strain distributions obtained from the simulations and HV measurements for the Type-2 90° bend

Figure 5.26 and Figure 5.27 shows that;

- For the Type-1 bend, the results are in agreement except the mid layers of the thickness. In these regions, strain values obtained from the simulations are lower than the ones obtained from the HV measurements. However, the distribution of strain is in good agreement with the measurements considering the scatter of the measurements.
- For the Type-2 bend, higher strain values are obtained compared to the Type-1 bend. HV measurements also verify this fact. However, HV measurements are higher than the simulation results as it is the case for the Type-1 bends.
- Briefly, for the two cases, strain values obtained from the simulations are lower than the measured ones, but the distributions are in agreement.

- In the Type-2 bends there is a region with high plastic strain and this region can not be captured with the simulations. This is due to an excessive deformation in that region.

In the simulations with pure bending thinning occurs in the bended regions. However, the actual workpiece undergoes thickening in some regions. There is no way to obtain this thickening by pure bending. Hence, the final geometry obtained from the simulations differs from the actual product in these thick regions (Figure 5.28). Other than these regions, obtained geometry is in agreement with the actual product. The overall dimensions of the cross-section have been checked with the technical drawings and seen that the overall geometry is correct (Figure 5.29).

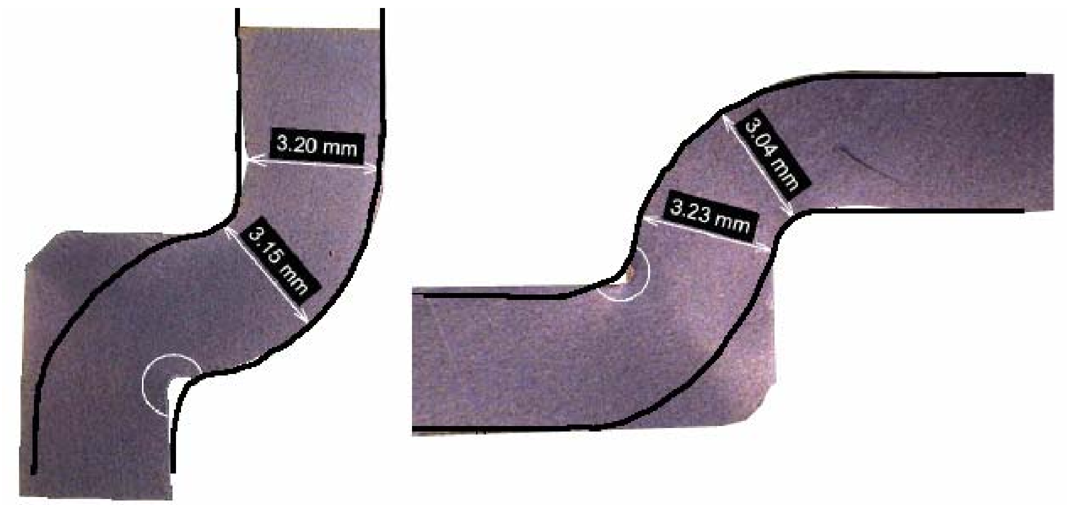

Figure 5.28 Geometrical comparison of simulation results (solid lines) with actual product

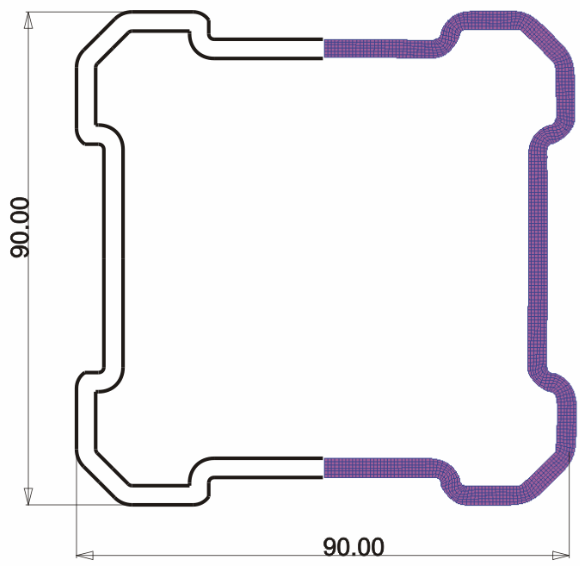

Figure 5.29 Overall geometry comparison

5.4.3 Alternative Roll-Forming Simulation Technique

Since the geometry and strain hardening pattern of the resulting cross-section differs from the actual workpiece, it is decided to simulate the roll-forming operations in a different manner. This time the simulations do not only include bending but also contain operations for the thickening regions. In order to obtain thickening, first the workpiece is bent for 90° over a rigid punch (Figure 5.30-a). Thenafter, the workpiece is formed between two dies (DIE1 and DIE2 in Figure 5.30-b) by moving both of the dies horizontally. This method enables the forming of the thick regions in the technical drawing of the channel.

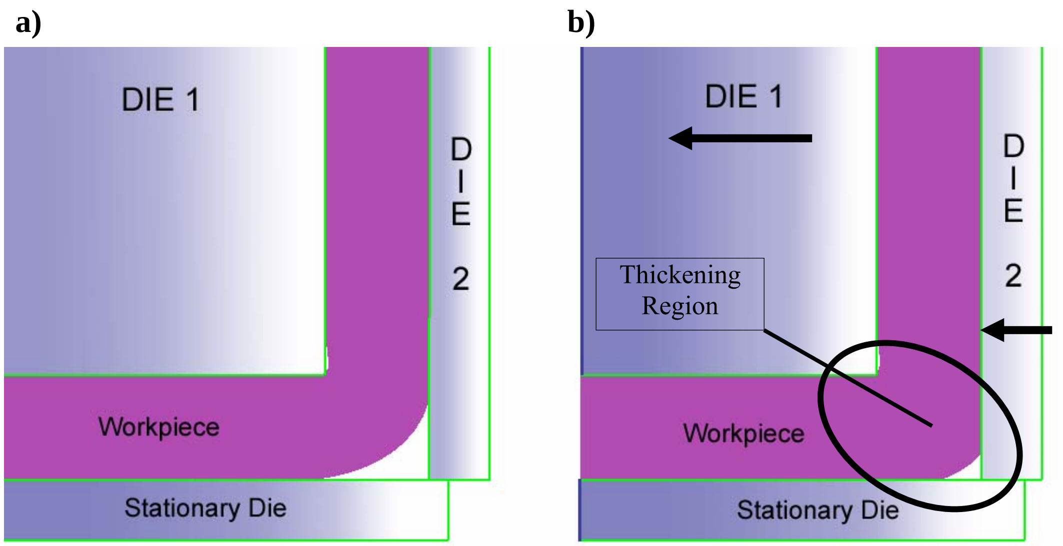

Figure 5.30 The new roll-forming simulation method: **a)** at the end of a bending process **b)** at the end of thickening stage

By this method, larger strain values are obtained and the resulting geometry coincides with actual product (Figure 5.31).

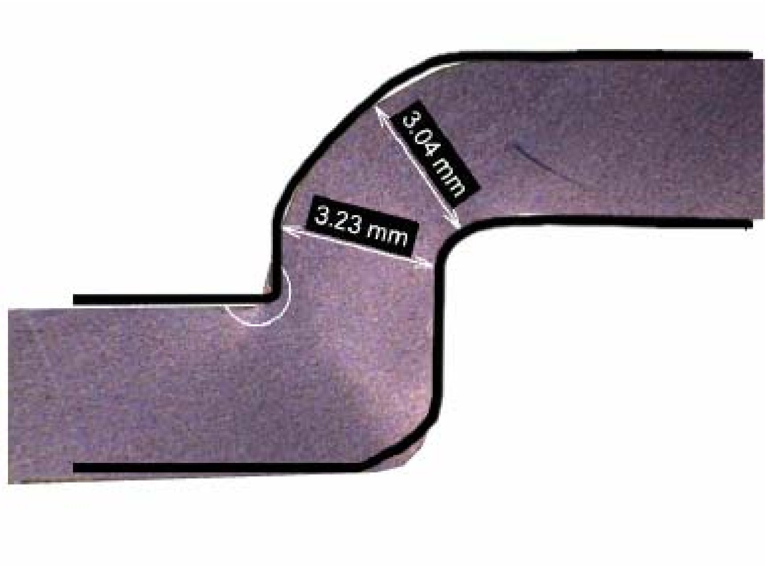

Figure 5.31 Comparison of resulting geometry of new forming simulation and the actual workpiece (Solid lines are the simulation results)

The strain values obtained from this new method are higher than the values obtained in the previous part. Figure 5.32 and Figure 5.33 present the strain distribution through the thickness of the workpiece compared with the strain values obtained from the HV measurements. Again in the Type-2 bends, strain values obtained from the HV measurements can not be compared with the computed values in the early parts of the plot since the values in here are too large that they are beyond the range of the flow curve. It is seen that, the strain values of the both bent regions are in agreement with the experimentally found ones.

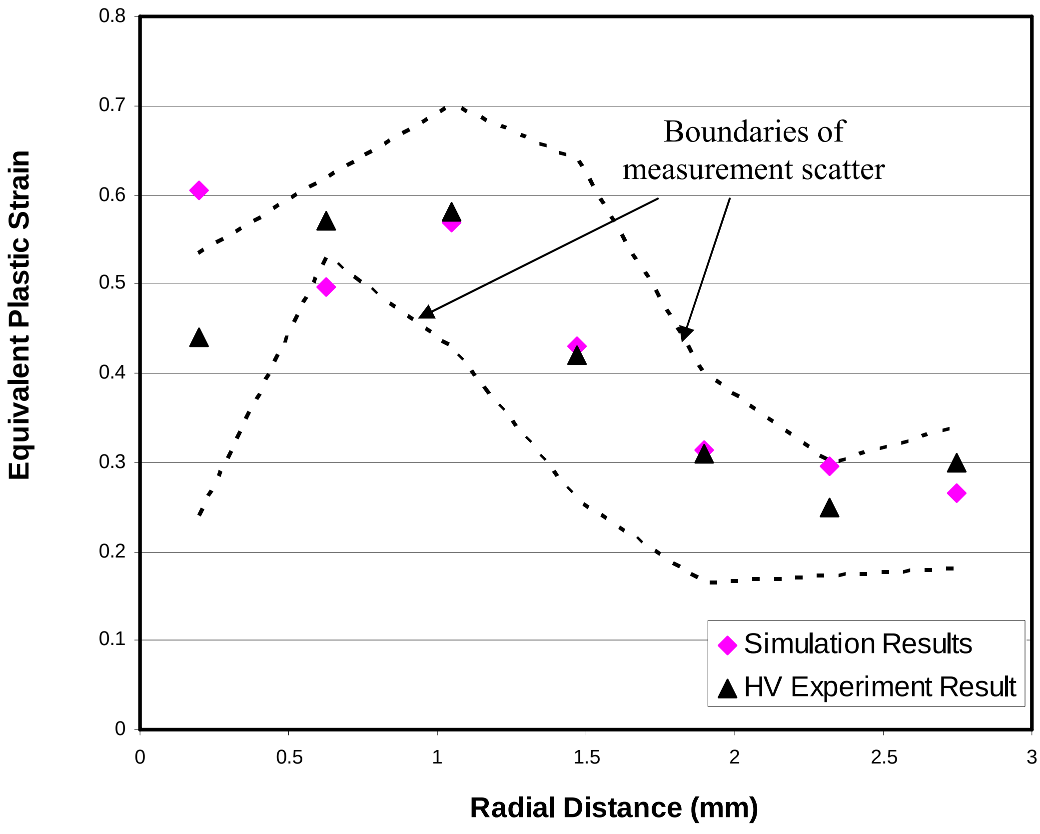

Figure 5.32 Strain distributions obtained from the new forming simulations and HV measurements for the Type-1 90° bend

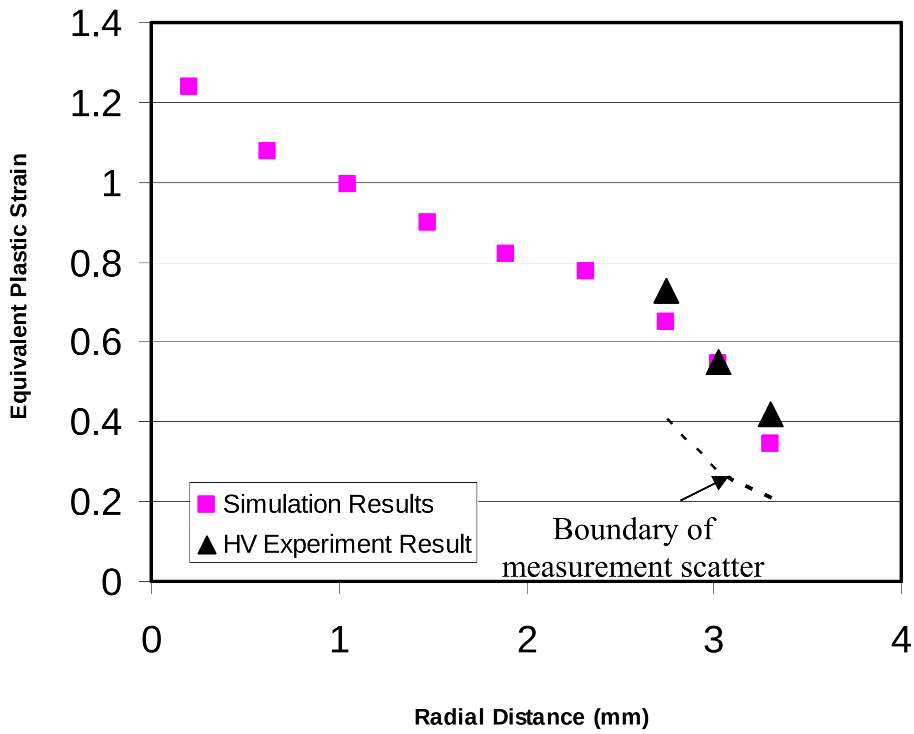

Figure 5.33 Strain distributions obtained from the new forming simulations and HV measurements for the Type-2 90° bend

5.5 Bending Experiment Simulations with Deformation Effects

Having completed the roll-forming simulations, the model is extruded to a 3-D model to perform the bending experiment simulations. The effects of plastic strain and residual stresses arising in the forming sequence will be investigated in this section.

5.5.1 Finite Element Model

The model used in this section resembles the model described in Section 5.4.1. 3D brick elements with assumed strain formulation are utilized in the simulations.

Because of symmetry of the geometry and the loads, only ¼ of the workpiece is modeled. In Section 5.4.1, the geometry is exactly the same as the technical drawings of the channel. However, this time the geometry obtained from the forming simulations is used. In addition, the workpiece has initial stresses and initial plastic strain transferred from the forming simulation results (Figure 5.34).

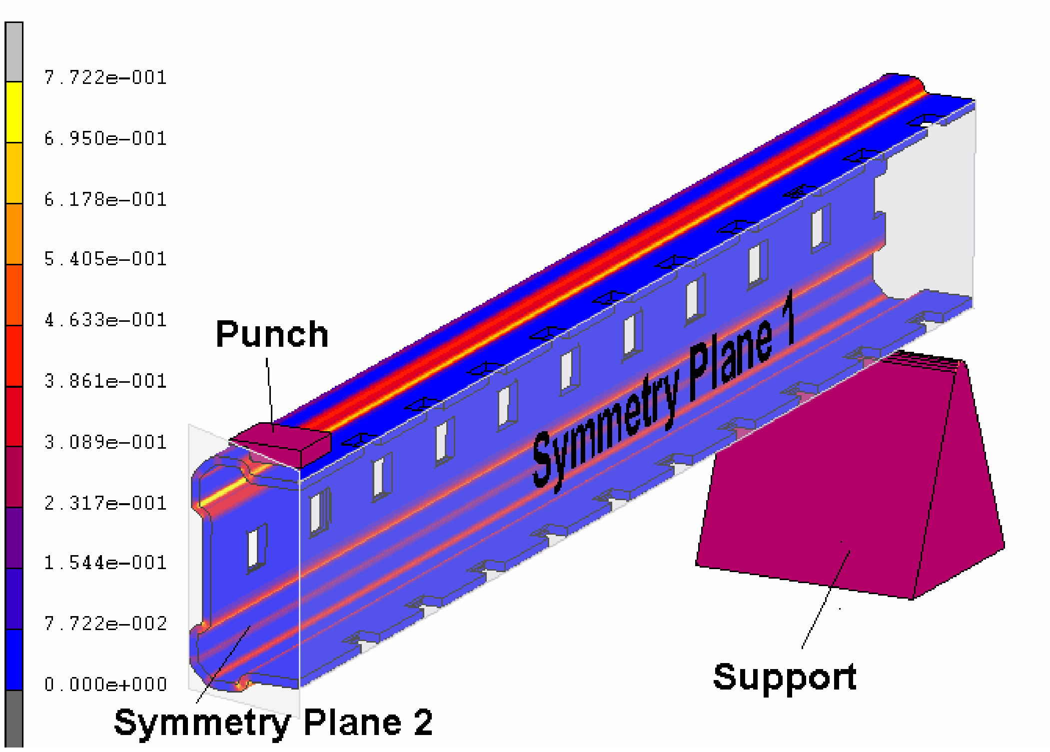

Figure 5.34 Initial plastic strain distribution along the workpiece

5.5.2 Comparison of the Simulation Results with the Experiments

When Figure 5.35 is examined, the outcomes are as follows;

- The manufacturing method 1, which is pure bending, increases the maximum reached force from 35 kN to 40 kN.

- The manufacturing method 2, which includes pressing the workpiece between dies, increases the maximum reached force from 35 kN to 45 kN.
- Method 2 predicts the maximum force with a 17% of error, while method 1 has a 25% error.
- In the experiment data, yielding occurs more gradually than the numerically computed ones.
- The general form of deformation is predicted well with the simulations. In other words, the character of the Force-Displacement curves obtained from the both simulations is consistent with the experiments.

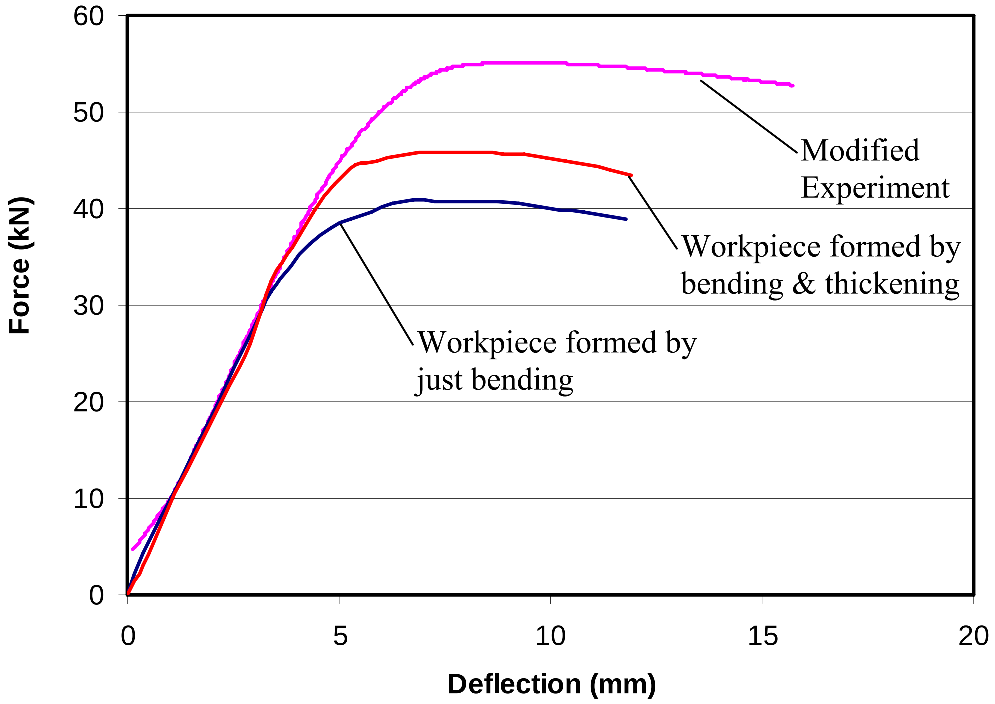

Figure 5.35 Comparison of bending simulation results and the bending experiment data

CHAPTER 6

CONCLUSIONS & FURTHER RECOMMENDATIONS

Roll-forming is an efficient way of producing long parts with constant cross-section. The process has several advantages such as high production capability up to 1800 m per working hour, capability of forming painted and coated material without injuring the fine surface, adaptability of auxiliary operations like piercing, notching and welding. The roll-formed sections have a higher strength to weight ratio than those, which are hot rolled or extruded.

Due to these advantages, roll-forming is widely used in the industry. However even today the deformation in roll-forming is not studied in detail. The production is mainly governed by empirical knowledge. Due to the complex nature of the process, simulation of roll-forming is cumbersome in terms of pre-processing and computation durations. Therefore, simulations are limited with simple geometries.

The thesis work is concentrated in two fields. The first one is the simulation of roll-forming process. This part compares 3D simulations utilizing solid and shell elements and 2D simulation with plane strain assumption. The conclusions are as follows.

- For 3D simulations, shell elements are found to be appropriate in terms of computation durations and results.

- 2D plane strain simulations predict the strain hardening in the bend regions with a good agreement with the 3D simulations. However, formulation predicts zero hardening in the web and flange of the sheet.
- The theoretical deformation length and longitudinal engineering strain values are found to be inconsistent with the experimental findings. The deformation length is low and the longitudinal engineering strain is over-predicted up to three times the experimental values.

The second concentrated field is the deformation features of the roll-forming process. The important geometrical parameters of the process are revealed and the effects of these parameters are studied. The conclusions are as follows.

- Deformation in roll-forming is mainly driven by the geometry of the sheet and rollers. The main geometrical parameters are angle change, flange length, roller radius and sheet thickness.
- The effect of roller radius on the plastification can only be seen at the very end of the flange where the sheet contacts the roller. The rest of the sheet is not affected by the change of the roller diameter.
- Effect of angle change and thickness of the sheet is tabulated for different locations on the flange of the sheet. As the angle change and thickness increase the severity of forming increases leading to higher plastic strains in the flange.
- The effect of the flange length is seen to lower the strain in the flange. The plastification in the bend region is not affected but the plastic strain in the flange of the sheet reduces. This is true for both thick and thin sheets.
- The deformation in thin sheets differs from the deformation in thick sheets. For the thin sheets the plastic strain values in the flange is low compared to the strain observed in the bend region except the end of the flange. There is steep increase of plastification when approached to the end of the flange.

- The main deformation directions in roll-forming are analyzed. It is seen that thick and thin sheets differ in deformation directions. The longitudinal strain components in thin sheets are more dominant. The deformation at the end of the flange and in the web is complex, meaning that most of the strain components are present. However, the strain in the bend area is almost a planar straining occurring in the cross-sectional plane.
- It is observed that the assumptions lying under the theory are not satisfied. This is the reason for the inconsistent predictions of the theory.
- The conditions in which the 2D plane strain simulations can be used are discussed. It is found that generally for thin sheets and thick sheets with relatively long flange lengths the assumption can be used.

In Chapter 5, these discussions are tested on a roll-formed product in a case study. It is seen that with only 2D plane strain simulation it is possible to obtain the hardening in a thick sheet with a relatively long flange length. The full 3D finite element simulation of the case study product would take weeks for the computation. However, plane strain simulations are fast and easy to model. The errors in the plane strain computation are known and the computation can be performed with the knowledge of these errors.

As a further study, the discussions in simulation of roll-forming process can be extended to explicit formulation. With the explicit formulation, the process can be simulated faster. However, there is also known drawbacks of the explicit formulation. Therefore, it would be comprehensive to compare implicit methods with the explicit method.

The study about the deformation of roll-formed sheets can be extended to the analysis of the effects of number of stages. The difference in plastification of the sheet that is bent from $0°$ to $\theta_2°$ or from 0° to $\theta_1°$ and $\theta_1°$ to $\theta_2°$ can be analyzed further. The applicability of 2D plane strain models to this case should be analyzed also.

Another extension of the study can be about the material of the sheet. The deformation features of the sheet can be analyzed with different materials having different yield stresses. By this way, effect of yield stress on the plastic deformation of the sheet can be examined.

REFERENCES

1. Tekkaya A.E.; ME 453 Metal Forming Technology, Lecture Notes. 2001: Middle East Technical University, Ankara.

2. Kiuchi M., Abe K., Onodera R.; Computerized Numerical Simulation of roll-forming process, Annals of CIRP Vol. 44/1/1995, pp. 239-242

3. Dykes, R.J.; Mander, S.J.; D. Bhattacharyya: Roll forming continious fibre-reinforced thermoplastic sheets: experimental analysis, Composites Part A, 31 (2000), pp. 1395-1407

4. Lyman, T.: Metals Handbook, 8th Edition, Vol. 4, Forming, “Cold Roll Forming”, published by American Society of Metals, Ohio, 1969, pp.224-239

5. FORMTAK Roll-form Machinery Corporation website, http://www.formtak.com, last accessed April, 2007

6. Johnson J.C.: Cold Roll Forming-the Changing Scene, sheet metal Industries, October 1975, pp. 555-572

7. Walker A.C.: Design and Analysis of Cold-Formed Sections, Sheet Metal Industries, October 1975, pp. 59-569

8. Dreistern Company, http://www.dreistern.com, last accessed April, 2007

9. Angel, R. T.: Designing Tools for Cold Roll Forming, The Iron Age, November 1949, Vol. 164, pp. 83-88.

10. Ona, H.; Jimma, T., Kozono, H.: A Computer Aided Design System for Cold Roll Forming, Advanced Technology of Plasticiy, Vol. 1, 1984, pp. 508-511.

11. Bhattacharyya, D.; Smith, P. D.; Yee, C. H.; Collins, I. F.: The Prediction of Forming Length in Cold Roll Forming, Journal of Mechanical Working Technology, Vol. 9, 1984, pp. 181-191.

12. Panton S. M., Zhu S. D., Duncan J. L.; Geometrical constraints on the forming path in roll forming channel sections, Proc. Instn. Mech. Engrs. Part B, 206 (1992), pp. 113-118

13. Panton S. M., Zhu S. D., Duncan J. L; Fundamental deformation types and sectional properties in roll forming, J. of Mech. Sci., 36 (8), pp. 725-735

14. Duggal N., Ahmetoglu M. A., Kinzel G. L., Altan T.; Computer aided simulation of cold roll forming- a computer program for simple section profiles, J. of Mater. Proc. Tech., 59 (1996), pp. 41-48

15. Heislitz F., Livatyali H., Ahmetoglu M. A., Kinzel G. L., Altan T.; Simulation of roll forming process with the 3-D FEM code PAM-STAMP, J. of Mater. Proc. Tech., 59 (1996), pp. 59-67

16. Livatyali H., Duggal N., Ahmetoğlu M.A., Altan T.; Investigation of crack formation on the Galvalume coationg of roll formed roof panels, J. of Mater. Proc. Tech., 98 (2000), pp. 53-61

17. Han Z., Liu C., Lu W., Ren L.; Simulation of a multi-stand roll-forming process for thick channel section, J. of Mater. Proc. Tech., 127 (2002), pp. 382-387

18. Kim N., Oh S.I.; Analysis Tool for Roll Forming of Sheet Metal Strips by the Finite Element Method, Annals off the CIRP, Vol. 48/1/1999, pp. 235-238

19. Brunet M., Ronel S.; Finite element analysis of roll-forming of thin sheet metal, J. of Mater. Proc. Tech., 45 (1994), pp. 255-260

20. Abdel-Rahman N., Sivakumaran K.S.; Material Properties Models for Analysis of Cold-Formed Steel Members, Journal of Structural Engineering, Vol. 123, No. 9, September 1997, pp. 1135-1143

21. Tabor D.; The Hardness and Strength of Metals, J. Inst. Metals, Vol.79, pp 1-18

22. Tabor D.; A Simple Theory of Static and Dynamic Hardness, Proc. Roy. Society Series A, Vol. 192, pp. 247-274

23. Ramaekers, J.A.H.; Harte und Verformung Metallischer Verkstoffe, Dr. –Ing. Dissertation, Technische Universitat Eindhoven, Eindhoven

24. Wilhelm, H.: 1969, Untersuchungen über den Zusammenhang zwischen Vickersharte und Vergleichsformanderung bei Kaltumformvor-gangen. Berichte aus dem Institut für Umformtechnik der Universitat Stuttgart, Essen: Girardet.

25. Dannenmann, E., Wilhelm, H., Steck, E.: “Uber den Zusammenhang zwishen Eindringharte und Umformgrad bei Kaltumformvorgangen”, Bander Bleche Rohre, (1968), pp 368-394.

26. Srinivasan K.; Venugopal, P.: J. Mat. Proc. Techn. 95 (1999), pp. 185- 190

27. Tekkaya A.E.; Hardness Measurements on Cold Formed Workpieces, Advanced Technology of Plasticity, Vol. II, Proceedings of the 6th ICTP, 1999

28. Tekkaya A.E.; "An Improved Relationship between Vickers Hardness and Yield Stress for Cold Formed Materials and its Experimental Verifications, Annals of the CIRP, Vol. 49, 2000

29. Yavuz B., Tekkaya A.E.; Correlations between Vickers Harness Number and Yield Stress of Cold Formed Products, 9th International Conference on Machine Design and Production, UMTIK 2000.

30. Bhattacharyya D., Smith P. D.; The Development of Longitudinal strain in cold roll forming and its influence on product straightness, First International Conference on Technology of Plasticity, Tokyo, 1984, pp. 422-427

31. M.S. Tehrani, P. Hartley, H. M. Naeini, H. Khademizadeh; Localized Edge Buckling in Cold Roll-Forming of Symmetric Channel Section, Thin-Walled Structures, 44 (2006), pp. 184-196

32. MSC.MARC Volume A, Theory and User

33. Mechanics of Materials, Ferdinand P. Beer, E. Russel Johnston, JR.,1992

APPENDIX A

PARAMETRIC STUDY OF 3D MODELS

A.1 Parametric Study of 3D Roll-Forming Simulation with Solid Elements

The parametric study is performed with a uniform mesh composed of 2600 elements with dimensions 0.6 mm in thickness direction, 1.5 mm in longitudinal direction and 1.5 mm in transverse direction. Therefore one element is used through the thickness of the sheet. The investigated parameters are convergence tolerance, contact tolerance, solution step size and matrix solver. The effects of these parameters are presented with longitudinal eng. strain plots, equivalent plastic strain on sheet surface plots and computation duration tables.

A.1.1 Effect of Convergence Tolerance

Both relative force tolerance and relative displacement tolerance are varied together through the values 0.1, 0.05 and 0.01. The longitudinal engineering strain results in Figure A.1a shows that the maximum reached values of strain does not change with the changing convergence tolerances. Figure A.1b shows the equivalent plastic strain on the upper surface of the sheet from web center to the flange end and again convergence tolerance has no effect on the final hardening on the sheet.

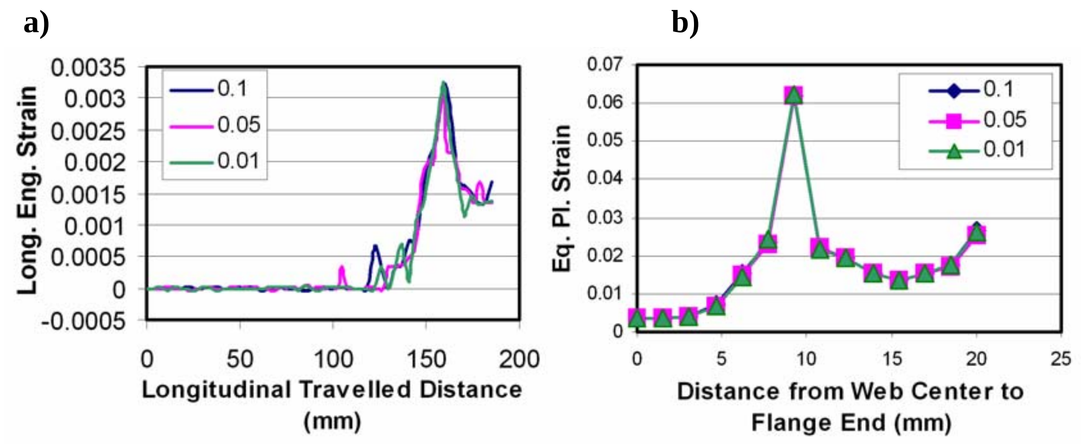

Figure A.1 Effect of convergence tolerances. a) Longitudinal engineering strain b) strain hardening on the sheet surface

However when the relative computation durations in Table A.1 are considered, there is a huge difference. As narrower convergence tolerances are used computation durations increase up to 3.3 times of the minimum duration. Therefore as a value of both force and displacement convergence tolerances 0.1 is selected.

Table A.1 Relative computation durations wrt. convergence tolerances

Convergence Tolerance	Relative Computation Durations
0.1	1.0
0.05	1.5
0.01	3.3

A.1.2 Effect of Contact Tolerance

When a node approaches a body with a distance equal to or less than the contact tolerance, the node is assumed to be in contact with the body. For that reason, the importance of contact tolerance increases in incremental processes since there is repetitive contact occurrences and releases during the process. Contact tolerance value is varied from 1% of the thickness to 8%. The results can be seen in Figure A.2a and Figure A.2b. As in the convergence tolerances, the contact tolerances values have a negligible effect on longitudinal engineering strain and hardening on the sheet. However relative computation durations are affected by the contact tolerances (Table A.2). As a result, 8% of the thickness is selected to be suitable because of the computation duration results.

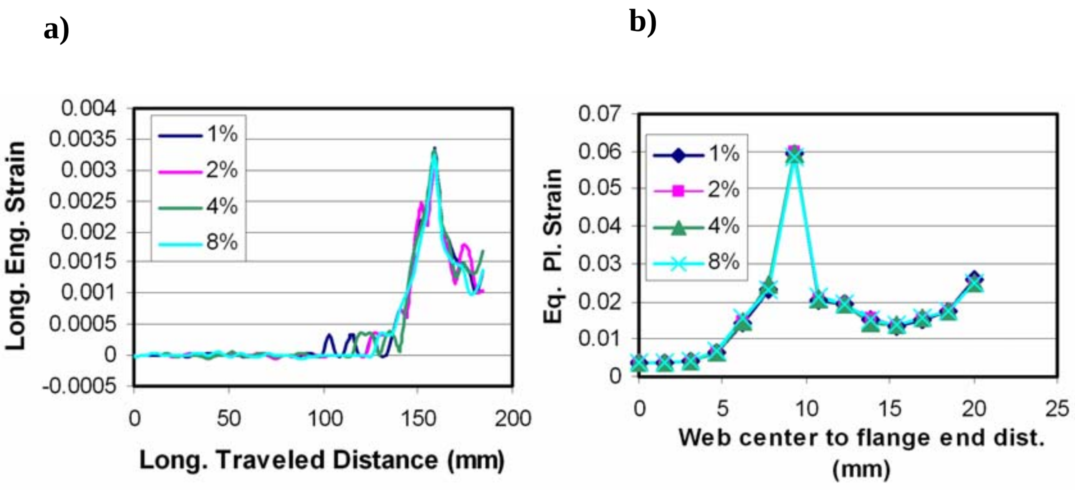

Figure A.2 Effect of contact tolerances. a) Longitudinal engineering strain b) strain hardening on the sheet surface

Table A.2 Relative computation durations wrt. convergence tolerances

Contact Tolerance	Relative Computation Durations
0.006	0.13
0.012	0.25
0.024	0.50
0.048	1.00

A.1.3 Effect of Step Size

Proper selection of step size plays an important role in finite element simulations. In roll-forming simulations, a large step size causes the nodes to move a large distance in one step over the curved surface of the roller and this large motion over the rigid surface sometimes turn out to be a problem that takes too much time to solve. In addition the details of the motion of the nodes on the roller can not be captured with a large step size. On the other hand a small step size will cause the overall computation time to increase because of the increased number of steps.
Therefore, for this problem step size is varied according to the longitudinal traveled distance from 3.7 mm/step to 0.9 mm/step. From Figure A.3a it is seen that step size affects the maximum reached longitudinal engineering strain. The difference between the maximum values of the results with 0.9 mm/step and 3.7 mm/step is 13% of the small value. The solution with the 1.2 mm/step can be said to converge since the difference with the 0.9 mm/step is less than 5%. When the strain hardening on the upper surface of the sheet in Figure A.3b is analyzed, it can be seen that step size has negligible effect on the hardening results.

a) b)

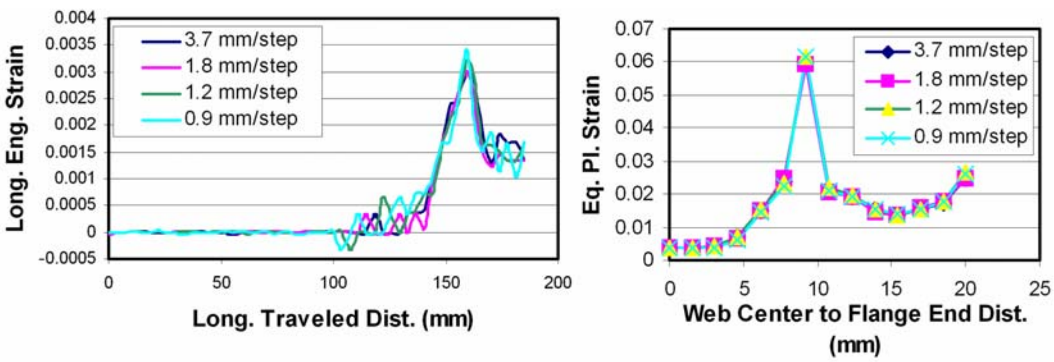

Figure A.3 Effect of step size: a) on longitudinal engineering strain b) on strain hardening on the sheet surface

The relative computation durations in Table A.3 shows that as the step size decreases in that range the solution time reduces. Therefore a step size of 1.2 mm/step is selected to be suitable for that problem since both convergence is achieved and solution duration is minimum.

Table A.3 Relative computation durations wrt. step size

Number of Steps	Relative Computation Durations
55	1.4
110	1.1
165	1.0
220	1.0

A.1.4 Effect of Solver

There are different solvers in literature to solve large matrix systems. They differ in terms of solution methods and handling of matrices during solution phase. Some solvers use analytical methods and some use numerical methods as solution methods. Handling of matrices during solution affects the allocated memory and solution duration of the system. The convenient solver for a problem is dependent on the distribution of the elements of the matrices and available memory. For this case three solvers are tried and the results can be seen in Table A.4.

Table A.4 Effect of solver on the computation duration

Solver	Relative Computation Durations
Multifrontal Sparse	1.3
Iterative Solver with 0.1 Tolerance	1.4
Iterative Solver with 0.001 Tolerance	2.8
Direct Sparse	1.0

The maximum computation duration is obtained with the iterative solvers. The convergence tolerance used in iterative solver is also varied and it is seen that it has an important effect on the solution duration. However values lower than 0.1 are not tried since lower values would give relatively poor results. As a result direct sparse solver is selected to be convenient for that specific problem.

A.1.5 Effect of Assumed Strain Formulation

As mentioned in Section 5.3.1 of Chapter 5, with the assumed strain formulation "the bending behavior of 3-D brick elements is improved by replacing the standard bi- or trilinear interpolation functions with an enriched group that is able to represent pure bending behavior. This formulation results in improved accuracy for isotropic behavior, but it should be noted that the computational costs increase" [32]. To examine the significance of the formulation, the simulations with the same mesh densities used in the study are performed with and without the formulation and the results for two cases can be seen in Figure A.4.

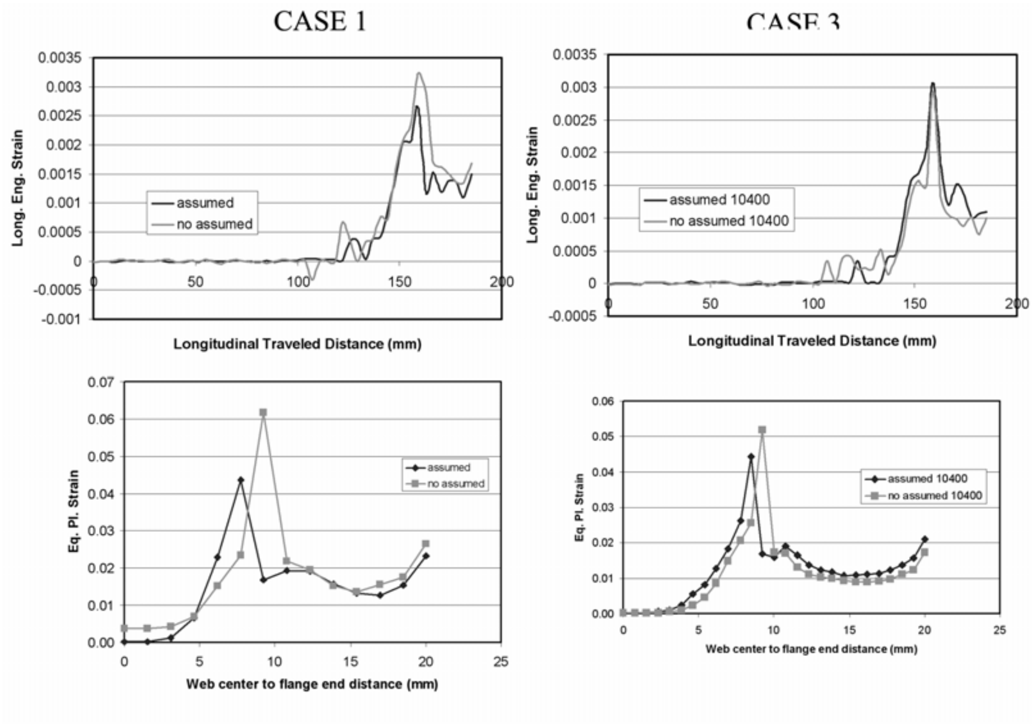

Figure A.4 Effect of Assumed Strain Formulation

It is seen that for the CASE 1 assumed strain formulation affects the longitudinal engineering strain values. The difference of the reached peak values is 20% of the high value. In addition the strain distribution across the sheet differs considerably. The maximum strain is reached at different locations. This means that maximum bending occurs at different location in the bend regions. When the CASE 3 is examined it is observed that the longitudinal strain values are not affected by the utilization of the formulations. In addition, the plastic strain values across the sheet from web center to the flange end are again similar in two cases. The location of the maximum plastic strain is again different. Therefore as the mesh is refined the significance of the formulation reduces. That's why the formulation is not used in the simulations using mesh densities CASE 3 and CASE 4, for the other cases the formulation has been utilized.

A.2 Parametric Study of 3D Roll-Forming Simulation with Shell Elements

The parametric study is performed with a uniform mesh composed of 2600 elements with dimensions 0.6 mm in thickness direction, 1.5 mm in longitudinal direction and 1.5 mm in transverse direction. The investigated parameters are number of layers, convergence tolerance, contact tolerance, solution step size and matrix solver. The effects of these parameters are presented with longitudinal eng. strain plots, equivalent plastic strain on sheet surface plots, equivalent plastic strain through the thickness and computation duration tables.

A.2.1 Effect of Number of Layers

The number of layers in shell elements has a great effect on the results. Insufficient number of layers causes the results to be poor. The points at which any field variable is calculated are defined by the layers. Therefore the number of layers is equal to the number of points that variables are output through the thickness. In this case, number of layers is varied from five to 11 and the results can be seen in Figure A.5. The maximum reached longitudinal strain values are all the same in each number of layers. However, the final reached strain differs with a maximum difference of 7% of the lowest value. In Figure A.5b the equivalent plastic strain values through the thickness in the bend region are plotted. It is seen that with five number of layers the nonlinearity of strain distribution is hard to capture. Starting with seven number of layers the strain distribution is observed to converge to its nonlinear distribution.

a) b)

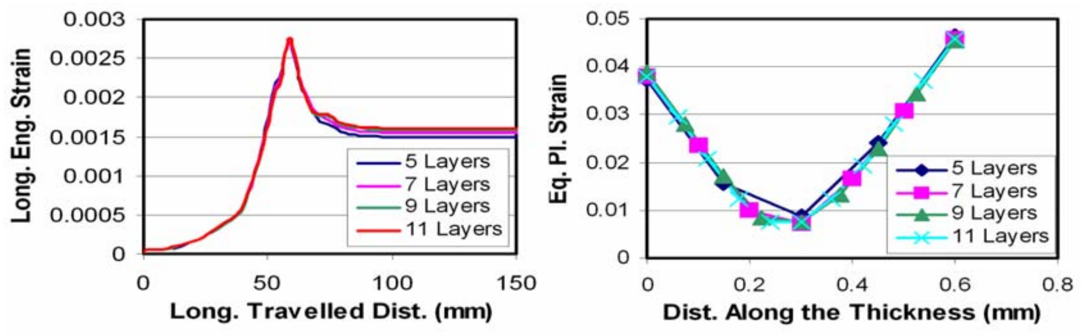

Figure A.5 Effect of number of layers: a) on longitudinal engineering strain b) on strain hardening on the sheet surface

When Table A.5 is observed, it is seen that number of layers does not affect the computation duration significantly. But with the increasing number of elements this effect will be a major factor influencing the computation durations. Therefore, seven number of layers is decided to be used in the simulations of roll-forming with shell elements.

Table A.5 Effect of number of layers on the computation durations

Number of Layers	Relative Computation Durations
5	1.00
7	1.01
9	1.08
11	1.10

A.2.2 Effect of Convergence Tolerance

As in the parametric study with solid elements relative force and displacement convergence tolerances are assigned values of 0.1, 0.05 and 0.01. The longitudinal engineering strain values and equivalent plastic strain values remain unchanged with the changing convergence tolerances. However, computation durations are highly affected by the convergence tolerances. This is tabulated in Table A.6. Since all convergence tolerances give the same results, it is convenient to select the tolerance with the least computation duration. Therefore convergence tolerance of 0.1 is selected for the simulations with shell elements.

Table A.6 Effect of convergence tolerance on the computation durations

Convergence Tolerance	Relative Computation Durations
0.10	1.0
0.05	1.8
0.01	4.0

A.2.3 Effect of Contact Tolerance

When contact tolerance is varied from 1% to 8% of the thickness which is 0.6 mm, no change is observed in the longitudinal engineering strain or plastic strain values. Therefore, the contact tolerance with the shortest simulation duration is selected, that is 8% of the thickness.

A.2.4 Effect of Step Size

Step size is varied from 1.85 mm/step to 0.9 mm/step according to the longitudinally traveled distance. The longitudinal engineering strain plots in Figure A.6 shows that all simulations give the same maximum value of engineering strain. However there is a maximum difference of 12% between the final reached strain values. With a step size of 1.2 mm/step the final engineering strain values converge. The equivalent plastic strain values do not show noticeable difference with respect to the step size. Therefore, 1.2 mm/step is selected to be appropriate for that case. Since the convergence is first achieved with this value of step size the computation duration is disregarded.

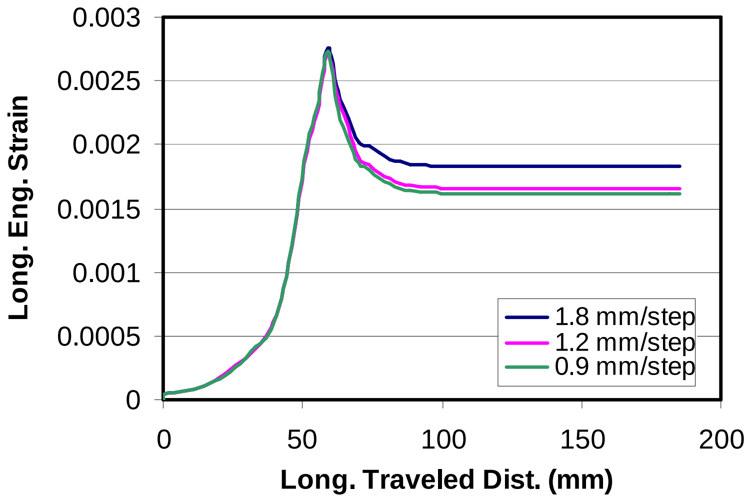

Figure A.6 Effect of step size

A.2.5 Effect of Solver

The same solvers checked in the parametric study of solid elements are tried for the shell elements and it is seen again that direct sparse solver is the fastest solver among the others.

APPENDIX B

CALCULATION OF DEFLECTION OF THE ROLL-FORMED PRODUCT

B.1 Beam Deflection Equations

The performed bending experiment with the product mentioned in Chapter 5 can be idealized as in the Figure B.1. This is a beam fixed at both ends. Force *P* is applied at the middle of the beam. The deflection is measured from the punch in the experiments. This deflection corresponds to the maximum deflection of the idealized model.

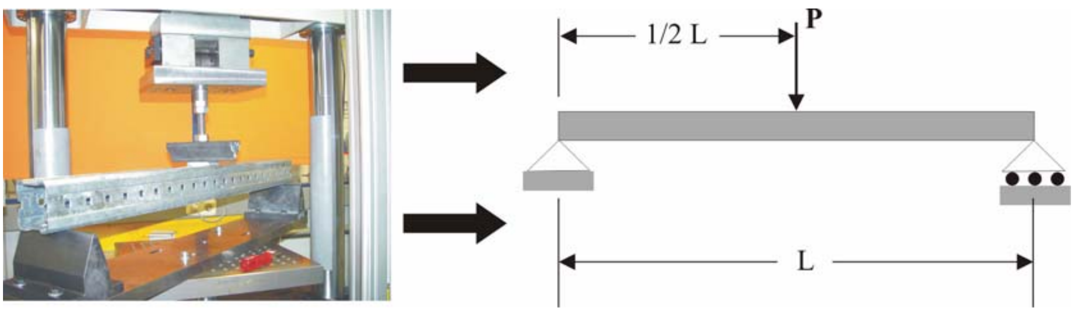

Figure B.1 Idealization of the bending experiment

According to the theory of elasticity maximum deflection of the beam can be found from the relation [33]

$$w = \frac{PL^3}{48EI} \tag{B.1}$$

where

w: Deflection

P: Applied Force

L: Total length of the beam

E: Modulus of Elasticity

I: Moment of Inertia

Among those variables, L and E are known from the geometry and the material properties of the product. w will be varied from zero to a value to obtain force vs. deflection plots. The only unknown is the moment of inertia of the beam. It has to be calculated for the geometry of the roll-formed product using the following equation.

$$I = \frac{l^3 t}{12}\sin^2(\alpha) + l \cdot t \cdot \bar{z}^2 \tag{B.2}$$

where

l: length of the sectional element

t: Thickness of the sectional element

α: Angle between the element and the axis that the moment inertia is calculated

$\bar{z}$: Perpendicular distance between the center of mass of the element and the axis that moment of inertia is calculated.

B.2 Calculation of the Moment of Inertia

In order to calculate the moment of inertia of the roll-formed product, the section should be simplified. The fillets and thick parts of the section are replaced by straight lines and sharp corners. The resulting geometry can be seen in Figure B.2.

The dashed line in Figure B.2 is the original cross-section of the product. The solid line shows the centroid of the idealized section.

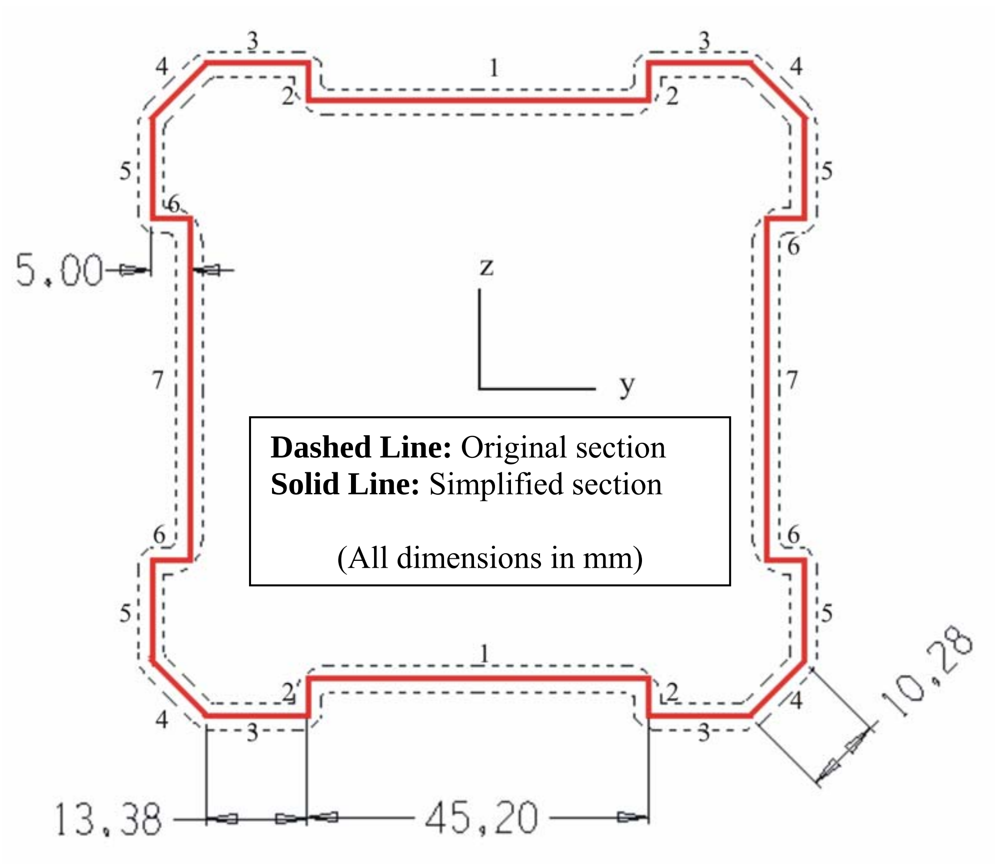

Figure B.2 Simplified section of the product

The elements on the section are numerated from one to seven. The elements with the same number have equal moment of inertias. The calculations are as follows.

$$I_{y_1} = \frac{45.2^3 \cdot 3.5}{12} \cdot \sin^2(0) + 45.2 \times 3.5 \times 38.25^2 = 231456.5 \ mm^4$$

$$I_{y_2} = \frac{5^3 \cdot 3.5}{12} \cdot \sin^2(90) + 5 \times 3.5 \times 42.25^2 = 31275.1 \ mm^4$$

$$I_{y_3} = \frac{13.38^3 \cdot 3.5}{12} \cdot \sin^2(0) + 13.38 \times 3.5 \times 43.25^2 = 87598.4 \ mm^4$$

$$I_{y_4} = \frac{10.28^3 \cdot 3.5}{12} \cdot \sin^2(45) + 10.28 \times 3.5 \times 39.62^2 = 56637.8 \ mm^4$$

$$I_{y_5} = \frac{13.38^3 \cdot 3.5}{12} \cdot \sin^2(90) + 13.38 \times 3.5 \times 29.29^2 = 40874.3\ mm^4$$

$$I_{y_6} = \frac{5^3 \cdot 3.5}{12} \cdot \sin^2(0) + 5 \times 3.5 \times 22.60^2 = 8938.3\ mm^4$$

$$I_{y_7} = \frac{45.2^3 \cdot 3.5}{12} \cdot \sin^2(90) + 45.2 \times 3.5 \times 0^2 = 26934.1\ mm^4$$

$$I_y = 2 \cdot I_{y_1} + 4 \cdot I_{y_2} + 4 \cdot I_{y_3} + 4 \cdot I_{y_4} + 4 \cdot I_{y_5} + 4 \cdot I_{y_6} + 2 \cdot I_{y_7} \tag{B.3}$$

$$I_y = 1418076.8\ mm^4$$

B.3 Calculation of the Maximum Deflection

Having obtained the moment of inertia, the force vs. deflection curve of the beam can be obtained by the equation B.1 with the following known values.

$P =$ will be calculated
$w =$ varied from 0 to 5 mm
$L =$ 1000 mm
$E =$ 200 GPa
$I_y =$ 1418076.8 mm^4

The obtained values are given in Table B.1.

Table B.1 Calculated force-deflection values

Deflection (mm)	Force (kN)
0	0.0
1	13.6
2	27.2
3	40.8
4	54.5
5	68.1